University of Alberta

Forced Stationary Free-surface and Internal Solitary Waves in Channel Flows

By

Lianger Gong

A Thesis
Submitted to the Faculty of Graduate Studies and Research
in Partial Fulfillment of the Requirements for the Degree
of Doctor of Philosophy

Department of Mathematical Sciences

Edmonton, Alberta
Fall, 1994

Canada

Name __LIANGER GONG__

Dissertation Abstracts International is arranged by broad, general subject categories. Please select the one subject which most nearly describes the content of your dissertation. Enter the corresponding four-digit code in the spaces provided.

Subject Categories

THE HUMANITIES AND SOCIAL SCIENCES

COMMUNICATIONS AND THE ARTS
Architecture	0729
Art History	0377
Cinema	0900
Dance	0378
Fine Arts	0357
Information Science	0723
Journalism	0391
Library Science	0399
Mass Communications	0708
Music	0413
Speech Communication	0459
Theater	0465

EDUCATION
General	0515
Administration	0514
Adult and Continuing	0516
Agricultural	0517
Art	0273
Bilingual and Multicultural	0282
Business	0688
Community College	0275
Curriculum and Instruction	0727
Early Childhood	0518
Elementary	0524
Finance	0277
Guidance and Counseling	0519
Health	0680
Higher	0745
History of	0520
Home Economics	0278
Industrial	0521
Language and Literature	0279
Mathematics	0280
Music	0522
Philosophy of	0998
Physical	0523

Psychology	0525
Reading	0535
Religious	0527
Sciences	0714
Secondary	0533
Social Sciences	0534
Sociology of	0340
Special	0529
Teacher Training	0530
Technology	0710
Tests and Measurements	0288
Vocational	0747

LANGUAGE, LITERATURE AND LINGUISTICS
Language
General	0679
Ancient	0289
Linguistics	0290
Modern	0291

Literature
General	0401
Classical	0294
Comparative	0295
Medieval	0297
Modern	0298
African	0316
American	0591
Asian	0305
Canadian (English)	0352
Canadian (French)	0355
English	0593
Germanic	0311
Latin American	0312
Middle Eastern	0315
Romance	0313
Slavic and East European	0314

PHILOSOPHY, RELIGION AND THEOLOGY
Philosophy	0422

Religion
General	0318
Biblical Studies	0321
Clergy	0319
History of	0320
Philosophy of	0322
Theology	0469

SOCIAL SCIENCES
American Studies	0323

Anthropology
Archaeology	0324
Cultural	0326
Physical	0327

Business Administration
General	0310
Accounting	0272
Banking	0770
Management	0454
Marketing	0338
Canadian Studies	0385

Economics
General	0501
Agricultural	0503
Commerce-Business	0505
Finance	0508
History	0509
Labor	0510
Theory	0511
Folklore	0358
Geography	0366
Gerontology	0351

History
General	0578

Ancient	0579
Medieval	0581
Modern	0582
Black	0328
African	0331
Asia, Australia and Oceania	0332
Canadian	0334
European	0335
Latin American	0336
Middle Eastern	0333
United States	0337
History of Science	0585
Law	0398

Political Science
General	0615
International Law and Relations	0616
Public Administration	0617
Recreation	0814
Social Work	0452

Sociology
General	0626
Criminology and Penology	0627
Demography	0938
Ethnic and Racial Studies	0631
Individual and Family Studies	0628
Industrial and Labor Relations	0629
Public and Social Welfare	0630
Social Structure and Development	0700
Theory and Methods	0344
Transportation	0709
Urban and Regional Planning	0999
Women's Studies	0453

THE SCIENCES AND ENGINEERING

BIOLOGICAL SCIENCES
Agriculture
General	0473
Agronomy	0285
Animal Culture and Nutrition	0475
Animal Pathology	0476
Food Science and Technology	0359
Forestry and Wildlife	0478
Plant Culture	0479
Plant Pathology	0480
Plant Physiology	0817
Range Management	0777
Wood Technology	0746

Biology
General	0306
Anatomy	0287
Biostatistics	0308
Botany	0309
Cell	0379
Ecology	0329
Entomology	0353
Genetics	0369
Limnology	0793
Microbiology	0410
Molecular	0307
Neuroscience	0317
Oceanography	0416
Physiology	0433
Radiation	0821
Veterinary Science	0778
Zoology	0472

Biophysics
General	0786
Medical	0760

EARTH SCIENCES
Biogeochemistry	0425
Geochemistry	0996

Geodesy	0370
Geology	0372
Geophysics	0373
Hydrology	0388
Mineralogy	0411
Paleobotany	0345
Paleoecology	0426
Paleontology	0418
Paleozoology	0985
Palynology	0427
Physical Geography	0368
Physical Oceanography	0415

HEALTH AND ENVIRONMENTAL SCIENCES
Environmental Sciences	0768

Health Sciences
General	0566
Audiology	0300
Chemotherapy	0992
Dentistry	0567
Education	0350
Hospital Management	0769
Human Development	0758
Immunology	0982
Medicine and Surgery	0564
Mental Health	0347
Nursing	0569
Nutrition	0570
Obstetrics and Gynecology	0380
Occupational Health and Therapy	0354
Ophthalmology	0381
Pathology	0571
Pharmacology	0419
Pharmacy	0572
Physical Therapy	0382
Public Health	0573
Radiology	0574
Recreation	0575

Speech Pathology	0460
Toxicology	0383
Home Economics	0386

PHYSICAL SCIENCES

Pure Sciences

Chemistry
General	0485
Agricultural	0749
Analytical	0486
Biochemistry	0487
Inorganic	0488
Nuclear	0738
Organic	0490
Pharmaceutical	0491
Physical	0494
Polymer	0495
Radiation	0754
Mathematics	0405

Physics
General	0605
Acoustics	0986
Astronomy and Astrophysics	0606
Atmospheric Science	0608
Atomic	0748
Electronics and Electricity	0607
Elementary Particles and High Energy	0798
Fluid and Plasma	0759
Molecular	0609
Nuclear	0610
Optics	0752
Radiation	0756
Solid State	0611
Statistics	0463

Applied Sciences
Applied Mechanics	0346
Computer Science	0984

Engineering
General	0537
Aerospace	0538
Agricultural	0539
Automotive	0540
Biomedical	0541
Chemical	0542
Civil	0543
Electronics and Electrical	0544
Heat and Thermodynamics	0348
Hydraulic	0545
Industrial	0546
Marine	0547
Materials Science	0794
Mechanical	0548
Metallurgy	0743
Mining	0551
Nuclear	0552
Packaging	0549
Petroleum	0765
Sanitary and Municipal	0554
System Science	0790
Geotechnology	0428
Operations Research	0796
Plastics Technology	0795
Textile Technology	0994

PSYCHOLOGY
General	0621
Behavioral	0384
Clinical	0622
Developmental	0620
Experimental	0623
Industrial	0624
Personality	0625
Physiological	0989
Psychobiology	0349
Psychometrics	0632
Social	0451

University of Alberta

Release Form

NAME OF AUTHOR: **Lianger Gong**
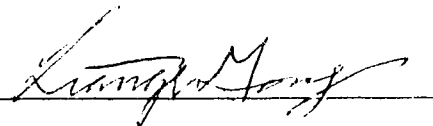
TITLE OF THESIS:

Forced Stationary Free-surface and Internal

Solitary Waves in Channel Flows

DEGREE FOR WHICH THESIS WAS PRESENTED: **Doctor of Philosophy**

YEAR THIS DEGREE GRANTED: **1994**

(Signed)_____

Permanent Address:
Department of Mathematical Sciences
University of Alberta
Edmonton, Alberta
Canada T6G 2G1
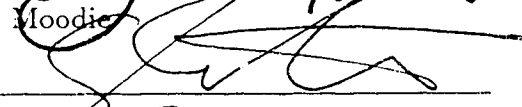
Date: 23(D), Sept/94

Uɴɪᴠᴇʀꜱɪᴛʏ ᴏꜰ Aʟʙᴇʀᴛᴀ

Fᴀᴄᴜʟᴛʏ ᴏꜰ Gʀᴀᴅᴜᴀᴛᴇ Sᴛᴜᴅɪᴇꜱ ᴀɴᴅ Rᴇꜱᴇᴀʀᴄʜ
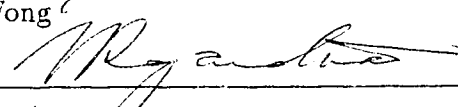
The undersigned certify that they have read, and recommend to the Faculty of Graduate Studies and Research for acceptance, a thesis entitled **Forced Stationary Free-surface and Internal Solitary Waves in Channel Flows** submitted by **Lianger Gong** here in partial fulfillment of the requirements for the degree of **Doctor of Philosophy** in Applied Mathematics.

S. S. Shen

T. B. Moodie

G. E. Swaters

Y. S. Wong

N. Rajaratnam

M. J. Ablowitz

Date: Sept. 9, 1994

To my parents, my wife, Peggy, and my daughter, Danielle

ABSTRACT

This dissertation consists of a joint study of mathematical analysis, numerical computation and experimental investigation on nonlinear long free-surface and internal waves in channel flows subject to external forcings. The fluids are assumed to be inviscid and incompressible. The external forcing is an obstruction mounted on the bottom or the top lid in the channel. By using a perturbation expansion, the forced Korteweg–de Vries (fKdV) equation is derived from a two-layer fluid flow in a closed channel. The main results obtained in the study are summarized as follows Analytic properties of solutions to the stationary forced Korteweg–de Vries (sfKdV) equation are studied. Analytic supercritical solitary wave solutions (SSWS) to the sfKdV equation are expressed in terms of Weierstrass' elliptic functions for a rectangular bump/dent or two local forcings. The existence of multiple SSWS is illustrated by depicting complicated bifurcation diagrams. There are at most two SSWS for a rectangular bump and more than two SSWS for a rectangular dent and two local bumps. A criterion for the stability of SSWS is provided, which stems from the nonlinear stability analysis developed by Benjamin. Based on our numerical simulations, only one of multiple SSWS is stable and all the others are unstable. Solitary waves on a shelf are discovered by solving a boundary value problem of the sfKdV equation. The uniform flows on a shelf are found analytically, which agree with the previous results obtained by King and Bloor through numerical computation. The uniform flow is always stable according to the nonlinear stability criterion. A series of experiments are carried out to verify the validity of the sfKdV model for forced stationary solitary waves and hydraulic falls. Experimental results agree reasonably well with the sfKdV prediction.

ACKNOWLEDGEMENTS

Contents

List of Tables

List of Figures

List of Plates

Chapter 1

Introduction

The purpose of this dissertation is to provide a joint study of mathematical analysis, numerical computation and experimental investigation on nonlinear long waves in response to external forcings. A practical motivation for studying forced nonlinear waves is to investigate the blocking effects of atmospheric currents by mountains and oceanic currents by seabed topography. The study deals primarily with the characteristics of supercritical solitary wave solutions (SSWS) of the stationary forced Korteweg–de Vries (sfKdV) equation, the bifurcation of multiple SSWS, the stability of forced SSWS, and the validity of the sfKdV model. The research results are anticipated to apply in the areas of meteorology, oceanography and other related fields.

The subject of nonlinear long waves has attracted the interest of many mathematicians and physical scientists over the last 160 years since John Scott Russell observed *the Wave of Translation* in 1834, which he characterized as *the solitary wave* [27]. The essential feature of the solitary wave is a balance between the nonlinearity and the dispersion of long wave modes in a physical system. The need

of a mathematical description for this type of wave stimulated the development of the theory of nonlinear long waves at the time and later in the nineteenth century. In 1895, Korteweg and de Vries derived their famous equation (referred to as the KdV equation now) for the propagation of unidirectional waves on the free surface of a shallow channel flow [19]. The KdV model provides a simple and approximate mathematical description of Russell's observation. By the mid-1960's, a renewed interest in studying solitary waves had become much more intense since they had been observed in many other fields, such as meteorology, elementary particle physics, plasma physics, and laser physics. A crucial discovery was made by two applied mathematicians, M. Kruskal and N. Zabusky, at Princeton University in 1965 [30]. By solving the KdV equation numerically, they demonstrated Fermi–Pasta–Ulum (FPU) recurrence. Meanwhile, they realized that nonlinear waves can interact strongly when they meet and then continue to move thereafter almost as if there had been no interaction at all. This led them to coin the name "soliton" to emphasize the particle-like character of these waves which seem to retain their identities in a collision. Intensive studies of solitons have fostered greater understanding of the physical world and helped to develop many powerful mathematical methods. A comprehensive bibliography about this interdisciplinary subject can be found in a recent book [1].

Particular interest in uniform soliton generation has recently stemmed from the remarkable numerical findings by Wu and Wu [47] and the pioneering experimental work by Huang, et al. [16]. The distinguished feature of their studies on free-surface waves of shallow water in a channel is that an external forcing was introduced by applying a steadily moving surface pressure. It was found that when the external forcing steadily moves at a velocity close to the critical speed $\sqrt{gH}$, where H is the

depth of undisturbed water and g is the gravitational acceleration, a succession of solitons of the same size can be generated periodically. Then the solitons advance ahead of the disturbance while there exists a region of depressed water just behind the disturbance and a train of dispersive waves propagate away from the disturbance in a direction opposite to that of the disturbance itself. This wave phenomenon does not occur in the absence of the external forcing. Since 1982, many mathematical models have been developed and applied to this intriguing problem. Among them are (i) the generalized Boussinesq equations by Wu and Wu [47]; (ii) the Green−Naghdi (G-N) models by Erterkin, et al. [10]; and (iii) the forced Korteweg−de Vries (fKdV) equation by Akylas [2], Mei [25], Wu [46] and Lee, et al. [21]. The most appealing model is perhaps the fKdV model because of its simple structure. In addition, Grimshaw and Smyth [15] investigated the same problem in a density-stratified fluid system. Katsis and Akylas [17] studied an analogue problem in three dimensional space by using the forced Kadomstev−Petviashvili equation. A detailed review related to the research of this topic can be found in the reference [21].

To give a brief summary of major published results, let us consider free-surface waves of a single-layer fluid flow over a bottom obstacle in a channel. The wave phenomena are classified by the upstream Froude number F. Here, the upstream Froude number F is defined as the ratio of the velocity U of the upstream flow to the shallow water wave speed $\sqrt{gH}$. It has been found that there exist two crucial values F_L (< 1) and F_C (> 1) such that the flow is classified into three categories: (i) supercritical régime, $F \geq F_C$, (ii) transcritical régime, $F \in (F_L,\ F_C)$, and (iii) subcritical régime, $F \leq F_L$. According to this classification, all possible wave phenomena are (i) multiple stationary solitary waves sustained on the site of the bump when $F > F_C$ and two branches of solitary waves merge into one at $F = F_C$

(Vanden-Broeck [43] and Shen [35]); (ii) run-away solitons (Wu & Wu [47], and others [2], [21]) when $F \in (F_L, F_C)$; (iii) only one stationary downstream cnoidal wave matched with the upstream flat region when $F < F_L$ (Forbes & Schwarz [13]) and the hydraulic fall occurs when $F = F_L$ (Sivakumaran et al. [41], Forbes [12], and Shen & Shen [39]).

However, many problems in the forced physical system are still unsolved. For example, the basic mechanism of soliton generation in a forced transcritical flow remains so far unexplained. The stability analysis of forced supercritical stationary solitary waves seems too difficult to apply for the general cases of arbitrary forcings although there is a remarkable progress on smooth sech^2-like solitary waves due to Camassa and Wu [7]–[8]. It is these interesting problems and intriguing phenomena which lead us to conduct this study.

Our main concern in this study is the stationary flow problem in the supercritical régime. Physical models include internal waves of two-layer fluid flows in a closed channel and free-surface waves of single-layer fluid flows in an open channel subject to the channel bottom obstacle. The sfKdV equation will be used as our mathematical model. Based on the sfKdV model, we study analytical properties of forced SSWS, discern the bifurcation of multiple SSWS, and investigate the instability and stability of forced SSWS. In addition, we attempt to test the validity of the sfKdV model by an experimental procedure.

The following results constitute the novel features of this dissertation:

(1) Proof of the positivity of SSWS to the sfKdV equation with a positive forcing;

(2) Ordered properties and extreme properties of the SSWS;

(3) Analytic expressions of the SSWS when the forcing is a rectangular bump or

dent, and two local forcings;

(4) Bifurcation analysis of multiple SSWS;

(5) Stability criterion of forced SSWS;

(6) Numerical simulations on the instability of the SSWS;

(7) Solitary waves and uniform flows on a shelf;

(8) Experimental validation of the sfKdV model for forced supercritical solitary waves and hydraulic falls.

Most analytical results such as the existence of the positive SSWS for the positive forcing and the nonexistence of three mutual ordered SSWS are motivated by numerical calculations. The ordered properties and extreme properties are useful in understanding the difference among multiple SSWS, envisaging the bifurcation behavior of the boundary value problem for the sfKdV equation, and determining the stability of an SSWS. These properties, some of which are sharp, are included in our recent paper [14].

Analytic solutions explicitly reveal the multiplicity of the solutions and make the complicated sfKdV bifurcation behavior more clear. Although the analytic solutions are constructed for a particular forcing, some of their properties which depend only on the area of the forcing (i.e. $\int_{-\infty}^{\infty} f(x)\ dx$) are applicable to the forcing of other shapes.

A criterion for the stability of SSWS is provided. This result is obtained employing the nonlinear stability analysis developed by Benjamin [5]. Numerical simulations based on a psuedo-spectral scheme are carried out to test the instability and stability of SSWS. Our numerical results show that only one of the multiple SSWS is

stable and all the others are unstable. Meanwhile, the numerical simulation reveals many remarkable features of forced long wave evolution in supercritical flows, which warrant further research.

For a shelf forcing, there exists an almost complete solitary wave sustained on the shelf while a tail of the solitary wave downstream connects smoothly to the upstream solitary wave [38]. This new finding, although not proved rigorously, can be justified intuitively. It is well known that there exists a stable solitary wave in each single-layer free-surface flow at a supercritical speed. A bottom obstruction, such as a shelf, only alters the shape of the solitary wave called the free solitary wave in the flat channel, but does not completely remove it. The altered solitary wave is considered to be a perturbation of the free solitary wave by the obstruction as explained by Vanden-Broeck [43].

A series of experiments with open channel water flows over a segment of a cylinder were conducted to confirm the validity of the sfKdV model for forced supercritical solitary waves and hydraulic falls. Our experimental results agree qualitatively with the results obtained from the sfKdV model. These results confirm the previous conclusion in Shen's paper [36]. Namely, the sfKdV equation is a parsimonious asymptotic model as long as the corresponding physics exists and the height of the bump is lower than the half of the upstream flow. Here, "parsimonious", meaning "simple" and "correct" in the sense of small error, is a word adopted from Ludwig's paper [22]. In addition, experimental uncertainties, which were not explicitly explained in the previous reports [12] and [41], will also be analyzed.

We have arranged the contents of this dissertation as follows. In Chapter 2, we present a detailed derivation of the fKdV equation for the motion of internal waves of two-layer fluid flows over topography in a closed channel. In the following

chapters, the sfKdV equation is used to explore the features of forced stationary solitary waves. Analytic properties of SSWS to the sfKdV equation are studied in Chapter 3. These properties include the existence of the positive SSWS, ordered and extreme properties of forced stationary solitary waves. In Chapter 4, we solve the sfKdV BVP analytically for (i) a nonlocal rectangular bump or dent, where "nonlocal" means that the support base of the forcing is much longer than the height of the forcing, and (ii) two local forcings, where "local" means that the forcing height is comparable with the forcing length. In Chapter 5, a nonlinear stability criterion of forced stationary solitary waves is proved, which provides a simple and sufficient condition. Numerical simulations on the instability and stability of the SSWS are illustrated by means of graphics obtained from our computations. In Chapter 6, solitary waves and uniform flows on a shelf are discussed. Experimental validation of the sfKdV model for forced supercritical stationary solitary waves and hydraulic falls are reported in Chapter 7. Finally, in Chapter 8, a brief summary of this dissertation and several remarks about future research in this area are given.

Chapter 2

Forced KdV Equation for Internal Waves in Two-layer Flows

It is important to investigate nonlinear long waves of near-critical stratified flows forced by external forcings since near-critical conditions are relatively common in meteorology and oceanography (see Baines [4] and Patoine & Warn [32]). Asymptotic analyses on this problem have been conducted by many people (Patoine & Warn [32], Grimshaw & Smyth [15], Melville & Helfrich [26], and Shen [36]).

In this chapter, an approximate mathematical model will be derived for the motion of internal waves in a two-layer fluid flow over topography. Our model is different from Melville and Helfrich's inhomogeneous extended KdV equation where the third-order nonlinearity is included. Here, we demonstrate that when the flow is near transcritical and the amplitude of the forcing is small compared to the depth of the lower layer fluid, the first order asymptotic approximation of the elevation of the interface between two fluids must satisfy a fKdV equation, which displays a balance of the quadratic nonlinearity, the dispersion of long internal wave modes

8

and the external forcing.

The procedure of our formulation is similar to that in Shen's paper [36].

2.1 Physical problem and basic equations

The two fluids under consideration are immiscible, inviscid and incompressible: a lower one of density ρ_- and upstream depth H_- and an upper, lighter one of density ρ_+ (i.e., $\rho_+ < \rho_-$) and upstream depth H_+. The two fluids are confined in a closed channel by a rigid top flat lid and a rigid uneven bottom wall. The flow is assumed to be two-dimensional and irrotational in both layers. The effects of surface tension are neglected.
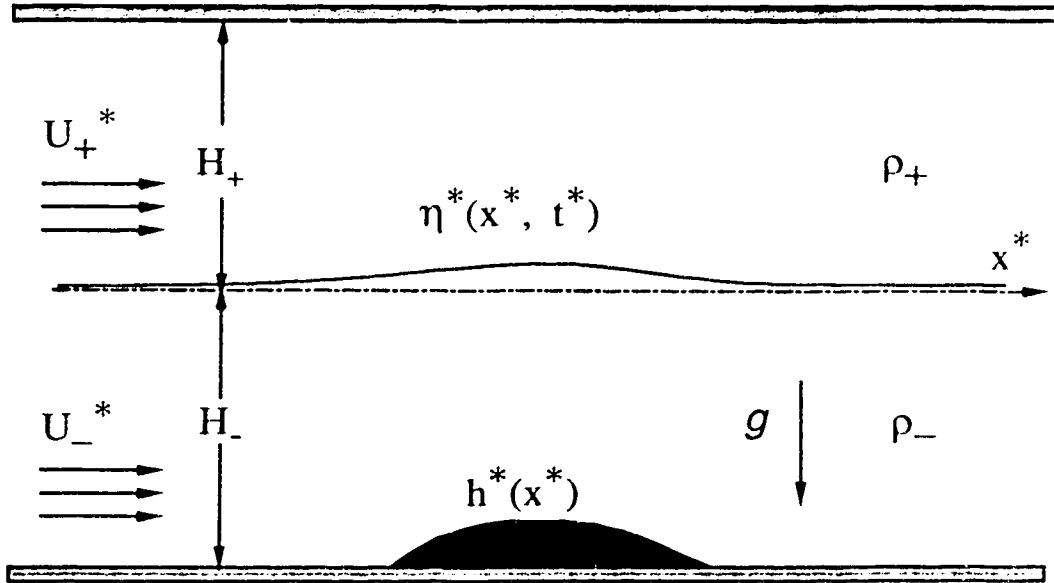
Figure 2.1: The sketch of a two-layer fluid flow over a bump.

The reference frame is fixed on the undisturbed interface (shown in Figure 2.1). Let the x^*-axis be aligned along the longitudinal direction, and the y^*-axis vertically opposite to the gravitational direction. The subscripts '$\pm$' signify the quantities of the upper and lower fluid layers, respectively. The flow potential functions are $\Phi^*_\pm(x^*, y^*, t^*)$. The upstream uniform velocities are $U^*_\pm$. The gravitational acceleration is g. The upper boundary, the interface and the lower boundary are $y^* = H_+$, $y^* = \eta^*(x^*, t^*)$, and $y^* = -H_- + h^*(x^*)$, respectively. By the conservation of mass and the irrotationality of the flow, the potential functions $\Phi^*_\pm$ satisfy Laplace equations in the domain of the fluids, that is,

$$\Phi^*_{\pm,x^*x^*} + \Phi^*_{\pm,y^*y^*} = 0, \tag{2.1}$$

subject to the following boundary conditions on the top lid at $y^* = H_+$

$$\Phi^*_{+,y^*} = 0, \quad \text{(kinematic B.C.)} \tag{2.2}$$

on the interface $y^* = \eta^*$

$$\Phi^*_{\pm,y^*} = \Phi^*_{\pm,x^*}\eta^*_{x^*} + \eta^*_{t^*}, \quad \text{(kinematic B.C.)} \tag{2.3}$$

$$\rho_+ \mathcal{B}\left[\Phi^*_+, \eta^*\right] = \rho_- \mathcal{B}\left[\Phi^*_-, \eta^*\right] \quad \text{(dynamic B.C.)} \tag{2.4}$$

where the differential operator $\mathcal{B}$ is defined as

$$\mathcal{B}\left[\Phi^*_\pm, \eta^*\right] = \Phi^*_{\pm,t^*} + \frac{1}{2}\left(\Phi^{*2}_{\pm,x^*} + \Phi^{*2}_{\pm,y^*} - U^{*2}_\pm\right) + g\eta^*,$$

and on the bottom $y^* = -H_- + h^*$

$$\Phi^*_{-,y^*} = h^*_{x^*}\Phi^*_{-,x^*}. \quad \text{(kinematic B.C.)} \tag{2.5}$$

In general, it is difficult to solve the nonlinear system of (2.1)–(2.5) due to the fact that the interface can not be prescribed. The objective of this chapter is to

reduce the above problem to a simple model. This model should be convenient for mathematical analysis and numerical computation, and it also give insights into major physical features. It is of our interest to investigate the propagation of long internal wave motion for the case when the flow is near critical and the amplitude of the forcing is small. We anticipate that main features will display a balance of the nonlinearity and the dispersion of long internal wave modes in response to the external forcing. Our formulation is based on suitable asymptotic expansions.

2.2 Linear dispersion relation

The linear dispersion relation of weakly nonlinear waves usually follows from the solvability condition of the first order expansion. Before proceeding to the formulation of this problem, we try to find out the linear dispersion relation in the absence of the forcing. Linearizing the system of (2.1)-(2.5), we obtain the following equations: for the upper and lower layers

$$\Phi^*_{\pm,x^*x^*} + \Phi^*_{\pm,y^*y^*} = 0, \tag{2.6}$$

on the top lid $y^* = H_+$

$$\Phi^*_{+,y^*} = 0, \tag{2.7}$$

on the interface $y^* = 0$

$$\Phi^*_{\pm,y^*} = \eta^*_{t^*}, \tag{2.8}$$

$$\rho_+ \left(\Phi^*_{+,t^*} + g\eta^*\right) = \rho_- \left(\Phi^*_{-,t^*} + g\eta^*\right), \tag{2.9}$$

on the bottom $y^* = -H_-$ is

$$\Phi^*_{-,y^*} = 0. \tag{2.10}$$

Suppose that a sinusoidal wave is taken as $\eta^* = a \exp\{i(kx^* - \omega t^*)\}$, k and ω being the wave number and the angular frequency, respectively. Then, the velocity potentials in both layers must be taken in the form

$$\Phi_\pm^* = (A_\pm\, e^{\pm k y^*} + B_\pm\, e^{\mp k y^*})\, e^{i(kx^*-\omega t^*)}. \tag{2.11}$$

The form (2.11) is chosen in order to satisfy (2.9). Equations (2.7), (2.8) and (2.10) give the constants $A_\pm$ and $B_\pm$ in terms of the given amplitude a:

$$A_\pm = \pm\frac{i\omega a\, e^{\mp k H_\pm}}{2k\,\sinh k H_\pm}, \tag{2.12}$$

$$B_\pm = \pm\frac{i\omega a\, e^{\pm k H_\pm}}{2k\,\sinh k H_\pm}. \tag{2.13}$$

Substituting (2.12)–(2.13) into (2.9) results in

$$\omega^2(\rho_+\,\coth k H_+ + \rho_-\,\coth k H_-) = gk(\rho_- - \rho_{-+}). \tag{2.14}$$

Under the assumption of the long wave approximation, i.e. $k H_\pm \ll 1$, we have

$$\coth k H_\pm \simeq 1/(k H_\pm),$$

and the dispersion relation between k and ω becomes

$$(\rho_- H_+ + \rho_+ H_-)\omega^2 + (\rho_+ - \rho_-)g H_+ H_- k^2 = 0.$$

Hence, the phase velocity of long linear internal oscillatory waves can be written as

$$c^{*2} \equiv \frac{\omega^2}{k^2} = \frac{\rho_- H_+ - \rho_+ H_+}{\rho_- H_+ + \rho_+ H_-} g H_-, \tag{2.15}$$

which, according to Lamb's book "Hydrodynamics" ([20] pp. 370), was first investigated by Stokes. This is similar to the critical velocity of free-surface waves in

shallow water of depth H_-. It is shown by the above equation that internal waves, in general, propagate slower than free-surface waves since

$$\frac{\rho_- H_+ - \rho_+ H_+}{\rho_- H_+ + \rho_+ H_-} \leq 1.$$

Also, we remark that this phase velocity (2.15) is expected to be the critical velocity of nonlinear long internal wave modes which will be discussed in §2.5.

2.3 Nondimensionalization

To carry out the procedure of asymptotic expansion, (2.1)–(2.5) need to be nondimensionalized. Let L (the typical wavelength) and H_- be the horizontal and vertical length scales, respectively. The following dimensionless variables are introduced

$$\varepsilon = (H_-/L)^2 \ll 1, \quad \eta = \eta^*/H_- \quad \text{(long wave assumption)},$$

$$\sigma = H_+/H_-, \quad \rho = \rho_+/\rho_-, \quad \gamma = U_+^*/U_-^*,$$

$$U_\pm = U_\pm^*/\sqrt{gH_-}, \quad \Phi_\pm = \varepsilon^{\frac{1}{2}}\Phi_\pm^*/\sqrt{gH_-^3},$$

$$(x,y) = (\varepsilon^{\frac{1}{2}}x^*, y^*)/H_-, \quad t = \varepsilon\sqrt{gH_-}\,t^*/L,$$

$$h = \varepsilon^{-2}h^*/H_- \quad \text{(small bottom obstacle assumption)}.$$

In terms of the dimensionless variables, the upper boundary, the interface, and the lower boundary are $y = \sigma$, $y = \eta$ and $y = -1 + \varepsilon^2 h$, respectively.

Let $\phi_\pm(x,y,t)$ denote the perturbations of the flow potentials about the upstream uniform flows. Then the flow potentials $\Phi_\pm(x,y,t)$ take the forms

$$\Phi_\pm(x,y,t) = U_\pm\, x + \phi_\pm(x,y,t). \tag{2.16}$$

Using the dimensionless variables and (2.16), (2.1)–(2.5) can be written as follows:

$$\varepsilon\phi_{+,xx} + \phi_{+,yy} = 0, \qquad \text{when} \quad \eta < y < \sigma, \tag{2.17}$$

$$\varepsilon\phi_{-,xx} + \phi_{-,yy} = 0, \qquad \text{when} \quad -1 + \varepsilon^2 h < y < \eta, \tag{2.18}$$

$$\phi_{+,y} = 0, \qquad \text{on} \quad y = \sigma, \tag{2.19}$$

$$\phi_{\pm,y} = \varepsilon(U_{\pm} + \phi_{\pm,x})\eta_x + \varepsilon^2\eta_t, \qquad \text{on} \quad y = \eta, \tag{2.20}$$

$$\rho\mathcal{B}_\varepsilon[\phi_+, \eta] = \mathcal{B}_\varepsilon[\phi_-, \eta], \qquad \text{on} \quad y = \eta, \tag{2.21}$$

$$\phi_{-,y} = \varepsilon^3(U_- + \phi_{-,x})h_x, \qquad \text{on} \quad y = -1 + \varepsilon^2 h. \tag{2.22}$$

In the formula (2.21), the differential operator $\mathcal{B}_\varepsilon$ is defined as

$$\mathcal{B}_\varepsilon[\phi_{\pm}, \eta] = \varepsilon\phi_{\pm,t} + \frac{1}{2}\left(\phi_{\pm,x}^2 + \varepsilon^{-1}\phi_{\pm,y}^2\right) + U_{\pm}\phi_{\pm,x} + \eta.$$

2.4 Asymptotic expansions

Now let us proceed with asymptotic expansions in the strips $S_- = \{(x,y) \in \mathcal{R} \mid -1 \leq y \leq 0\}$ and $S_+ = \{(x,y) \in \mathcal{R} \mid 0 \leq y \leq \sigma\}$. Hence, it is required to approximate the boundary conditions on the interface and the bottom so that the boundary conditions are approximately prescribed on $y = 0$ and $y = -1$, respectively. Taking the first order approximation of Taylor expansions of (2.20)–(2.21) about $y = 0$ and (2.22) about $y = -1$, we can get

$$\phi_{\pm,y} + \eta\phi_{\pm,yy} = \varepsilon^2\eta_t + \varepsilon\eta_x(U_{\pm} + \phi_{\pm,x} + \eta\phi_{\pm,xy}) \qquad \text{on} \quad y = 0, \tag{2.23}$$

$$\rho\mathcal{L}_\varepsilon[\phi_+, \eta] = \mathcal{L}_\varepsilon[\phi_-, \eta] \qquad \text{on} \quad y = 0, \tag{2.24}$$

$$\phi_{-,y} + \varepsilon^2 h\phi_{-,yy} = \varepsilon^3(U_- + \phi_{-,x})h_x \qquad \text{on} \qquad y = -1. \tag{2.25}$$

In the formula (2.24), the differential operator $\mathcal{L}_\epsilon$ is defined as

$$\mathcal{L}_\epsilon \left[\phi_\pm, \eta\right] = \epsilon(\phi_{\pm,t} + \eta\phi_{\pm,yt}) + U_\pm(\phi_{\pm,x} + \eta\phi_{\pm,xy}) + \eta$$
$$+ \frac{1}{2}\left[(\phi_{\pm,x} + \eta\phi_{\pm,xy})^2 + \epsilon^{-1}(\phi_{\pm,y} + \eta\phi_{\pm,yy})^2\right]. \tag{2.26}$$

Therefore, with this approximation, all of the above equations are confined in the two strips S_- and S_+.

The response of the interface to the order ϵ^2 forcing is assumed to be of order ϵ which implies that the internal wave is a dispersive wave with the second-order nonlinearity. Hence, the asymptotic expansions for $(\phi_\pm, \eta)$ are taken as follows

$$\phi_\pm = \epsilon\phi_\pm^{(1)}(x,y) + \epsilon^2\phi_\pm^{(2)}(x,y) + O(\epsilon^3), \tag{2.27}$$

$$\eta = \epsilon\eta^{(1)}(x) + \epsilon^2\eta^{(2)}(x) + O(\epsilon^3). \tag{2.28}$$

Also, it is our intention to investigate the displacement of the interface for near-critical flows in both layers. The precise meaning of near-critical velocity is that the upstream uniform velocities $U_\pm$ take the form

$$U_\pm = U^{(0)}{}_\pm + \epsilon\lambda_\pm. \tag{2.29}$$

Here, $U^{(0)}{}_\pm$ are the critical velocities which will be determined by the solvability condition of the second-order perturbation problem derived in the next section. The quantities $\lambda_\pm$ are constants which signify the perturbations of the upstream uniform velocities about the corresponding critical velocities. When $\lambda_+ > 0$ (< 0), the upper layer flow is said to be supercritical (subcritical). A similar definition applies to the lower layer flow.

2.5 Forced KdV equation

Substituting the above asymptotic expansions (2.27)–(2.29) into the approximate governing equations (2.17)–(2.19) and (2.23)–(2.25) in the strips S_- and S_+ yields the first three order problems according to the powers of ϵ.

The first-order problem: In the upper layer S_+ and the lower layer S_-

$$\phi_{\pm,yy}^{(1)} = 0, \tag{2.30}$$

on $y = \sigma$

$$\phi_{+,y}^{(1)} = 0, \tag{2.31}$$

on $y = 0$

$$\phi_{\pm,y}^{(1)} = 0, \tag{2.32}$$

$$\rho\left(\frac{1}{2}\phi_{+,y}^{(1)\,2} + U_+^{(0)}\phi_{+,x}^{(1)} + \eta^{(1)}\right) = \frac{1}{2}\phi_{-,y}^{(1)\,2} + U_-^{(0)}\phi_{-,x}^{(1)} + \eta^{(1)}, \tag{2.33}$$

and on $y = -1$

$$\phi_{-,y}^{(1)} = 0. \tag{2.34}$$

It is easy to show from (2.30)–(2.32) and (2.34) that $\phi_{\pm,y}^{(1)}(x,y,t) = 0$ everywhere. Hence, $\phi_\pm^{(1)}(x,y,t)$ are independent of y and (2.33) is reduced to

$$\rho(U_+^{(0)}\phi_{+,x}^{(1)} + \eta^{(1)}) = U_-^{(0)}\phi_{-,x}^{(1)} + \eta^{(1)}. \tag{2.35}$$

The quantities $U_\pm^{(0)}$ are the critical velocities of the upstream uniform flows that will be determined by the solvability condition for the second-order problem. The first-order approximation of the interface elevation $\eta^{(1)}$ will be determined by the solvability condition of the third-order problem.

The second-order problem: In the upper layer S_+ and the lower layer S_-

$$\phi_{\pm,xx}^{(1)} + \phi_{\pm,yy}^{(2)} = 0, \tag{2.36}$$

on $y = \sigma$

$$\phi_{+,y}^{(2)} = 0, \qquad (2.37)$$

on $y = 0$

$$\phi_{\pm,y}^{(2)} = U_{\pm}^{(0)}\eta_x^{(1)}, \qquad (2.38)$$

$$\rho\left[\phi_{+,t}^{(1)} + \frac{1}{2}\phi_{+,x}^{(1)}{}^2 + U_+^{(0)}\phi_{+,x}^{(2)} + \lambda_+\phi_{+,x}^{(1)} + \eta^{(2)}\right] =$$
$$\phi_{-,t}^{(1)} + \frac{1}{2}\phi_{-,x}^{(1)}{}^2 + U_-^{(0)}\phi_{-,x}^{(2)} + \lambda_-\phi_{-,x}^{(1)} + \eta^{(2)}, \qquad (2.39)$$

and on $y = -1$

$$\phi_{-,y}^{(2)} = 0. \qquad (2.40)$$

From (2.36)–(2.40), one can derive that

$$\phi_{+,y}^{(2)} = (\sigma - y)\phi_{+,xx}^{(1)}, \qquad (2.41)$$

$$\phi_{-,y}^{(2)} = -(1 + y)\phi_{-,xx}^{(1)}, \qquad (2.42)$$

$$\phi_{+,xx}^{(1)} = \frac{U_+^{(0)}}{\sigma}\eta_x^{(1)}, \qquad (2.43)$$

$$\phi_{-,xx}^{(1)} = -U_-^{(0)}\eta_x^{(1)}. \qquad (2.44)$$

These equations further lead to

$$\phi_{+,x}^{(1)} = \frac{U_+^{(0)}}{\sigma}\eta^{(1)}, \qquad (2.45)$$

$$\phi^{(1)}{}_{-,x} = -U_-^{(0)}\eta^{(1)}. \qquad (2.46)$$

Substituting (2.45)–(2.46) into (2.35) results in

$$\rho\left(\frac{U_+^{(0)2}}{\sigma} + 1\right)\eta^{(1)} = \left(-U_-^{(0)2} + 1\right)\eta^{(1)}. \qquad (2.47)$$

For a nontrivial solution, $\eta^{(1)}$ is not identically equal to zero. Therefore, the solvability condition of the second-order problem is

$$\rho\left(\frac{U_+^{(0)^2}}{\sigma}+1\right) = -U_-^{(0)^2}+1. \qquad (2.48)$$

This is the dispersion relation which determines the critical velocities $U_\pm^{(0)}$. If γ denotes the ratio of the upstream uniform velocity of the upper layer to that of the lower layer, i.e. $\gamma = U_+^*/U_-^*$, we have $U_+^{(0)} = \gamma U_-^{(0)}$ and $\lambda_+ = \gamma\lambda_-$. Therefore, the critical velocities $U_\pm^{(0)}$ can be determined by

$$U_-^{(0)^2} = \frac{\sigma(1-\rho)}{\sigma+\gamma^2\rho} \quad \text{and} \quad U_+^{(0)} = \gamma U_-^{(0)} \qquad (2.49)$$

in terms of ρ,σ, and γ. When $\gamma = 1$, the first equation in (2.49) coincides with (2.15) which is the phase velocity of linear long internal wave modes in the absent of the external forcing.

It is worth noting that, by differentiating with respect to x, (2.39) can be rewritten in the form

$$\rho\left[\phi_{+,xt}^{(1)} + \phi_{+,x}^{(1)}\phi_{+,xx}^{(1)} + U_+^{(0)}\phi_{+,xx}^{(2)} + \lambda_+\phi_{+,xx}^{(1)} + \eta_x^{(2)}\right] =$$
$$\phi_{-,xt}^{(1)} + \phi_{-,x}^{(1)}\phi_{-,xx}^{(1)} + U_-^{(0)}\phi_{-,xx}^{(2)} + \lambda_-\phi_{-,xx}^{(1)} + \eta_x^{(2)}. \qquad (2.50)$$

Substituting (2.45)-(2.46) into (2.50) yields

$$\rho\left[\frac{U_+^{(0)}}{\sigma}\eta_t^{(1)} + \left(\frac{U_+^{(0)}}{\sigma}\right)^2\eta^{(1)}\eta_x^{(1)} + U_+^{(0)}\phi_{+,xx}^{(2)} + \lambda_+\frac{U_+^{(0)}}{\sigma}\eta_x^{(1)} + \eta_x^{(2)}\right] =$$
$$-U_-^{(0)}\eta_t^{(1)} + U_-^{(0)^2}\eta^{(1)}\eta_x^{(1)} + U_-^{(0)}\phi_{-,xx}^{(2)} - \lambda_-U_-^{(0)}\eta^{(1)} + \eta_x^{(2)}. \qquad (2.51)$$

It is easy to see from (2.51) that the first-order approximation of the interface elevation $\eta^{(1)}$ can be determined if the terms related to $\phi_\pm^{(2)}$ and $\eta^{(2)}$ are eliminated.

In fact, we are able to achieve this by considering the third-order problem and using (2.41)–(2.42) and the dispersion relation (2.48).

The procedure is carried out as follows. Integrating equations (2.41) and (2.42) with respect to y, one can derive that

$$\phi_+^{(2)} = \phi_+^{(2)}\big|_{y=0} + \frac{y(2\sigma - y)}{2}\phi_{+,xx}^{(1)}, \tag{2.52}$$

$$\phi_-^{(2)} = \phi_-^{(2)}\big|_{y=0} - \frac{y(2+y)}{2}\phi_{+,xx}^{(1)}. \tag{2.53}$$

Then, taking twice differentiation of the above two equations with respect to x, we have

$$\phi_{+,xx}^{(2)} = \phi_{+,xx}^{(2)}\big|_{y=0} + \frac{y(2\sigma - y)}{2}\phi_{+,xxxx}^{(1)}, \tag{2.54}$$

$$\phi_{-,xx}^{(2)} = \phi_{-,xx}^{(2)}\big|_{y=0} - \frac{y(2+y)}{2}\phi_{-,xxxx}^{(1)}. \tag{2.55}$$

Further, in order to eliminate $\phi_{\pm,xx}^{(2)}$ and $\eta_x^{(2)}$, we need to consider the following third-order problem.

The third-order problem: In the upper layer S_+ and the lower layer S_-

$$\phi_{\pm,xx}^{(2)} + \phi_{\pm,yy}^{(3)} = 0, \tag{2.56}$$

on $y = \sigma$

$$\phi_{+,y}^{(3)} = 0, \tag{2.57}$$

on $y = 0$

$$\phi_{\pm,y}^{(3)} + \phi_{\pm,yy}^{(2)}\eta^{(1)} = \eta_t^{(1)} + (\lambda_\pm + \phi_{\pm,x}^{(1)})\eta_x^{(1)} + U_\pm^{(0)}\eta_x^{(2)}, \tag{2.58}$$

and on $y = -1$

$$\phi_{-,y}^{(3)} = U_-^{(0)}h_x. \tag{2.59}$$

Using the boundary conditions (2.57)–(2.59), integrating equations (2.54) and (2.55) in $[0,\sigma]$ and $[-1,0]$ with respect to y results in the following:

$$\phi^{(2)}_{+,xx}\,|_{y=0} \;=\; -\frac{\sigma^2}{3}\phi^{(1)}_{+,xxxx}$$

$$+\frac{1}{\sigma}\left[\eta^{(1)}_t + \left(\lambda_+ + \phi^{(1)}_{+,x}\right)\eta^{(1)}_x + U^{(0)}_+\eta^{(2)}_x + \phi^{(1)}_{+,xx}\eta^{(1)}\right], \quad (2.60)$$

$$\phi^{(2)}_{-,xx}\,|_{y=0} \;=\; -\frac{1}{3}\phi^{(1)}_{-,xxxx} - \eta^{(1)}_t$$

$$+U^{(0)}_-(h_x - \eta^{(2)}_x) - \left(\lambda_- + \phi^{(1)}_{-,x}\right)\eta^{(1)}_x - \phi^{(1)}_{-,xx}\eta^{(1)}. \quad (2.61)$$

Then, substituting (2.60)–(2.61) into (2.51) and using equations (2.45)–(2.46), we can obtain a fKdV equation for the first-order approximation of the interface elevation

$$m_1\eta^{(1)}_t + m_2\eta^{(1)}_x + m_3\eta^{(1)}\eta^{(1)}_x + m_4\eta^{(1)}_{xxx} = f_x, \quad (2.62)$$

where the coefficients m_k ($k = 1,2,3,4$) and the forcing term f are given by

$$m_1 = 2\left(\frac{\rho}{\sigma}U^{(0)}_+ + U^{(0)}_-\right), \quad (2.63)$$

$$m_2 = 2\left(\frac{\rho}{\sigma}\lambda_+ U^{(0)}_+ + \lambda_- U^{(0)}_-\right), \quad (2.64)$$

$$m_3 = 3\left(\frac{\rho}{\sigma^2}U^{(0)^2}_+ - U^{(0)^2}_-\right), \quad (2.65)$$

$$m_4 = -\frac{1}{3}\left(\sigma\rho U^{(0)^2}_+ + U^{(0)^2}_-\right), \quad (2.66)$$

$$f = U^{(0)^2}_- h. \quad (2.67)$$

Here, we have also used the dispersion relation (2.48) to eliminate $\eta^{(2)}_x$.

For a single-layer open channel flow, $H_+ = 0$, $\rho = 0$, and $U^{(0)}_+ = 0$. Then, $U^{(0)}_- = 1$ from (2.47), and in (2.63)–(2.67), $m_1 = 2$, $m_2 = 2\lambda_-$, $m_3 = -3$, $m_4 = -\frac{1}{3}$, $m_5 = h$. Equation (2.62) in this case coincides with the fKdV equation for a rectangular channel derived by Shen [34]. This may be considered as a verification of the correctness of the coefficients (2.63)–(2.67).

The fKdV equation has been discussed extensively over the last decade since Patoine and Warn [32] derived a similar equation for Rossby waves forced by topography. This simple model has been successfully used for describing the generation of advancing upstream solitons by Akylas [2], Lee, et al. [21], and showing the existence of hydraulic falls and multiple stationary forced solitary waves by Shen [36]. All of these results confirmed the innovative discoveries by Wu and Wu [47], Forbes and Schwartz [13], Vanden-Broek [43] and Forbes [12]. But, the research in this area is far from the end. An analytic method of solving an initial value problem of the fKdV equation still needs to be developed although Fokas and Ablowitz made a first try five years ago [11]. The bifurcation behavior of multiple stationary forced solitary waves is, in general, very complicated. The mathematical analysis on the stability of forced solitary waves hardly achieves much for the general case of forcings owing to the complicated structure of the wave profiles. In this dissertation, we will primarily study the time-independent fKdV model, and in particular, examine the bifurcation behavior of multiple forced stationary solitary waves, the stability of forced stationary solitary waves, and the validation of the sfKdV model.

Chapter 3

Analysis on the Supercritical Stationary Forced KdV Equation

When the flow is steady, the fKdV equation (2.62) is reduced to a nonlinear third order ordinary differential equation:

$$\lambda \eta_x + 2\alpha \eta \eta_x + \beta \eta_{xxx} = f_x, \tag{3.1}$$

where $\lambda = m_2$, $\alpha = m_3/2$, $\beta = m_4$ are constants, and $\eta = \eta^{(1)}$. The equation (3.1) is referred to as the stationary forced Korteweg–de Vries (sfKdV) equation.

The fKdV equation has been derived from single-layer flows and density-stratified flows by many authors. For convenience to explain the physical meaning of our mathematical analysis, we regard $\eta(x)$ in (3.1) as the first order approximation of the free-surface elevation of a single-layer flow and λ specifies the upstream velocity of the flow. The upstream flow is supercritical (subcritical) if $\lambda > 0$ ($\lambda < 0$). The constants α and β are determined by the geometric shape of the cross section of the channel and the function $f(x)$ represents the external forcing, such as a bottom bump in the channel.

22

Further, we assume that $\lambda > 0$, $\alpha < 0$, $\beta < 0$, and the forcing function $f(x) \in$ $C_0(\Re)$. Here, $C_0(\Re)$ is defined as a set of functions which are continuous and have a compact support in $\Re$. It is interesting to study analytical properties of solutions to the sfKdV equation (3.1) with the boundary conditions

$$\eta(\pm\infty) = \eta_x(\pm\infty) = \eta_{xx}(\pm\infty) = 0. \tag{3.2}$$

Integrating (3.1) once over $(-\infty, x)$ and using the boundary condition (3.2) results in

$$\lambda\eta + \alpha\eta^2 + \beta\eta_{xx} = f. \tag{3.3}$$

A function $\eta(x) \in C^2(\Re)$ which satisfies (3.3) and the boundary condition (3.2) is referred to as a supercritical solitary wave solution (SSWS) to the sfKdV equation since the wave profile represented by $\eta(x)$ resembles a single solitary wave. This wave is stationary and different from the regular KdV solitary wave which is a traveling wave.

We will present (i) a complete proof of the existence of supercritical positive solitary wave solutions (SPSWS) for the positive forcing in §3.1, (ii) two ordered properties of SSWS in §3.2, and (iii) some extreme properties of SSWS in §3.3.

3.1   Supercritical positive solitary wave solutions

Consider the following sfKdV BVP

$$\lambda\eta + \alpha\eta^2 + \beta\eta_{xx} = f, \qquad -\infty < x < +\infty, \tag{3.4}$$

$$\eta(\pm\infty) = \eta_x(\pm\infty) = 0, \tag{3.5}$$

where $\lambda > 0$, $\alpha < 0$, $\beta < 0$ and $f(x) \in C_0(\Re)$.

Shen proved that the sfKdV BVP (3.4)-(3.5) has at least one SSWS if λ is sufficiently large [34]. Many results from numerical calculations suggest that every solution is positive for the positive forcing $f(x) \geq 0$. Here, we prove this general statement.

Theorem 1 (Positivity Property) *Suppose that $\eta(x)$ is an SSWS of the sfKdV BVP (3.4)-(3.5) and $f(x) \geq 0$, then $\eta(x) > 0$ for any $x \in \Re$, i.e. $\eta(x)$ is an SPSWS.*

Proof: If $\eta(x)$ is an SSWS of the sfKdV BVP (3.4)-(3.5) with the positive forcing $f(x) \geq 0$, then we have

$$\eta(x) = \frac{1}{\beta} \int_{-\infty}^{+\infty} K(x,\xi) \left(\alpha \eta^2(\xi) - f(\xi) \right) d\xi, \tag{3.6}$$

where $K(x,\xi) = \frac{1}{2\nu} \exp(-\nu|\xi - x|)$ is the Green's function satisfying

$$\begin{cases} K_{\xi\xi} - \nu^2 K = -\delta(\xi - x), \\ K(\xi = \pm\infty, x) = 0, \quad \nu = \sqrt{-\lambda/\beta}. \end{cases} \tag{3.7}$$

Clearly, $\eta(x) \geq 0$ holds for any $x \in \Re$ since $\alpha < 0$, $\beta < 0$, $K(x,\xi) \geq 0$ and $f(\xi) \geq 0$ for any $\xi \in \Re$.

Now, suppose that there exists a point $a \in \Re$ such that $\eta(a) = 0$. From (3.6),

$$\eta(a) = \frac{1}{\beta} \int_{-\infty}^{+\infty} K(a,\xi) \left(\alpha \eta^2(\xi) - f(\xi) \right) d\xi = 0.$$

Since $K(a,\xi) > 0$ and $\alpha \eta^2(\xi) - f(\xi) \leq 0$ we have $\alpha \eta^2(\xi) = f(\xi)$ for any $\xi \in \Re$. This is a contradiction since $f(\xi_1) > 0$ for some $\xi_1 \in \Re$ whereas $\alpha \eta^2(\xi_1)$ is always less or equal to zero. Hence, $\eta(x) > 0$ for any $x \in \Re$.

3.2   Ordered properties

After resolving the existence question of SPSWS to the sfKdV equation with $f(x) \in C_0(\Re)$, we discuss various properties of SSWS to the sfKdV equation. For multiple solutions, it is interesting to investigate the relative position of the solutions. When we say that two solutions $\eta_1(x)$ and $\eta_2(x)$ of the sfKdV BVP (3.4)-(3.5) are ordered, we mean that $\eta_1(x) \neq \eta_2(x)$ for any $x \in \Re$. Numerous numerical solutions we obtained seem to suggest that if there exists a third solution of the sfKdV BVP (3.4)-(3.5), then it can not be ordered with respect to the other two already ordered solutions. Indeed, this is generally true. We have found that the solutions of the sfKdV BVP (3.4)-(3.5) have the following ordered properties.

Theorem 2 (Ordered Property I) *The* sfKdV BVP (3.4)-(3.5) *admits at most two ordered* SPSWS;

Proof: If the theorem were not true, the sfKdV BVP (3.4)-(3.5) would admit at least three ordered SPSWS. Assume that η_i ($i = 1, 2, 3$) are three ordered solutions and, without loss of generality, $0 < \eta_1 < \eta_2 < \eta_3$. Let $w_1 = \eta_2 - \eta_1$, and $w_2 = \eta_3 - \eta_2$. From (3.4), it follows that

$$\beta w_{1,xx} = [-\lambda - \alpha(\eta_1 + \eta_2)]w_1, \tag{3.8}$$

$$\beta w_{2,xx} = [-\lambda - \alpha(\eta_2 + \eta_3)]w_2. \tag{3.9}$$

Multiplying (3.8) by w_2 and (3.9) by $-w_1$, adding the two resulting equations together and integrating the sum from $-\infty$ to ∞, we have

$$\int_{-\infty}^{\infty} (w_1 + w_2)w_1 w_2 \, dx = 0.$$

Clearly, w_1 and w_2 are positive for any $x \in \Re$. This is a contradiction and the proof of the theorem is finished.

Hence, if there exists a third SPSWS of the sfKdV BVP (3.4)-(3.5), then it cannot be ordered with the other two.

Next, let us show a condition for two SPSWS being ordered. This condition is simple to apply if the SPSWS profiles are known.

Theorem 3 (Ordered Property II) *If two distinct solutions $\eta_1(x)$ and $\eta_2(x)$ of the sfKdV BVP (3.4)-(3.5) satisfy $\| \eta_1 \|_\infty > \| \eta_2 \|_\infty$ and $\| \eta_2 \|_\infty \leq -\frac{\lambda}{2\alpha}$, then $\eta_1(x) > \eta_2(x)$ for each $x \in \Re$.*

Proof: The second ordered property is based on the following two facts. First, under the assumptions of **Theorem 3**, $\eta_1(x) \geq \eta_2(x)$ for any $x \in \Re$. If this were not true, there would exist $x_0 \in \Re$ such that $\eta_1(x_0) < \eta_2(x_0)$. Let $w(x) = \eta_1(x) - \eta_2(x)$. Then, putting $\eta_1(x) = w(x) + \eta_2(x)$ into (3.4), one gets

$$(\lambda + 2\alpha\eta_2(x))\, w(x) + \alpha w^2(x) + \beta w_{xx}(x) = 0, \qquad x \in \Re. \tag{3.10}$$

On the other hand, the function $w(x)$ has at least a local minimum point a such that $w(a) < 0$ and $w_{xx}(a) \geq 0$ since $w(x_0) < 0$ and $w(\pm\infty) = 0$. Also, by the above assumption $\lambda + 2\alpha\eta_2(a) \geq 0$, we have

$$(\lambda + 2\alpha\eta_2(a))\, w(a) + \alpha w^2(a) + \beta w_{xx}(a) < 0.$$

This contradicts (3.10). Hence, $\eta_1(x) \geq \eta_2(x)$ for all $x \in \Re$.

Now, according to the theory of ordinary differential equations, the following IVP:

$$(\lambda + 2\alpha\eta_2(x))\, w(x) + \alpha w^2(x) + \beta w_{xx}(x) = 0, \qquad x \in \Re, \tag{3.11}$$

$$w(x_0) = w_x(x_0) = 0, \qquad\qquad x_0 \in \Re, \tag{3.12}$$

has only a trivial solution when $\eta_2(x)$ is a given bounded function. In fact, the IVP (3.11)-(3.12) can be viewed as a system of first order differential equations:

$$\frac{dw}{dx} = v, \tag{3.13}$$

$$\frac{dv}{dx} = -\frac{1}{\beta}\left[(\lambda + 2\alpha\eta_2)w + \alpha w^2\right] \tag{3.14}$$

with initial value conditions: $w(x_0) = 0$ and $v(x_0) = 0$.

Since the right hand side of (3.13)-(3.14) is obviously in C^1 and hence satisfies Lipschitz condition, the IVP (3.13)-(3.14) has only a trivial solution, that is $w(x) = 0$, for all $x \in \Re$.

Now, let us return to the proof of **Theorem 3**. Suppose that the conclusion fails to hold. There must exist $x_0 \in \Re$ such that $\eta_1(x_0) = \eta_2(x_0)$, i.e. $w(x_0) = 0$. By the first fact, x_0 is a minimum point of $w(x)$, hence, $w_x(x_0) = 0$. Then, by the second fact, $\eta_1(x) = \eta_2(x)$ for all $x \in \Re$. This is a contradiction to the assumption and completes our proof.

3.3 Extreme properties

It is clear that every solution to the sfKdV BVP (3.4)-(3.5) is bounded for the forcing $f(x) \in C_0(\Re)$. The extreme properties is very useful in determining the stability of an SSWS, which will be discussed in Chapter 5. Regarding a general forcing, we first show that the crest of supercritical solitary waves is either higher than a certain point or lower than another point.

Theorem 4 (Extreme Property I) *If $\eta(x)$ is a solution of the sfKdV BVP (3.4)- (3.5) and $f(x) \in C_0^1(\Re)$, then either*

$$\| \eta \|_\infty \leq \frac{\sqrt{\lambda^2 + 4\alpha \| f \|_\infty} - \lambda}{2\alpha} \quad or \quad \| \eta \|_\infty \geq -\frac{\sqrt{\lambda^2 + 4\alpha \| f \|_\infty} + \lambda}{2\alpha} \tag{3.15}$$

where $\| f \|_\infty = \max\{|f(x)|, x \in \Re\}$.

Proof: By (3.6), one can get

$$|\eta(x)| \le \frac{1}{|\beta|}(|\alpha| \| \eta \|_\infty^2 + \| f \|_\infty) \int_{-\infty}^{+\infty} K(x,\xi)d\xi.$$

Direct calculation of the above integral yields

$$\int_{-\infty}^{+\infty} K(x,\xi)d\xi = |\beta|/\lambda.$$

Thus

$$|\alpha| \| \eta \|_\infty^2 - \lambda \| \eta \|_\infty + \| f \|_\infty \ge 0,$$

which is equivalent to (3.15).

However, for a negative forcing, we can prove the crest of supercritical positive solitary waves must be higher than a certain point. This is included in the following theorem whose conclusion is stronger than (3.15).

Theorem 5 (Extreme Property II) *If* $\eta(x)$ *is an* SPSWS *of the* sfKdV BVP (3.4)–(3.5) *and* $f(x) \le 0$, *then* $\| \eta \|_\infty \ge -\lambda/\alpha$.

Proof: By the continuity of $\eta(x)$, there exists $x_0 \in \Re$ such that $\eta(x_0) = \| \eta \|_\infty$, $\eta'(x_0) = 0$, and $\eta_{xx}(x_0) \le 0$. Since $f(x) \le 0$, from (3.4), we have

$$\lambda\eta(x_0) + \alpha\eta^2(x_0) = f(x_0) - \beta\eta_{xx}(x_0) \le 0.$$

The condition $\eta(x_0) > 0$ implies that $\lambda + \alpha\eta(x_0) \le 0$. Therefore, $\| \eta \|_\infty = \eta(x_0) \ge -\lambda/\alpha$.

For forced supercritical solitary waves, there might exist both the crest and the trough. The following theorem specifies the trough of the wave profile must always be lower than a certain height.

Theorem 6 (Extreme Property III) *If $\eta(x)$ is an SPSWS of the sfKdV BVP (3.4)-(3.5) and $f(x) \geq 0$ and x_0 is a local minimum point of $\eta(x)$ in $\Re$, then $\eta(x_0) \leq -\lambda/\alpha$.*

Proof: Since x_0 is a local minimum point of $\eta(x)$, then $\eta_x(x_0) = 0$, and $\eta_{xx}(x_0) \geq 0$. By (3.4), the condition $f(x) \geq 0$ implies

$$\lambda\eta(x_0) + \alpha\eta^2(x_0) = f(x_0) - \beta\eta_{xx}(x_0) \geq 0.$$

Hence, from $\eta(x_0) > 0$, we have $\lambda + \alpha\eta(x_0) \geq 0$, i.e. $\eta(x_0) \leq -\lambda/\alpha$.

The following property concerns the numbers of crests and troughs of supercritical solitary waves.

Theorem 7 (Extreme Property IV) *If $\eta(x)$ is an SPSWS of the sfKdV BVP (3.4)-(3.5), and if $\eta(x) \geq -\lambda/\alpha$ and $f(x) \geq 0$ for all $x \in$ supp(f), then $\eta(x)$ has at most one local extreme point in supp(f).*

Proof: Suppose that $\eta(x)$ has two local extreme points a and b with $a < b$ in supp(f), then $\eta_x(a) = \eta_x(b) = 0$. Integrating (3.4) with respect to x from a to b yields

$$\int_a^b \left[\lambda\eta(x) + \alpha\eta^2(x)\right] dx + \beta\left[\eta_x(b) - \eta_x(a)\right] = \int_a^b f(x)dx.$$

This implies that

$$\int_a^b \left[\lambda\eta(x) + \alpha\eta^2(x)\right] dx > 0 \tag{3.16}$$

since $f(x) > 0$ for any $x \in [a,b] \subset$ supp(f). On the other hand, the assumption $\eta(x) \geq -\lambda/\alpha > 0$ for all $x \in$ supp(f) leads to

$$\int_a^b \left[\lambda\eta(x) + \alpha\eta^2(x)\right] dx \leq 0.$$

This contradicts (3.16), and our proof is completed.

Chapter 4

Analytic Solitary Wave Solutions

It is well known that the solutions to the sfKdV BVP (3.4)−(3.5) represent station-
ary solitary waves of an open channel flow in response to external forcings. These
solutions may play a significant role in developing stability theory of nonlinear evo-
lution equations. It is interesting to solve this problem analytically. The explicit
expression of solutions is useful for exploring the complicated bifurcation behavior
of the sfKdV BVP (3.4)−(3.5).

In the sfKdV equation, the forcing is usually classified into two categories. ac-
cording to [36]. One type of forcing, called "local" forcing, has the height of the
bump comparable with the length of the bump support and can be approximated by
the Dirac delta function in the nondimensional long wave coordinates. For a local
forcing, Shen has recently shown that the sfKdV equation has at most two branches
of SPSWS by finding the analytic expression [35]. A forcing which is not the "lo-
cal" type is called a "nonlocal" forcing. For a nonlocal forcing bump, it means its
support is much longer than its height. Patoine and Warn [32], and Wu [46] found
analytic expressions for the solutions of the sfKdV BVP (3.4)−(3.5) for a sech^4-like

and sech^2-like forcing, respectively. These forcings belong to the category of nonlocal forcing. They also demonstrated the existence of two branches of SPSWS.

In this chapter, our main goal is to solve the sfKdV BVP (3.4)−(3.5) analytically for (i) a nonlocal rectangular bump/dent (§4.1) and (ii) two local forcings (§4.2). Meanwhile, we will elucidate the complicated bifurcation behavior of multiple SP-SWS in these cases by displaying many graphs from the computations.

4.1   Analytical SPSWS for a bump or dent

Let us consider the rectangular bump or dent forcing which is defined as

$$f(x) = \begin{cases} \gamma, & |x| \le a/2, \\ 0, & \text{otherwise.} \end{cases}$$

When $\gamma > 0$ (< 0), $f(x)$ represents the forcing of a rectangular bump (dent). All SPSWS in this case can be expressed in terms of Weierstrass' elliptic functions in the region of the rectangular bump or dent and matched by hyperbolic sech^2-type of functions outside of the support base of the forcing. Here, a is a positive constant which represents the length of the rectangular bump or dent. Since the forcing function $f(x)$ has a jump discontinuity, all SPSWS $\eta(x)$ of the sfKdV BVP (3.4)−(3.5) are in $C^1(\Re)$.

4.1.1   Explicit expression of SPSWS

When $x \le -a/2$, an SPSWS $\eta(x)$ of the sfKdV BVP(3.4)−(3.5) can be expressed by

$$\eta(x) = -\frac{3\lambda}{2\alpha}\text{sech}^2\sqrt{\frac{-\lambda}{4\beta}}(x - L_0),$$

where the phase shift L_0 is to be determined.

When $|x| < a/2$, the SPSWS $\eta(x)$ must satisfy the equation

$$\lambda\eta + \alpha\eta^2 + \beta\eta_{xx} = \gamma. \tag{4.1}$$

The continuity of η and η_x at $x = -a/2$ and $x = a/2$ yields

$$\eta(-a/2) = -\frac{3\lambda}{2\alpha}\text{sech}^2\sqrt{\frac{-\lambda}{4\beta}}(a/2 + L_0) \equiv \eta_0, \tag{4.2}$$

$$\eta_x(-a/2) = \sqrt{\frac{-\lambda}{\beta}}\eta_0 \tanh\sqrt{\frac{-\lambda}{4\beta}}(a/2 + L_0) \equiv \eta_1, \tag{4.3}$$

$$\eta(-a/2) = \eta(a/2), \tag{4.4}$$

$$\eta_x(-a/2) = \eta_x(a/2), \quad \text{or} \quad \eta_x(-a/2) = -\eta_x(a/2). \tag{4.5}$$

The first integral of (4.1) from $-a/2$ to x ($< a/2$) satisfies

$$(\eta_x)^2 = b_1\eta^3 + b_2\eta^2 + b_3\eta + b_4, \tag{4.6}$$

where $b_1 = -(2\alpha)/(3\beta)$, $b_2 = -\lambda/\beta$, $b_3 = 2\gamma/\beta$, and $b_4 = -b_3\eta_0$. By making a transform $\eta = c_1 u + c_2$, (4.6) is converted into

$$(u_x)^2 = 4u^3 - g_2 u - g_3, \tag{4.7}$$

where $c_1 = 4/b_1$, $c_2 = -b_2/(3b_1)$, $g_2 = -(b_2 c_2 + b_3)/c_1$, and $g_3 = -(b_1 c_2^3 + b_2 c_2^2 + b_3 c_2 + b_4)/c_1^2$. Here, g_2 is a constant and g_3 is a function of L_0 for given λ, α, β, and a. The general solution of (4.7) can be expressed in terms of Weierstrass' elliptic function $u = \wp(x + \tau, g_2, g_3)$ (cf. [44], pp. 470). Thus, when $|x| < a/2$, the SPSWS $\eta(x)$ can be put in the form

$$\eta(x) = c_1\wp(x + \tau, g_2, g_3) + c_2. \tag{4.8}$$

Equations (4.2) and (4.3) yield

$$\eta_0 = c_1 \wp(-a/2 + \tau, g_2, g_3) + c_2,$$ (4.9)

$$\eta_1 = c_1 \wp'(-a/2 + \tau, g_2, g_3).$$ (4.10)

Further, by using the identity of Weierstrass' elliptic function (cf. [44], pp. 482)

$$\wp(x + y, g_2, g_3) + \wp(x, g_2, g_3) + \wp(y, g_2, g_3) = \frac{1}{4} \left\{ \frac{\wp'(x, g_2, g_3) - \wp'(y, g_2, g_3)}{\wp(x, g_2, g_3) - \wp(y, g_2, g_3)} \right\}^2,$$

Weierstrass' elliptic function $\wp(x + \tau, g_2, g_3)$ in (4.8) can be rewritten in the form:

$$\wp(x + \tau, g_2, g_3) = \frac{1}{4} \left\{ \frac{c_1 \wp'(x + a/2, g_2, g_3) - \eta_1}{c_1 \wp(x + a/2, g_2, g_3) - \eta_0 + c_2} \right\}^2 - \wp(x + a/2, g_2, g_3) - \frac{\eta_0 - c_2}{c_1}.$$

Then, (4.4) results in an equation

$$B(\lambda, L_0) \equiv \frac{c_1}{4} \left\{ \frac{c_1 \wp'(a, g_2, g_3) - \eta_1}{c_1 \wp(a, g_2, g_3) - \eta_0 + c_2} \right\}^2 - c_1 \wp(a, g_2, g_3) + 2c_2 - 2\eta_0 = 0, \quad (4.11)$$

which determines the phase shift L_0.

On the other hand, when $x \geq a/2$, the SPSWS can be expressed by

$$\eta(x) = -\frac{3\lambda}{2\alpha} \text{sech}^2 \sqrt{\frac{-\lambda}{4\beta}} (x - L_1),$$

where the phase shift L_1 is to be determined by the continuity conditions $(4.4)-(4.5)$.

Consequently, for each solution L_0 of (4.11), we are able to construct an SPSWS to the sfKdV BVP $(3.4)-(3.5)$, which is expressed by

$$\eta(x) = \begin{cases} -\frac{3\lambda}{2\alpha} \text{sech}^2 \sqrt{\frac{-\lambda}{4\beta}} (x - L_0), & -\infty < x \leq -a/2, \\ c_1 \wp(x + \tau, g_2, g_3) + c_2, & -a/2 < x < a/2, \\ -\frac{3\lambda}{2\alpha} \text{sech}^2 \sqrt{\frac{-\lambda}{4\beta}} (x - L_1), & a/2 \leq x < \infty. \end{cases} \quad (4.12)$$

4.1.2 Existence of multiple SPSWS

A salient feature of the sfKdV BVP (3.4)–(3.5) for a nonlocal forcing is that it may admit more than two SPSWS. In fact, (4.11) may define L_0 as a multi-valued function of λ and determines the bifurcation of the sfKdV BVP (3.4)–(3.5). Namely, for a given λ, the number of the corresponding solutions for L_0 to equation (4.11) is equal to the number of SPSWS. Obviously, a contour plot of $z = B(\lambda, L_0)$ at level zero is able to show the bifurcation behavior of multiple SPSWS. In this section, we would like to illustrate our numerical results obtained by using Mathematica (cf. Appendix A). For. simplicity, let us take $\alpha = -3/4$, $\beta = -1/6$, γ and a as parameters.

CASE I. $\gamma > 0$

In this case, our numerical results suggest that there are at most two branches of SPSWS, which are always ordered. For a fixed $\lambda > 0$, when γ approaches zero, which corresponds to the unforced case, two branches of SPSWS reduce to free solitary waves and uniform null solutions, respectively. As explained in [43], a higher solitary wave solution may be viewed as the perturbation of an unforced solitary wave solution and a lower solitary wave solution branch is the response to the perturbation of an unforced uniform wave solution. Our computational results are shown as follows.

(i) For $\gamma = 1$ and $a = 1$, the contour plot (Figure 4.1 (a)) of $z = B(\lambda, L_0)$ at level zero shows that (4.11) has at most two zeros for $0 < \lambda \le 3$. Precisely, there are no solutions, one solution, and two solutions to the sfKdV BVP (3.4)–(3.5) for $\lambda < \lambda_C (\approx 1.2)$, $\lambda = \lambda_C$, and $\lambda_C < \lambda \le 3$, respectively. This λ_C is called the turning point of the SPSWS bifurcation. Figure 4.1 (b) displays two SPSWS for $\lambda = 1.5 > \lambda_C$.
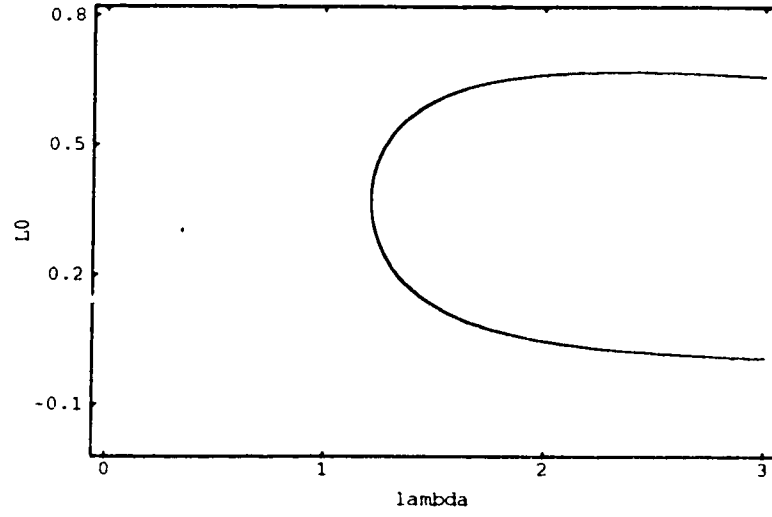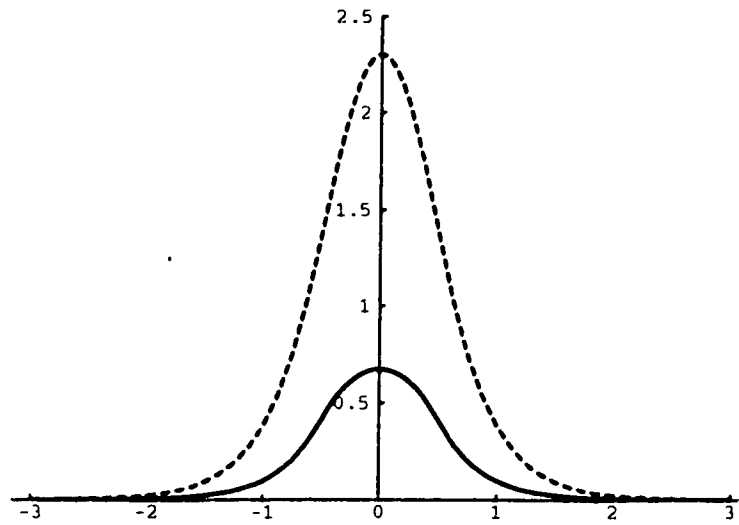
Figure 4.1: (a) Bifurcation diagram of the SPSWS in the plane (λ, L_0) for $\gamma = 1$ and $a = 1$. (b) Two SPSWS of the sfKdV BVP when $\lambda = 1.5$ corresponding to $L_{01} = 0.601315225$ (solid line) and $L_{02} = 0.1270480543$ (dashed line).

(ii) For $\gamma = 0.5$ and $a = 1$, the contour plot (Figure 4.2 (a)) of $z = B(\lambda, L_0)$ at level zero shows that (4.11) has at most two zeros for $0 < \lambda \leq 3$. The turning point λ_C is close to 0.785. Hence, there are no solutions, one solution, and two solutions to the sfKdV BVP (3.4)–(3.5) for $\lambda < \lambda_C$ $\lambda = \lambda_C$, and $\lambda_C < \lambda \leq 3$, respectively. Figure 4.2 (b) displays two SPSWS for $\lambda = 1.5 > \lambda_C$.
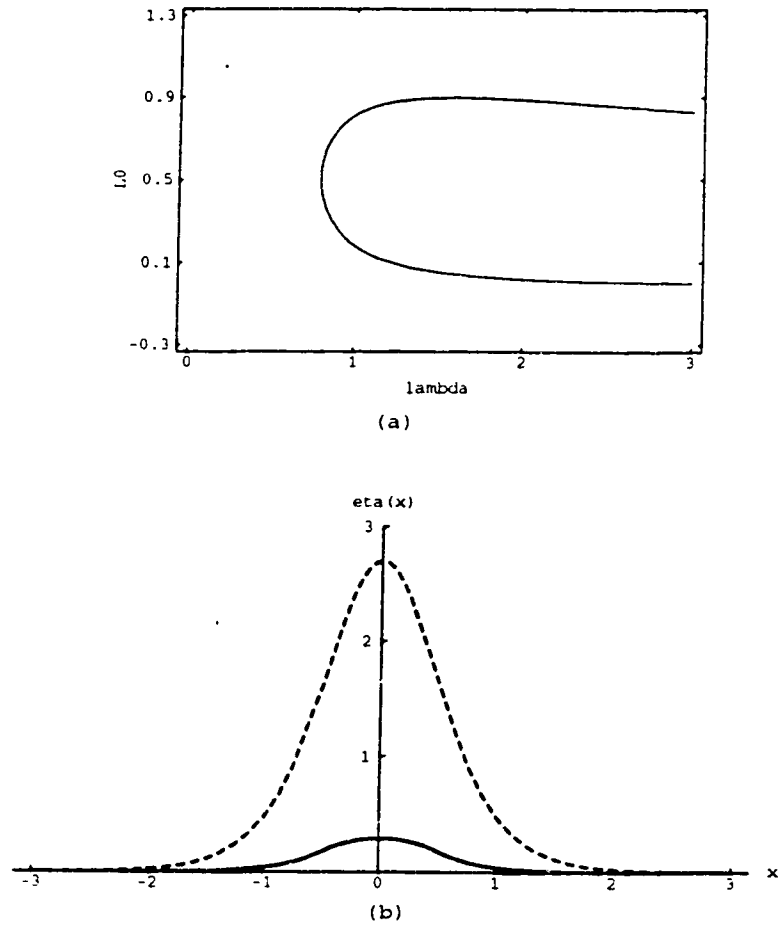
Figure 4.2: (a) Bifurcation diagram of the SPSWS in the plane (λ, L_0) for $\gamma = 0.5$ and $a = 1$. (b) Two SPSWS of the sfKdV BVP when $\lambda = 1.5$ corresponding to $L_{01} = 0.8985087523$ (solid line) and $L_{02} = 0.05288336998$ (dashed line).

(iii) For $\gamma = 0.1$ and $a = 1$, the contour plot (Figure 4.3 (a)) of $z = B(\lambda, L_0)$ at level zero shows that (4.11) has at most two zeros for $0 < \lambda \leq 2$. The turning point λ_C is close to 0.283. Therefore, there are no solutions, one solution, and two solutions to the sfKdV BVP (3.4)–(3.5) for $\lambda < \lambda_C(\approx 1.2)$, $\lambda = \lambda_C$, and $\lambda_C < \lambda \leq 3$, respectively. Figure 4.3 (b) displays two SPSWS for $\lambda = 1.5 > (\lambda_C)$.

(a)

(b)
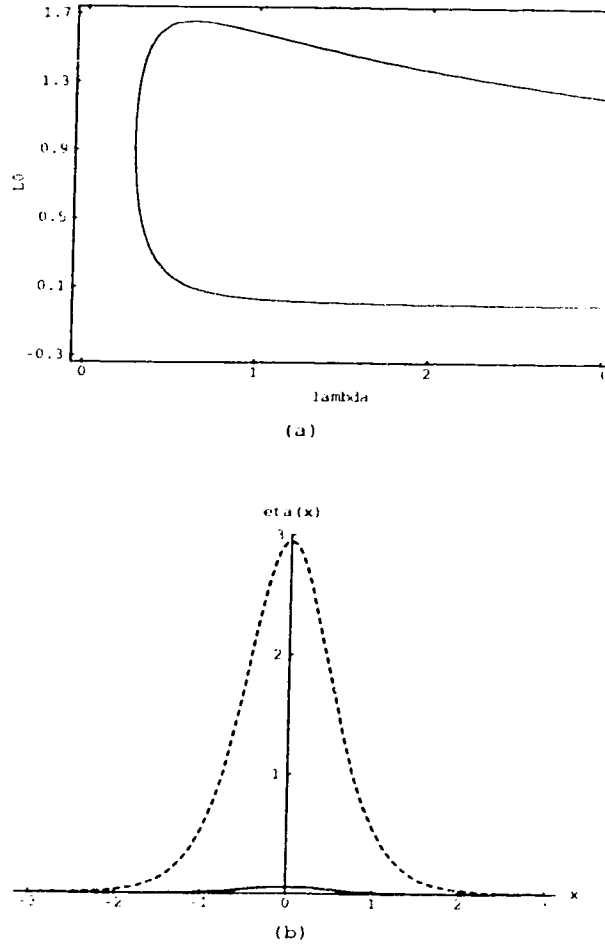
Figure 4.3: (a) Bifurcation diagram of the SPSWS in the plane (λ, L_0) for $\gamma = 0.1$ and $a = 1$. (b) Two SPSWS of the sfKdV BVP when $\lambda = 1.5$ corresponding to $L_{01} = 1.471252106$ (solid line) and $L_{02} = 0.00964251$ (dashed line).

CASE II. $\gamma < 0$

For a dent forcing, we have found numerically that the sfKdV BVP (3.4)−(3.5) might admit infinitely many SPSWS for fixed α and β, and sufficiently large values λ and a, the number of the SPSWS is an increasing function of λ and a, and all SPSWS are not always ordered.

(i) When $\gamma = -1$ and $a = 1$, the contour plot (Figure 4.4) of $z = B(\lambda, L_0)$ at level zero shows that (4.11) has at most two zeros for $0 < \lambda \leq 4$. The turning point λ_C is close to 0.9916. Hence, there are no solution, one solutions, and two solutions to the sfKdV BVP (3.4)−(3.5) for $\lambda < \lambda_C$, $\lambda = \lambda_C$, and $\lambda_C < \lambda \leq 3$, respectively.
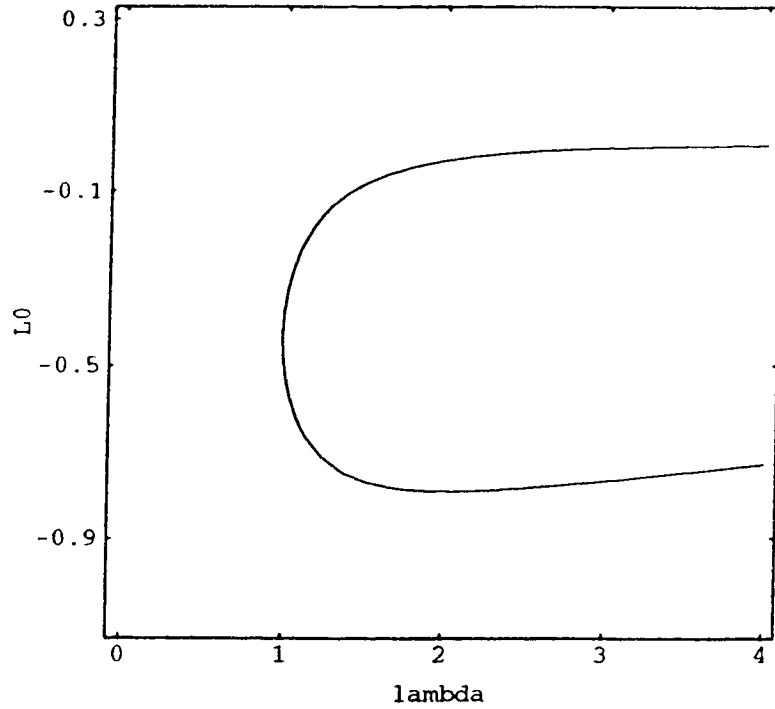
Figure 4.4: Bifurcation of the SPSWS in the plane (λ, L_0) for $\gamma = -1$ and $a = 1$.

(ii) Figure 4.5 (a) shows that there are four SPSWS for sufficiently large $\lambda > \lambda_{C_2}$ when $\gamma = -1$ and $a = 2$. There are two turning points in this case. One is $\lambda_{C_1}(\approx 0.22175)$ and the other is $\lambda_{C_2}(\approx 0.339)$. A remarkable feature of this bifurcation is that there exists a pitchfork bifurcation at the turning point λ_{C_2}. Figure 4.5 (b) displays the local bifurcation diagram in the neighborhood of the two turning points. The gaps in Figures 4.5 (a)–(b) are due to numerical errors.

(a)

(b)
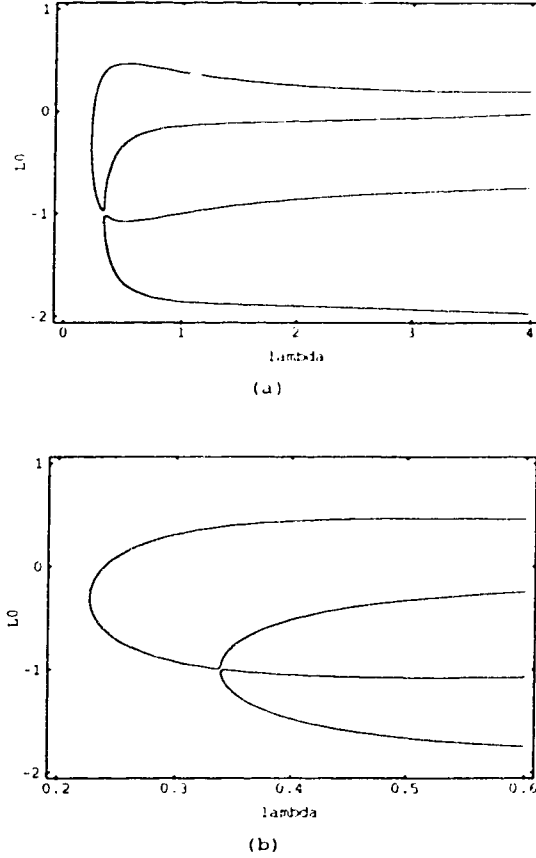
Figure 4.5: (a) Bifurcation diagram of the SPSWS in the plane (λ, L_0) for $\gamma = -1$ and $a = 2$. (b) Local bifurcation diagram of the SPSWS near two turning points.

Another interesting feature is that there exist nonsymmetric solutions in response to symmetric forcing and nonsymmetric solutions must occur in pairs. In fact, for a symmetric forcing, $\eta(-x)$ is also an SPSWS if $\eta(x)$ is an SPSWS. Hence, the number of nonsymmetric solutions must be even. Figures 4.6 (a)–(b) show the graphs of two symmetric SPSWS and two nonsymmetric SPSWS when $a = 2$ and $\lambda = 3$, respectively. Two nonsymmetric SPSWS in Figure 4.6 (b) are indeed antisymmetric.

eta(x)

(a)

eta(x)

(b)
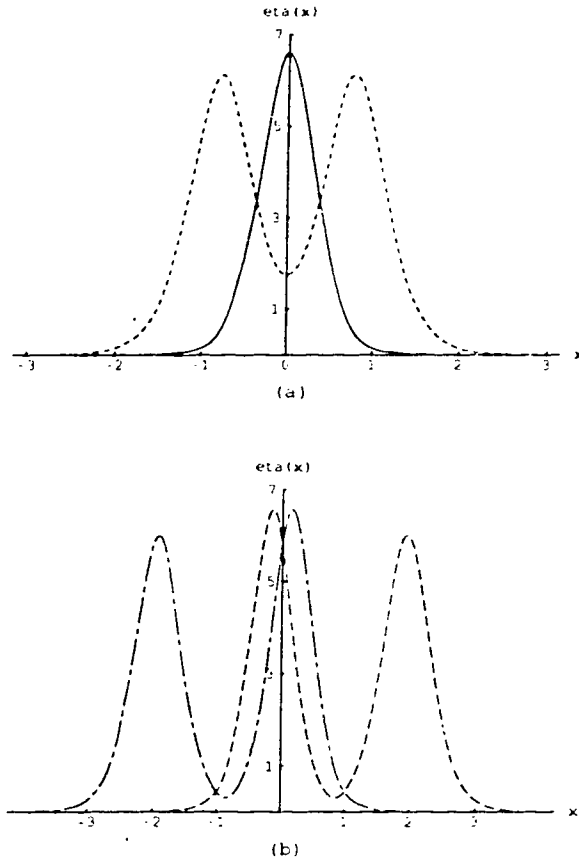
Figure 4.6: (a) Two symmetric SPSWS of the sfKdV BVP when $a = 2$ and $\lambda = 3$ corresponding to $L_{01} = 0.201436$ (solid line) and $L_{02} = -0.793253$ (dashed line). (b) Two nonsymmetric SPSWS of the sfKdV BVP when $a = 2$ and $\lambda = 3$ corresponding to $L_{03} = -0.0669117$ (dashed line) and $L_{04} = -1.93309$ (dot-dashed line).

(iii) Moreover, we have found that there exist eight SPSWS to the sfKdV BVP (3.4)–(3.5) when $\gamma = -1$ and $a = 8$. In this case, there are four turning points: $\lambda_{C_1}(\approx 0.3132)$, $\lambda_{C_2}(\approx 0.3395)$, $\lambda_{C_3}(\approx 1.3866)$, and $\lambda_{C_4}(\approx 2.2545)$. Figure 4.7 (a) shows the bifurcation diagram for $0 < \lambda \le 4$ and Figure 4.7 (b) shows the local bifurcation diagram for $0.3 < \lambda < 0.4$. Our numerical results have clearly demonstrated the existence of two pitchfork bifurcations at the turning point λ_{C_2} (Figure 4.7 (b)) and λ_{C_4} (Figure 4.7 (a)).
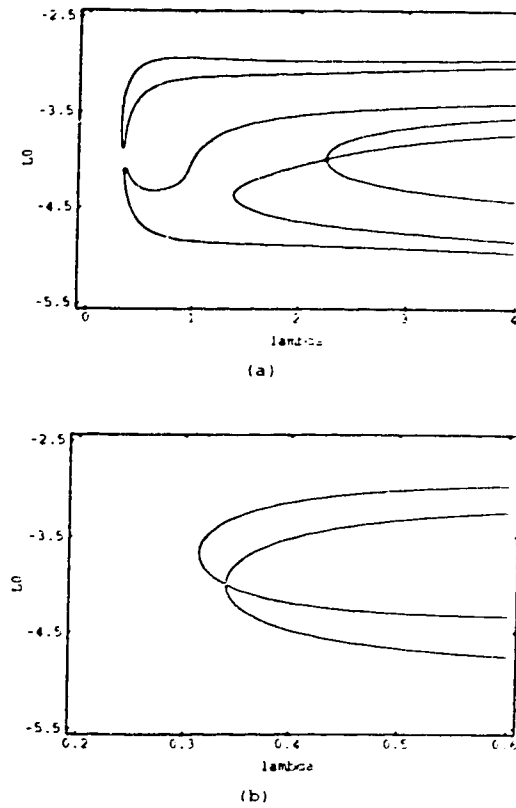
Figure 4.7: (a) Bifurcation diagram of the SPSWS in the plane (λ, L_0) for $\gamma = -1$ and $a = 8$. (b) Local bifurcation diagram of the SPSWS near the first two turning points.

All eight SPSWS are displayed in Figures 4.8: four symmetric SPSWS (a)-(b) and four nonsymmetric SPSWS (c)-(d).

(a)

(b)

eta(x)

(c)

eta(x)

(d)
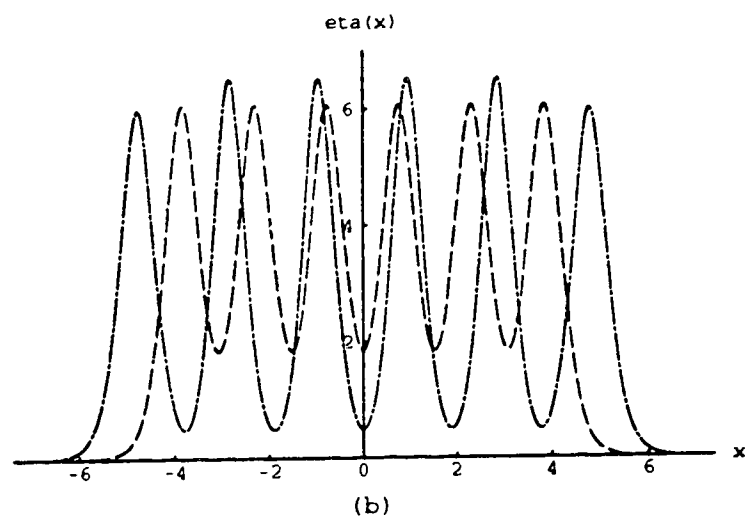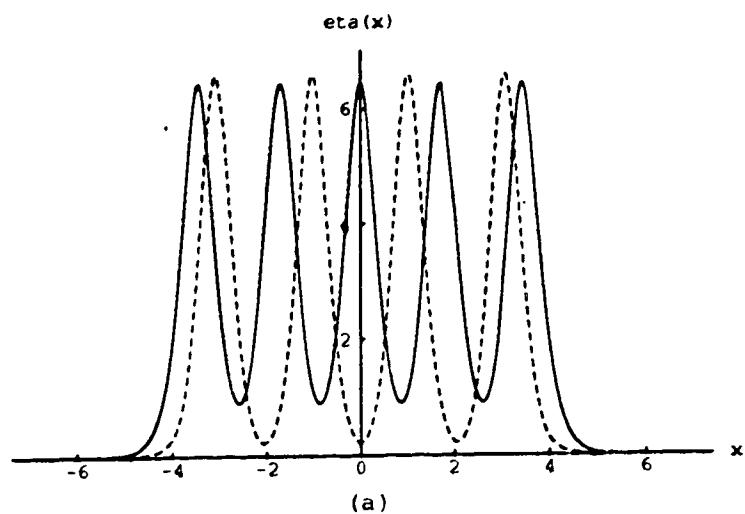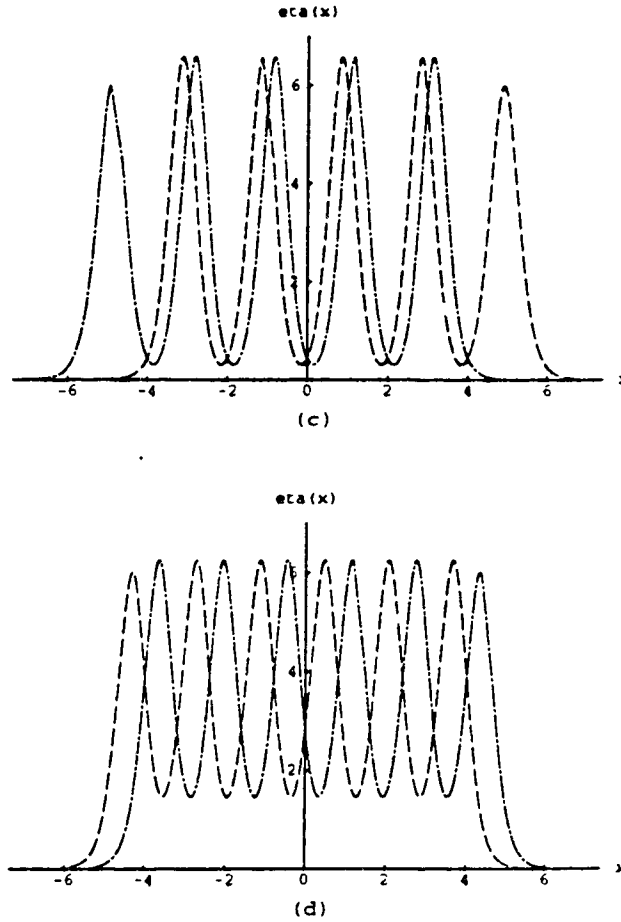
Figure 4.8: (a) Two symmetric SPSWS of the sfKdV BVP when $a = 8$ and $\lambda = 3$ corresponding to $L_{01} = -3.4566$ (solid line) and $L_{02} = -2.96922$ (dashed line). (b) Other two symmetric SPSWS correspond to $L_{03} = -3.84921$ (dashed line) and $L_{04} = -4.77441$ (dot-dashed line). (c) Two nonsymmetric SPSWS correspond to $L_{05} = -3.06691$ (dashed line) and $L_{06} = -3.67532$ (dot-dashed line). (d) Other two nonsymmetric correspond to $L_{07} = -4.32468$ (dashed line) and $L_{08} = -4.93309$ (dot-dashed line).

4.2 Analytical SPSWS for two local bumps

For two local forcings at $x = -a$ and $x = a$, the forcing function can be approximated by

$$f(x) = P_1\delta(x + a) + P_2\delta(x - a),$$

where a, P_1 and P_2 are constants. Since the forcing function is a generalized function, we require that the SPSWS $\eta(x)$ of the sfKdV BVP (3.4)--(3.5) must be in $C(\Re)$ and possess at least the second order continuous derivatives in $\Re$ except two singular points $x = -a$ and $x = a$ at which it satisfies the following jump conditions:

$$\eta_x(-a_+) - \eta_x(-a_-) = P_1/\beta, \tag{4.13}$$

$$\eta_x(a_+) - \eta_x(a_-) = P_2/\beta. \tag{4.14}$$

The procedure of solving the sfKdV BVP (3.4)--(3.5) with the above forcing and conditions is similar to that discussed in §4.1. All SPSWS in this case can be expressed in terms of Weierstrass' elliptic functions in the interval $(-a, a)$ matched by hyperbolic sech^2-type of functions outside of that interval.

The SPSWS $\eta(x)$ of the sfKdV BVP(3.4)--(3.5) can be expressed by

$$\eta(x) = -\frac{3\lambda}{2\alpha}\text{sech}^2\sqrt{\frac{-\lambda}{4\beta}}(x - L_0), \quad \text{for } x < -a,$$

and

$$\eta(x) = -\frac{3\lambda}{2\alpha}\text{sech}^2\sqrt{\frac{-\lambda}{4\beta}}(x - L_1), \quad \text{for } x > -a,$$

where the phase shifts L_0 and L_1 are to be determined.

When $-a < x < a$, the SPSWS $\eta(x)$ must satisfy the equation

$$\lambda\eta + \alpha\eta^2 + \beta\eta_{xx} = 0. \tag{4.15}$$

The continuity of η and the jump conditions of η_x at $x = -a$ and $x = a$ yields

$$\eta(-a_+) = \eta(-a_-), \tag{4.16}$$

$$\eta_x(-a_+) = \eta_x(-a_-) + P_1/\beta, \tag{4.17}$$

$$\eta(a_+) = \eta(a_-), \tag{4.18}$$

$$\eta_x(a_+) = \eta_x(a_-) + P_2/\beta, \tag{4.19}$$

where

$$\eta_0 \equiv \eta(-a_-) = \frac{3\lambda}{2\alpha}\mathrm{sech}^2\sqrt{\frac{-\lambda}{4\beta}}(a + L_0), \tag{4.20}$$

$$\hat{\eta}_0 \equiv \eta_x(-a_-) = \sqrt{\frac{-\lambda}{\beta}}\eta_0 \tanh\sqrt{\frac{-\lambda}{4\beta}}(a + L_0), \tag{4.21}$$

$$\eta_1 \equiv \eta(a_+) = \frac{3\lambda}{2\alpha}\mathrm{sech}^2\sqrt{\frac{-\lambda}{4\beta}}(a - L_1), \tag{4.22}$$

$$\hat{\eta}_1 \equiv \eta_x(a_+) = -\sqrt{\frac{-\lambda}{\beta}}\eta_1 \tanh\sqrt{\frac{-\lambda}{4\beta}}(a - L_1). \tag{4.23}$$

The first integral of (4.15) from $-a$ to x ($< a$) satisfies

$$(\eta_x)^2 = b_1\eta^3 + b_2\eta^2 + S. \tag{4.24}$$

Here, $b_1 = -(2\alpha)/(3\beta)$, $b_2 = -\lambda/\beta$, and the integration constant S must be determined. The continuity of η and the jump condition of η_x at $x = -a$ results in

$$S = \frac{P_1(P_1 + 2\beta\hat{\eta}_0)}{2\beta^2}. \tag{4.25}$$

By making a transform $\eta = c_1 u + c_2$, (4.24) is converted into

$$(u_x)^2 = 4u^3 - g_2 u - g_3, \tag{4.26}$$

where $c_1 = 4/b_1$, $c_2 = -b_2/(3b_1)$, $g_2 = -b_2 c_2/c_1$, and $g_3 = -(b_1 c_2^3 + b_2 c_2^2 + S)/c_1^2$. Here, g_2 is a constant and g_3 is a function of L_0 for given λ, α, β, and a. The

general solution of (4.26) can be expressed in term of Weierstrass' elliptic function $u = \wp(x + \tau, g_2, g_3)$. Thus, when $|x| < a$, the SPSWS $\eta(x)$ can be put in the form

$$\eta(x) = c_1\wp(x + \tau, g_2, g_3) + c_2. \tag{4.27}$$

Equations (4.20) and (4.21) are rewritten as

$$\eta_0 = c_1\wp(-a + \tau, g_2, g_3) + c_2, \tag{4.28}$$

$$\hat{\eta}_0 = c_1\wp'(-a + \tau, g_2, g_3) - \frac{P_1}{\beta}. \tag{4.29}$$

Further, Weierstrass' elliptic function $\wp(x + \tau, g_2, g_3)$ in (4.28) can be rewritten as

$$\wp(x + \tau, g_2, g_3) = \frac{1}{4}\left\{\frac{c_1\wp'(x + a, g_2, g_3) - d_1}{c_1\wp(x + a, g_2, g_3) - d_2}\right\}^2 - \wp(x + a, g_2, g_3) - \frac{d_2}{c_1}.$$

where $d_1 = \hat{\eta}_0 - P_1/\beta$ and $d_2 = \eta_0 - c_2$. The continuity (4.18)of η and the jump condition (4.19) of η_x at $x = a$ results in a nonlinear system of equations:

$$\eta_1 = \eta(a_-), \tag{4.30}$$

$$\hat{\eta}_1 = \eta_x(a_-) + \frac{P_2}{\beta}, \tag{4.31}$$

where $\eta(a_-)$ and $\eta_x(a_-)$ can be calculated from (4.27). This system determines two phase shifts L_0 and L_1. Substituting (4.30)–(4.31) into (4.24) yields

$$\hat{\eta}_1 = \frac{P_2^2 - S\beta^2}{2P_2\beta}. \tag{4.32}$$

Eliminating η_1 and $\hat{\eta}_1$ from (4.30)–(4.32), one finally obtains one equation for L_0

$$B_\lambda(L_0) \equiv b_1\eta^3(a_-) + b_2\eta^2(a_-) - \left(\frac{P_2^2 - S\beta^2}{2P_2\beta}\right)^2 = 0 \tag{4.33}$$

Any solution L_0 of (4.30)−(4.31) satisfies (4.33). But, (4.33) may have extra zeros for (4.30)−(4.31). Therefore, unlike the equation (4.11), (4.33) cannot give an explicit

expression for discerning the bifurcation. However, (4.33) is useful to search for the SPSWS of the sfKdV BVP. We first find all roots L_0 of (4.33), then substitute each root into (4.30) to solve for L_1, and finally confirm whether each pair of (L_0, L_1) satisfies (4.31). Once such a pair of L_0 and L_1 is found, we are able to construct an SPSWS to the sfKdV BVP (3.4)–(3.5), which is expressed by

$$\eta(x) = \begin{cases} -\frac{3\lambda}{2\alpha}\text{sech}^2\sqrt{\frac{-\lambda}{4\beta}}(x - L_0), & -\infty < x \leq -a, \\ c_1\wp(x + \tau, g_2, g_3) + c_2, & -a < x < a, \\ -\frac{3\lambda}{2\alpha}\text{sech}^2\sqrt{\frac{-\lambda}{4\beta}}(x - L_1), & a \leq x < \infty. \end{cases} \quad (4.34)$$

One example is displayed in Figure 4.9 for $a = 1$, $P_1 = P_2 = 0.5$ and $\lambda = 1.0$. In this case, by using Mathematica (cf. Appendix B), we find that the system of (4.30)–(4.31) has four pairs of roots L_0, and L_1: {-0.16443883, 0.16443883}, {-0.5722933, 0.5722933}, {-0.21513488, 0.66210687}, and {-0.66210681, 0.21513506}. Hence, the sfKdV BVP (3.4)–(3.5) has four SPSWS: two symmetric and two non-symmetric. The two symmetric SPSWS shown in Figure 4.9 (a) are ordered and the two nonsymmetric shown in Figure 4.9 (b) are mutually antisymmetric.
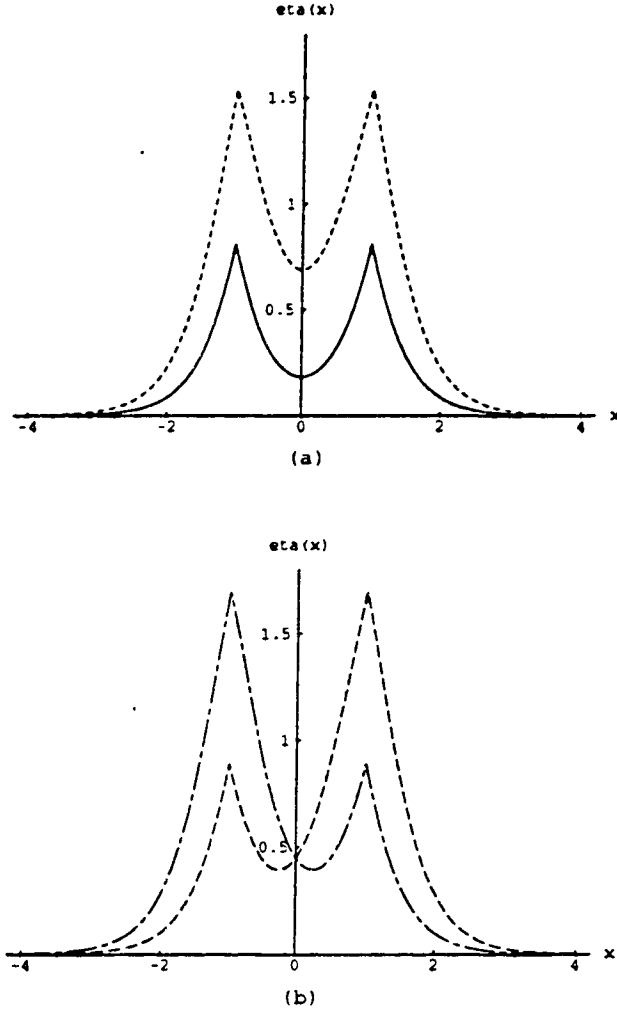
Figure 4.9: (a) Two symmetric SPSWS of the sfKdV BVP when $a = 1$ $P_1 = P_2 = 1$ and $\lambda = 1$ corresponding to $L_{01} = -0.16443883$, $L_{11} = 0.16443883$ (solid line) and $L_{02} = -0.5722933$, $L_{12} = 0.5722933$ (dashed line). (b) Two nonsymmetric SPSWS corresponding to $L_{03} = -0.21513488$, $L_{13} = 0.66210687$ (dashed line) and $L_{04} = -0.66210681$, $L_{14} = 0.21513506$ (long-dashed line).

Chapter 5

Stability of Forced Solitary Waves

We have shown analytically that there may exist multiple SSWS to the sfKdV BVP (3.4)–(3.5). A natural and important question is which solution is physically observable. The answer to this question is related to the stability of these forced stationary solitary waves.

It is worth remarking that Camassa and Wu have recently made remarkable progress in the research on the stability analysis for forced stationary sech^2-like solitary waves [7]–[8]. Through the linear instability analysis, they identified three different categories of forced stationary solitary waves, which occur in three different parametric régimes called a periodic bifurcating régime, an aperiodic bifurcating régime, and a supercritical stable régime. The steady state is unstable in the periodic bifurcating régime and the aperiodic bifurcating régime. The steady state in the supercritical stable régime is shown to be stable by means of nonlinear stability analysis based on the Hamiltonian functional formulation. But, in general, the stability and instability of the sfKdV SSWS seem difficult to be analyzed due to their complicated structure.

In this chapter, we investigate the stability of the sfKdV SSWS both analytically and numerically. Following the nonlinear stability theory developed by Benjamin [5], we will derive a criterion of nonlinear stability for forced stationary solitary waves in §5.1. This criterion is easy to use for discerning the stability of an SSWS provided that the magnitude of the wave profile is known. Alternatively, numerical simulations may be helpful in illustrating the features of the stability and instability of the sfKdV SSWS when the mathematical theory fails to apply. In §5.2, we will demonstrate numerical evidence for the stability and instability of supercritical stationary solitary waves forced by a rectangular bump and two local forcings described in Chapter 4.

5.1   Theory of linear and nonlinear stability

5.1.1   Basic concepts of stability theory

Suppose that $\eta_s(x)$ is an SSWS of the sfKdV equation and an arbitrary perturbation $v(x)$ is imposed on the given initial state $\eta_s(x)$, the resulting motion $\eta(x, t)$ is required to satisfy the fKdV equation with the following initial and boundary conditions

$$\eta_t + \lambda\eta_x + 2\alpha\eta\eta_x + \beta\eta_{xxx} = f_x, \quad -\infty < x < \infty, t > 0, \qquad (5.1)$$

$$\eta(x, t = 0) = \eta_s(x) + v(x), \quad -\infty < x < \infty, \qquad (5.2)$$

$$\eta(\pm\infty, t) = \eta_x(\pm\infty, t) = \eta_{xx}(\pm\infty, t) = 0, \quad t > 0. \qquad (5.3)$$

If $\eta(x, t)$ is decomposed into

$$\eta(x, t) = \eta_s(x) + \zeta(x, t),$$

then the perturbation $\zeta(x,t)$ of the primary motion $\eta_s(x)$ must satisfy a homogeneous nonlinear equation with the corresponding initial and boundary conditions

$$\zeta_t + \left[(\lambda + 2\alpha\eta_s(x))\zeta + \alpha\zeta^2 + \beta\zeta_{xx}\right]_x = 0, \quad -\infty < x < \infty, t > 0, \quad (5.4)$$

$$\zeta(x, t = 0) = v(x), \quad -\infty < x < \infty, \quad (5.5)$$

$$\zeta(\pm\infty, t) = \zeta_x(\pm\infty, t) = \zeta_{xx}(\pm\infty, t) = 0, \quad t > 0. \quad (5.6)$$

The primary motion $\eta_s(x)$ is said to be stable if $\zeta(x,t)$ remains arbitrarily small for all future time provided that the initial perturbation $v(x)$ is suitably small.

5.1.2 Formulation of linear stability

Linear stability analysis is based on the linearized equation of (5.4), i.e.,

$$\zeta_t + [(\lambda + 2\alpha\eta_s(x))\zeta + \beta\zeta_{xx}]_x = 0, \quad -\infty < x < \infty, t > 0 \quad (5.7)$$

with boundary conditions (5.6). By separating variables

$$\zeta(x, t) = e^{\sigma t} r(x)$$

where σ and $r(x)$ may be complex, (5.6) and (5.7) reduce to

$$[(\lambda + 2\alpha\eta_s(x))r(x) + \beta r_{xx}(x)]_x + \sigma r(x) = 0, \quad -\infty < x < \infty, \quad (5.8)$$

$$r(\pm\infty) = r_x(\pm\infty) = r_{xx}(\pm\infty) = 0. \quad (5.9)$$

This is an eigenvalue problem of a third order ordinary differential equation. The linear stability of $\eta_s(x)$ is determined by the signature of the real part of σ. Namely, $\eta_s(x)$ is referred to as linearly stable, neutrally stable, or unstable if $Re(\sigma)$ is negative, zero, or positive, respectively. It is remarked that no statement can be made for the nonlinear stability if $\eta_s(x)$ is neutrally stable. However, this eigenvalue problem (5.8)–(5.9) does not seem to have been resolved. This leads us to search for alternative approaches which will be discussed in the rest of this chapter.

5.1.3 Criterion of nonlinear stability

To our surprise, the nonlinear stability analysis actually results in a simple sufficient condition for the stability criterion. The concept of nonlinear stability is here interpreted in the usual Lyapunov sense. Precisely, suppose that the perturbed motion $\zeta(x,t)$ and initial perturbation $v(x)$ belong to the Sobolev space $\mathcal{H}^1$ where the norm is defined by $||\zeta||_1^2 = \int_{-\infty}^{\infty}(\zeta^2 + \zeta_x^2)dx$ for any $\zeta \in \mathcal{H}^1$. The SSWS $\eta_s(x)$ is stable if for any $\varepsilon > 0$, one can choose a $\delta > 0$ such that $||\zeta(x,t)||_1 < \varepsilon$ for all time $t > 0$ provided that $||v(x)||_1 < \delta$.

According to numerical results reported in the paper [40], an SSWS is stable if the crest of the SSWS profile is lower than a certain height. This is actually true in general. Following nonlinear analysis developed by Benjamin [5], we can prove the following criterion for the nonlinear stability of the sfKdV solitary waves.

Theorem 8 *Suppose that $\eta_s(x)$ is an SSWS of the* sfKdV *BVP (3.4)–(3.5). If* $\lambda + 2\alpha||\eta_s||_\infty > 0$, *then η_s is stable.*

Proof: The proof of this theorem can be done by following the procedure reported in Bona's paper [6]. To do this, we first introduce a functional

$$H \equiv \frac{1}{2}\int_{-\infty}^{\infty}\left[(\lambda + 2\alpha\eta_s)\zeta^2 + \frac{2\alpha}{3}\zeta^3 - \beta\zeta_x^2\right]dx$$

for the perturbation $\zeta(x,t)$ defined in §5.1.1. By a standard procedure, one can show that $dH/dt = 0$ for all time $t > 0$. In fact,

$$\frac{dH}{dt} = \int_{-\infty}^{\infty}\left[(\lambda + 2\alpha\eta_s)\zeta + \alpha\zeta^2\right]\zeta_t dx - \beta\int_{-\infty}^{\infty}\zeta_x\zeta_{xt}dx.$$

Integrating by part and using the boundary condition (5.6), we can rewrite the second integral in the above equation as

$$\int_{-\infty}^{\infty}\zeta_x\zeta_{xt}dx = -\int_{-\infty}^{\infty}\zeta_{xx}\zeta_t dx.$$

This implies that

$$\frac{dH}{dt} = \int_{-\infty}^{\infty} \left[(\lambda + 2\alpha\eta_s)\zeta + \alpha\zeta^2 + \beta\zeta_{xx} \right] \zeta_t dx.$$

Further, since $\zeta(x,t)$ satisfies (5.4) and (5.6), we have $dH/dt = 0$. Therefore, H is invariant in time t.

Secondly, one can show the operator

$$\frac{1}{2} \int_{-\infty}^{\infty} \left[(\lambda + 2\alpha\eta_s)\zeta^2 - \beta\zeta_x^2 \right] dx \qquad (5.10)$$

is always positive definite under our assumption, i.e. there is a positive constant c_1 such that

$$\frac{1}{2} \int_{-\infty}^{\infty} \left[(\lambda + 2\alpha\eta_s)\zeta^2 - \beta\zeta_x^2 \right] dx \geq c_1 \parallel \zeta \parallel_1^2,$$

since $\alpha < 0$, $\beta < 0$ and $\lambda + 2\alpha\eta_s \geq c_0 \equiv \lambda + 2\alpha||\eta_s||_\infty > 0$. Here, $c_1 = \min\{c_0, -\beta\}$.

We point out the difference between our estimate and Camassa and Wu's one. Indeed, the operator (5.10) can be put in another form

$$\frac{1}{2} \int_{-\infty}^{\infty} \left[(\lambda + 2\alpha\eta_s)\zeta^2 + \beta\zeta\zeta_{xx} \right] dx = \frac{1}{2} \int_{-\infty}^{\infty} \lambda\zeta^2 dx + \frac{\beta}{2} \int_{-\infty}^{\infty} \left(\frac{2\alpha}{\beta}\eta_s\zeta + \zeta_{xx} \right) \zeta dx.$$

For a forced stationary sech^2-like solitary wave, they have a sharp estimate for the second integral on the right hand side from elementary quantum mechanics (cf. [7], pp. 443), which will results in a sharp conclusion.

The third step is to use Sobolev's inequality [5]

$$\parallel \zeta \parallel_\infty \leq \frac{\parallel \zeta \parallel_1}{\sqrt{2}} \qquad (5.11)$$

to obtain the following estimates of the upper and lower bounds for the functional H

$$c_1 \parallel \zeta \parallel_1^2 - \frac{|\alpha|}{3\sqrt{2}} \parallel \zeta \parallel_1 \parallel \zeta \parallel^2 \leq H \leq M \parallel \zeta \parallel_1^2 + \frac{|\alpha|}{3\sqrt{2}} \parallel \zeta \parallel_1 \parallel \zeta \parallel^2, \qquad (5.12)$$

where $||\zeta||^2 = \int_{-\infty}^{\infty} \zeta^2 dx$, The proof of the above Sobolev's inequality is based on the theory of Fourier analysis. In fact, suppose $\zeta \in \mathcal{H}^1$, then $\zeta \in \mathcal{L}^2$ and $\zeta_x \in \mathcal{L}^2$. The Fourier's transform of ζ is defined as

$$\hat{\zeta}(k,t) = \int_{-\infty}^{\infty} e^{-ikx}\zeta(x,t)dx$$

and the inverse Fourier's transform is defined as

$$\zeta(x,t) = \frac{1}{2\pi} \int_{-\infty}^{\infty} e^{ikx}\hat{\zeta}(k,t)dk.$$

According to Parseval's identity, the norm of ζ in $\mathcal{H}^1$ can be put in the form

$$\|\zeta\|_1^2 = \int_{-\infty}^{\infty} (1+k^2)|\hat{\zeta}|^2 dk.$$

Now, using the Schwarz inequality, we get Sobolev's inequality (5.11).

It is noticed that $H \le \gamma(\delta) \equiv \gamma$ holds for all time $t > 0$ if it holds at $t = 0$ since it is invariant in time t. Finally, we use this fact to establish the stability condition for the sfKdV SSWS.

For simplicity, let us denote $A(t) = ||\zeta||$, and $B(t) = ||\zeta_x||$. Then, we have

$$
\begin{aligned}
-\frac{\beta}{2}B^2 &= H - \frac{1}{2}\int_{-\infty}^{\infty} \left[(\lambda + 2\alpha\eta_s)\zeta^2 + \frac{2\alpha}{3}\zeta^3 \right] dx \\
&\le \gamma + \frac{|\alpha|}{3\sqrt{2}}(A+B)A^2.
\end{aligned}
$$

Here, to get the last inequality, we have used Sobolev's inequality (5.11) once again. Solving this inequality yields

$$B \le F(A) \equiv \frac{\alpha}{3\sqrt{2}\beta}A^2 - \frac{1}{\beta}\left[\frac{|\alpha|}{18}A^4 - 2\beta\left(\gamma + \frac{|\alpha|}{3\sqrt{2}}A^2 \right) \right]^{\frac{1}{2}}. \qquad (5.13)$$

On the other hand, we have

$$\frac{c_0}{2}A^2 - \frac{|\alpha|}{3\sqrt{2}}(A+B)A^2 \le \gamma. \qquad (5.14)$$

Substituting (5.13) into (5.14) gives

$$G(A) \equiv \left(\frac{c_0}{2} - \frac{|\alpha|}{3\sqrt{2}}F(A)\right)A^2 - \frac{|\alpha|}{3\sqrt{2}}A^3 \leq \gamma.$$

Notice that $F(0) = \sqrt{-\frac{2\gamma}{\beta}}$ and $G(0) = G'(0) = 0$. Also, we have $G''(0) > 0$ if

$$\gamma < -\frac{9c_0^2\beta}{4\alpha^2}. \tag{5.15}$$

Two typical graphics of the function $G(A)$ are depicted in Figure 5.1.

Following Bona's arguments, we can conclude that there exists an A_γ for γ small enough such that A_γ approaches zero as γ approaches zero and $A \leq A_\gamma$ for all time $t > 0$. In turn, there also exists a B_γ such that B_γ approaches zero as γ approaches zero and $B \leq B_\gamma$ for all time $t > 0$.

Hence, by choosing δ small enough such that both (5.15) and $A^2 + B^2 \leq A_\gamma^2 + B_\gamma^2 < \varepsilon^2$ hold, we are able to establish the Lyapunov condition for the stability of an sfKdV SSWS in the Sobolev space $\mathcal{H}^1$. Hence, $\eta_s(x)$ is stable.

In the following, we would like to make several remarks about this nonlinear stability criterion.

Remark I   According to this stability criterion, the lower SSWS reported in our paper [40] and discussed in Case I of §4.2 must be stable. These results have been confirmed by our numerical simulations.

Remark II   It is also easy to prove another criterion by **Theorem 8**, which may be used to discern the stability of the uniform flow on a shelf discussed in §6.3. Since

$$\lambda + 2\alpha||\eta_s|| \geq \sqrt{\lambda^2 + 4\alpha \ || f \ ||_\infty} > 0,$$

following **Theorem 8**, we have the following corollary:

Corollary *Suppose that $\eta_s(x)$ is an SPSWS of the sfKdV BVP (3.4)–(3.5) and $\lambda^2 + 4\alpha \parallel f \parallel_\infty > 0$, then, η_s is stable if*

$$\parallel \eta_s \parallel_\infty \leq \frac{\sqrt{\lambda^2 + 4\alpha \parallel f \parallel_\infty} - \lambda}{2\alpha}.$$
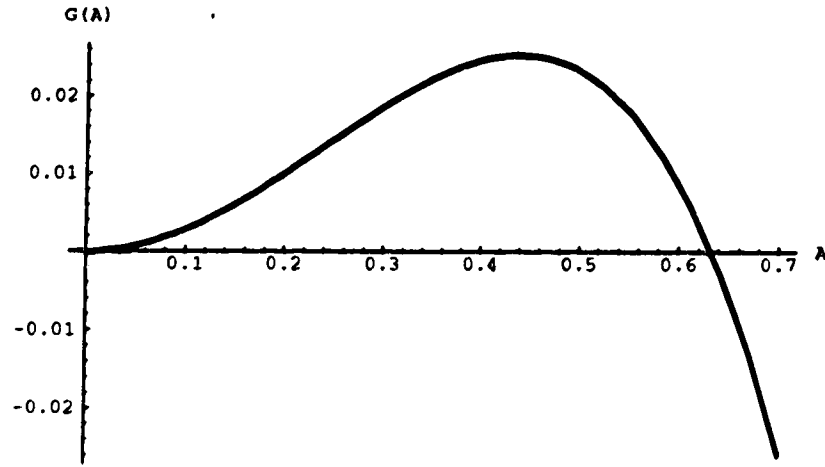
(a)
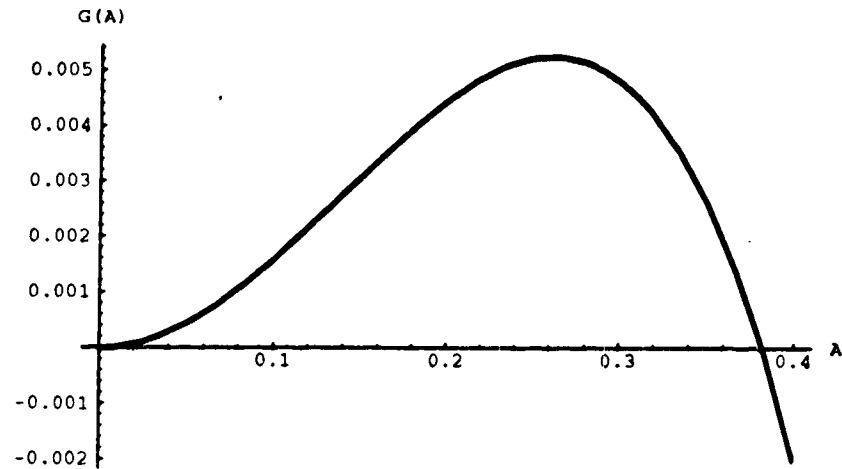
(b)

Figure 5.1: Two typical graphics of the function $G(A)$: (a) $\alpha = -3/4$, $\beta = -1/6, \gamma = 1/10, c_0 = 1$; (b) $\alpha = -3/4, \beta = -1/6, \gamma = 1/100; c_0 = 1/2$.

Remark III Following the proof of **Theorem 8**, we can also show that all negative SSWS, if they exist, must be stable.

Remark IV This stability criterion only provides a sufficient condition for the stability of an SSWS. It cannot be applied for the SSWS of the sfKdV equation which does not satisfy the condition. For example, any SSWS of the sfKdV equation with a negative forcing, i.e. $f(x) \leq 0$, does not satisfy this condition because of $\lambda + 2\alpha||\eta_s||_\infty < 0$ according to **Theorem 5**. Thus, this criterion cannot be applied for the case of a nonlocal rectangular dent discussed in Chapter 4. The stability and instability features have been illustrated by numerical simulations in our paper [14].

Remark V The condition in **Theorem 8** is simple and nice since we do not specify the shape of the forcing and the structure of the forced solitary wave. In the studies [32], [7] and [8], Camassa and Wu, Patoine and Warn restricted themselves to sech²-like forced solitary waves. With these specifications, they provided a sharper stability criterion which includes our results. Despite that our criterion is not sharp, it is applicable to a large variety of supercritical forced solitary waves and forcings. Hence, our criterion is a more general result.

Let us make a specific comparison of our results and Camassa and Wu's ones below. First, we look at the forcing defined by

$$f(x) = \frac{4}{3}(\mu - 4) \; \text{sech}^2 x.$$

Here μ is a parameter. This forcing was originally proposed by Wu [46]. In this case, the fKdV equation assumes the form

$$\eta_t + \mu\eta_x - 9\eta\eta_x - \eta_{xxx} = f_x$$

and the corresponding sfKdV equation admits a solitary wave solution

$$\eta_s(x) = \frac{4}{3}\text{sech}^2 x.$$

They proved that the above SSWS is stable when $\mu > 9$ [7]. According to our criterion, the above SSWS is stable when $\mu > 12$.

Another case is that

$$f(x) = \frac{1}{18}\alpha(12 - \alpha)\ \text{sech}^4 x.$$

Here, α is a parameter. This forcing was originally studied by Patoine and Warn [32]. In this case, the fKdV equation takes the form

$$\eta_t + 4\eta_x - 9\eta\eta_x - \eta_{xxx} = f_x$$

and the corresponding sfKdV equation admits a solitary wave solution

$$\eta_s(x) = \frac{1}{9}\alpha\ \text{sech}^2 x.$$

They showed that this SSWS is stable when $\alpha < 6$ [8]. According to our criterion, this SSWS is stable when $\alpha < 4$.

For the regions of $\mu < 9$ and $\alpha > 6$ corresponding to the above two cases, nonlinear stability analysis cannot be applied. Instead, they employed the method of asymptotic perturbation to explore linearized instability analysis. By means of this, they identified that forced solitary waves in the regions of $\mu < 9$ and $\alpha > 6$ are unstable. However, in general, the stability and instability of the sfKdV SSWS seems difficult to analyze due to their complicated structure. Thus, we seek for the numerical method to explore the stability and instability of general forced solitary waves in the next section.

5.2 Numerical investigation of the stability

Computer simulation is very helpful to discern the stability features of the sfKdV solitary waves. It may be used to verify the results obtained from mathematical analysis. Besides that, by means of numerical simulation, one can see whether an initial state is stable or unstable when mathematical theory fails to apply and how an unstable state evolves. .We have numerically shown that only one SPSWS is stable and all others are unstable in the cases of one local forcing [40] and a rectangular dent forcing [15]. In this section, we focus on numerical investigation of the stability and instability of stationary solitary waves in response to two types of forcings: (i) a rectangular bump and (ii) two δ-functions.

The fKdV equation (5.1) with a given SPSWS $\eta_s(x)$ as the initial profile is numerically solved up to a certain time t, (say, $t \leq 60$). Naturally, numerical results are approximations to the exact solutions with the error usually estimable. The small perturbation due to the truncation error (or called the numerical noise), which possesses waves of almost all wave numbers, is introduced to the system. If the solution is stable in response to this type of perturbation, then it should be stable in response to all types of perturbations. Therefore, we say that $\eta_s(x)$ is stable if this initial profile remains almost the same shape as the time evolves. Otherwise, it is unstable.

5.2.1 Chan and Kerkhoven's psuedo-spectral scheme

For the purpose of numerical simulations, the Chan and Kerkhoven's psuedo-spectral scheme [9] is extended to solve the fKdV IVP (5.1)–(5.3). This scheme was the most effective and accurate shown by Nouri and Sloan [31] and originally designed to solve

the KdV equation. The KdV equation is notorious for its fast propagation of waves possessing large wave numbers which are associated with the numerical noise. By using the Chan-Kerkhoven's scheme, the propagation of numerical noise does not occur seriously when a large integration interval and a small time step are taken and the efficiency is not yet given up.

Equation (5.1) is integrated in time by the leap-frog finite difference scheme in the spectrum space. The infinite domain in space is replaced by $-L < x < L$ with L sufficiently large and the periodic boundary condition $\eta(-L,t) = \eta(L,t)$ holds for any time $t > 0$. For a convenience, we make a substitution $X = \pi x/L + \pi$ so that the solution in X is 2π —periodic and write $s = \pi/L, u(X,t) = \eta(x,t)$ and $w = su^2$. Thus, the fKdV equation is rewritten as

$$u_t + \lambda s u_X + \alpha w_X + \beta s^3 u_{XXX} = s\frac{d}{dX}f(s^{-1}(X - \pi)), \quad 0 < X < 2\pi, t > 0. \quad (5.16)$$

Then, the interval $[0, 2\pi]$ is discretized by $N+1$ equidistant points $X_0 = 0, X_1, ..., X_{N-1}$, $X_N = 2\pi$ so that $\Delta X = 2\pi/N$, where N is always taken to be a power of 2. The numerical approximation of $u(X_j,t)$ is denoted by $U(X_j,t)$. The discrete Fourier transform of $\{U(X_j,t)|j = 0,1,2,...,N - 1\}$ is denoted by

$$\hat{U}(p,t) = \frac{1}{\sqrt{N}} \sum_{j=0}^{N-1} U(X_j,t)e^{(-2\pi jp/N)i}, p = -M, -M + 1, ..., M - 1, \quad (5.17)$$

where $M = N/2$ and $i = \sqrt{-1}$ is the imaginary unit. Taking the discrete Fourier transform of (5.16) with respect to X, we get

$$\hat{U}_t(p,t) + \lambda sip\hat{U}(p,t) + \alpha ip\hat{W}(p,t) - \beta s^3 ip^3\hat{U}(p,t) = ispF(p), \quad (5.18)$$

where $\hat{W}(p,t)$ and $F(p)$ are the discrete Fourier transforms of $\{W(X_j,t) = sU^2(X_j,t)\}_0^{N-1}$ and $\{f(s^{-1}(X_j - \pi))\}_0^{N-1}$, respectively. We adopt the leap-frog scheme to approxi-

mate for $\hat{U}_t(p,t)$ in (5.18)

$$\hat{U}_t(p,t) \approx \frac{\hat{U}(p,t+\Delta t) - \hat{U}(p,t-\Delta t)}{2\Delta t},$$

and Crank-Nicolson scheme to approximate linear dispersive term $p^3\hat{U}(p,t)$ in (5.18)

$$p^3\hat{U}(p,t) \approx p^3 \frac{\hat{U}(p,t+\Delta t) + \hat{U}(p,t-\Delta t)}{2}.$$

Given $U(X_j,t)$ and $U(X_j,t-\Delta t)$ for $j = 0,1,2,...,N-1$, we are able to calculate $\hat{U}(p,t+\Delta t)$ from (5.18) and obtain

$$
\begin{aligned}
\hat{U}(p,t+\Delta t) \;=\; & \frac{1}{1-i\beta s^3 p^3 \Delta t}\Big[\hat{U}(p,t-\Delta t) \\
& +i\beta s^3 p^3 \Delta t \hat{U}(p,t-\Delta t) - 2i\lambda s p \Delta t \hat{U}(p,t) \\
& -2i\alpha p \Delta t \hat{W}(p,t) + i s p \Delta t F(p)\Big],
\end{aligned}
$$

$$p = -M, -M+1, ..., M-1.$$

From $\{\hat{U}(p,t+\Delta t)\}_{-M}^{M-1}$, approximate solution $\{U(X_j,t+\Delta t)\}_0^{N-1}$ is resolved by inverse Fourier transformation

$$U(X_j,t+\Delta t) = \frac{1}{\sqrt{N}}\sum_{p=-M}^{M-1} \hat{U}(p,t+\Delta t)e^{(-2\pi jp/N)i}, \quad j = 0,1,...,N-1. \quad (5.19)$$

Since the leap-frog schem is used, we need to specify the values at first two time steps. By refining the time step to $\Delta t/10$, the values U at the time step Δt are calculated by

$$
\begin{aligned}
\hat{U}(p,t) \;=\; & \hat{U}(p,t-0.1\Delta t) + 0.1\Delta t[i\beta s^3 p^3 \hat{U}(p,t-0.1\Delta t) - i\lambda s p \hat{U}(p,t-0.1\Delta t) \\
& -i\alpha p \hat{W}(p,t-0.1\Delta t) + i s p F(p)]
\end{aligned}
$$

through 9 time steps from initial values assigned.

Based on the above scheme, a Mathematica program called sspsws.m (cf. Appendix C) is designed to solve the fKdV IVP (5.1)-(5.3). In order to implement

the above algorithm using Mathematica and take advantage of its command for built-in discrete Fourier transform, we change the indices $j = 0, 1, ..., N - 1$ and $p = -M, -M + 1, ..., M - 1$ to $k = j + 1$ and $q = p + M + 1$, respectively. Thus we have $\hat{V}(q, t)$ for $q = 1, 2, ..., N - 1$ in place of $\hat{U}(p, t)$ where

$$\hat{V}(q, t) = \frac{1}{\sqrt{N}} \sum_{j=0}^{N-1} V(X_j, t) e^{-2\pi i (k-1)(q-N/2-1)/N}, \quad q = 1, 2, ..., N. \quad (5.20)$$

Similarly, we have $V(k, t)$ in place of $U(X_j, t)$ such that

$$V(k, t) = \frac{1}{\sqrt{N}} \sum_{q=1}^{N} \hat{V}(q, t) e^{2\pi i (k-1)(q-N/2-1)/N}, \quad k = 1, 2, ..., N. \quad (5.21)$$

5.2.2 Numerical results

Let us illustrate our numerical calculations for two specific forcings below. All numerical computations are implemented on an HP 9000/755 workstation in the Department of Mathematics at the University of Alberta.

CASE I.   The forcing of a rectangular bump

In this case, all parameters are taken to be $\lambda = 1.5$, $\alpha = -3/4$, $\beta = -1/6$, $\gamma = 1$, and $a = 1$. The sfKdV BVP (3.4)–(3.5) has two SPSWS as shown in §4.1.2, **Case I** (i). According to the nonlinear stability criterion, the lower SSWS must be stable. This is confirmed by our numerical computation. Figure 5.2 (a) exhibits the evolution of the lower SPSWS $\eta_s^{(1)}(x)$ (solid line in Figure 4.1 (b)). The norm of $\zeta(x, t)$ in l^2 space is depicted in Figure 5.2 (b).

It is also noticed that the wave resistance coefficient

$$C_{D_w}(t) \equiv - \int_{-\infty}^{+\infty} f\eta_x dx = \frac{1}{2} \frac{d}{dt} \int_{-\infty}^{+\infty} \eta^2 dx, \quad (5.22)$$

introduced by Wu [46], characterizes the energy balance of the wave evolution. This quantity can be used to discern the instability feature of an SPSWS as well. Namely,

the stationary solution $\eta_s(x)$ is said to be unstable if the wave resistance coefficient $C_{D_w}(t)$ oscillates within computing time. Otherwise, it is stable. For a rectangular bump forcing, the wave resistance coefficient $C_{D_w}(t)$ is simply written as

$$C_{D_w}(t) = \eta(-a/2, t) - \eta(a/2, t).$$

Figure 5.2 (c) displays the curve of the wave resistance coefficient $C_{D_w}(t)$ versus time t. Thus, this SPSWS is stable since the initial wave profile remains in the same shape up to time $t = 50$ and the curve of the wave resistance coefficient $C_{D_w}(t)$ is almost flat. In the computation, we take $L = 8$, $\Delta x = 16/512$ and $\Delta t = 0.01$.

eta(x, t)
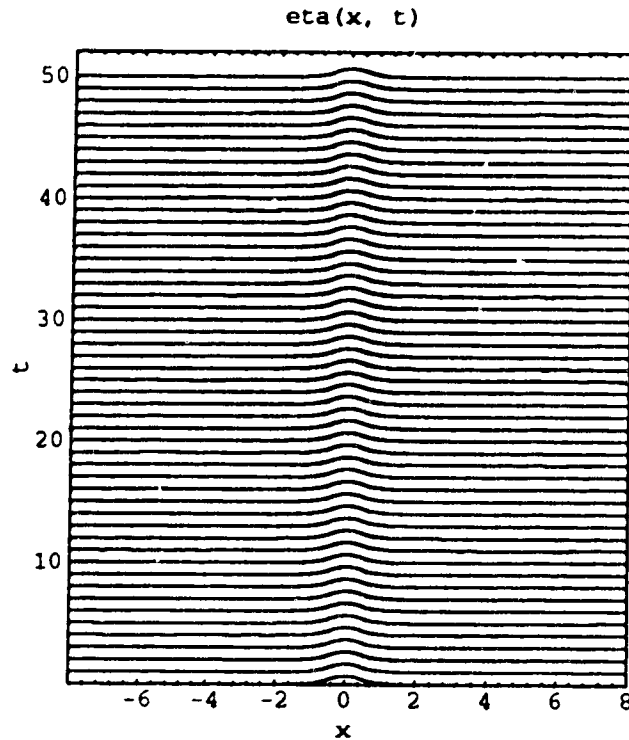
(a)
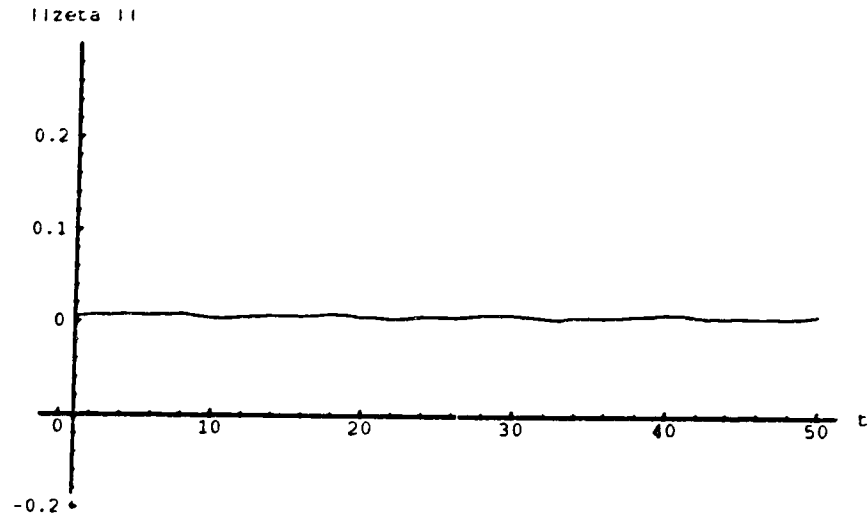
(b)
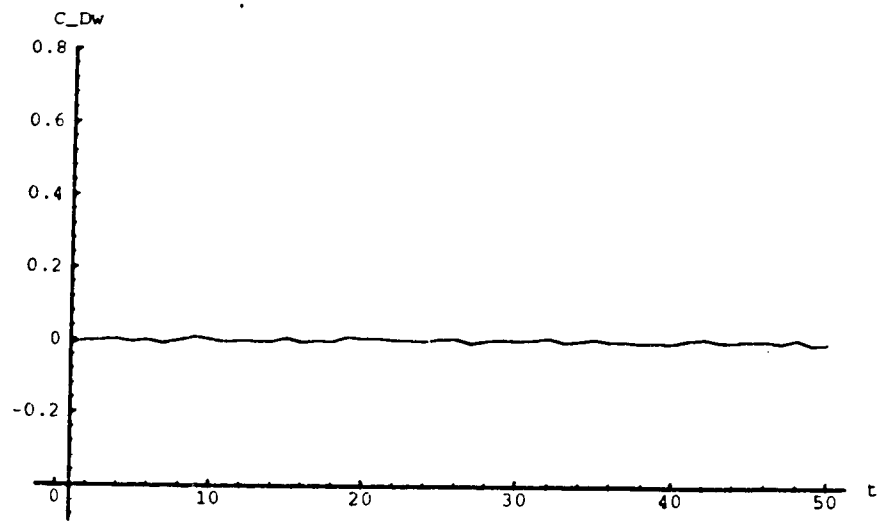
(c)

Figure 5.2:   (a) Evolution of the stable SPSWS $\eta_s^{(1)}(x)$ corresponding to the solid line in Figure 4.1 (b);   (b) The norm of $\zeta(x,t)$ in l^2 space versus time t;   (c) The curve of the wave resistance coefficient $C_{D_w}(t)$ versus time t.

Figure 5.3 (a) displays the evolution of the higher SPSWS $\eta_s^{(2)}(x)$ up to $t = 25$. The plot domain in x space is $(-30, 90)$. This SPSWS is unstable since the wave profile changes the shape of initial state after a certain time step. The system evolves into the stable state shown in Figure 5.2 (a) and generates a soliton advancing along the upstream while a train of dispersive waves propagates away along the downstream. In the computation, we take $L = 30$, $\Delta x = 120/512$ and $\Delta t = 0.01$. The package sspsws.m shown in Appendix C needs to be modified a little for the domain $(-L, 3L)$ in place of $(-L, L)$.

eta(x, t)
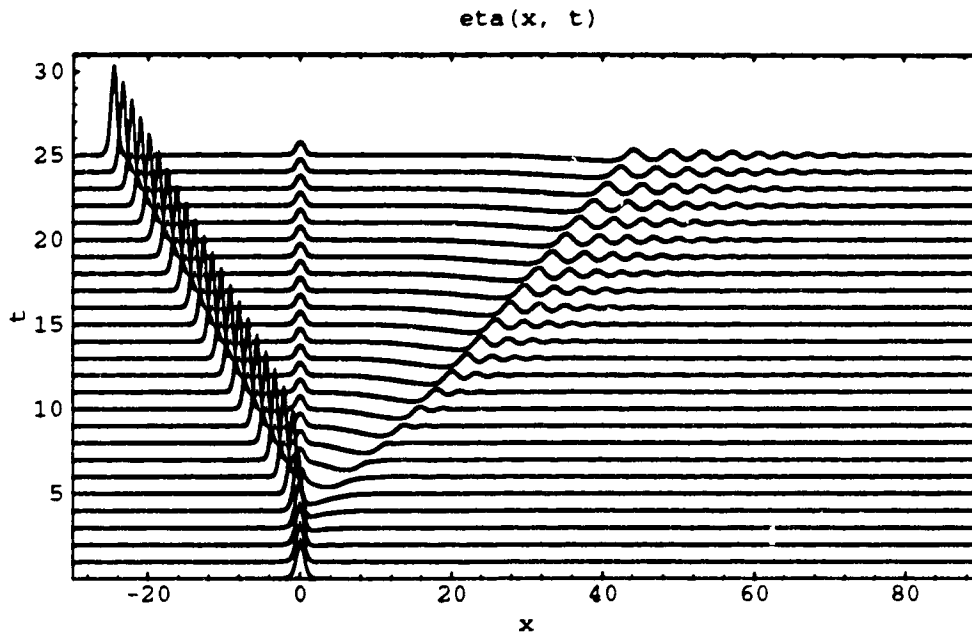
Figure 5.3: Evolution of the SPSWS $\eta_s^{(2)}(x)$ corresponding to the dashed line in Figure 4.1 (b).

CASE II.   The forcing of two δ-functions

In our numerical computation for the case of two local forcings, we take all parameters specified in §4.2, $\lambda = 1$, $\alpha = -3/4$, $\beta = -1/6$, $P_1 = P_2 = 0.5$ and $a = 1$. Then the forcing function and its discrete Fourier transform are approximated by

$$f(x) = 0.5 \left[\delta(x+1) - \delta(x-1) \right] \quad \text{and} \quad F(p) = 0.5pN \, \cos(sp)/(2L).$$

As we have shown in §4.2, the sfKdV BVP (3.4)-(3.5) has four SPSWS in this case. According to our numerical simulation, only one SPSWS is stable and all the others are unstable. The results are displayed throughout Figure 5.4-8.

Figure 5.4 exhibits the evolution of the symmetric SPSWS $\eta_s^{(1)}(x)$ (solid line in Figure 4.9 (a)). This SPSWS is stable since the initial wave profile remains in the same shape up to time $t = 50$. In the computation, we take $L = 12$, $\Delta x = 24/512$ and $\Delta t = 0.01$.

Figure 5.5 displays the evolution of another symmetric SPSWS $\eta_s^{(2)}(x)$ up to $t = 35$. This SPSWS is unstable since the wave profile changes the shape of initial state after a certain time steps. The system evolves into the stable state shown in Figure 5.4, and generates a soliton advancing along the upstream while a train of dispersive waves propagates away along the downstream. In the computation, we take $L = 40$, $\Delta x = 80/512$ and $\Delta t = 0.02$. To display the main character of the wave propagation, we only plot the wave profiles in the space domain $(-25, 40)$.

Figure 5.6 (a) displays the evolution of initial profile $\eta(x, 0) = \eta_s^{(3)}(x)$ up to $t = 60$. Figure 5.6 (b) shows four profiles of wave propagation corresponding to $t = 5, 15, 25, 35$. According to these numerical results, this nonsymmetric SPSWS is unstable as well and it eventually evolves into the stable steady-state with only some weak radiation downstream. In the computation, the infinite domain in space

is taken as $(-L, 3L)$ to display the main character of the wave propagation, $L = 20, \Delta x = 80/512$ and $\Delta t = 0.02$.

(a)

(b)
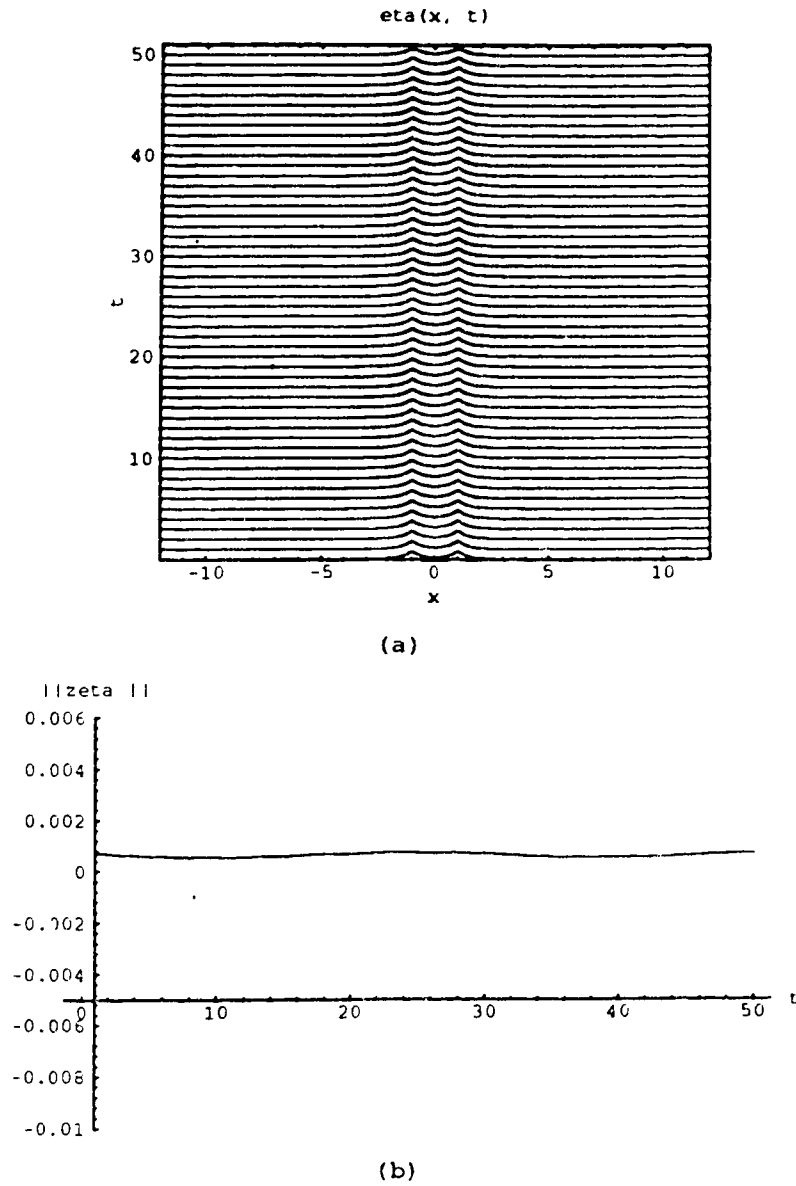
Figure 5.4: (a) Evolution of the stable SPSWS $\eta_*^{(1)}(x)$ corresponding to the solid line in Figure 4.9 (a); (b) The norm of $\zeta(x, t)$ in l^2 space versus time t.
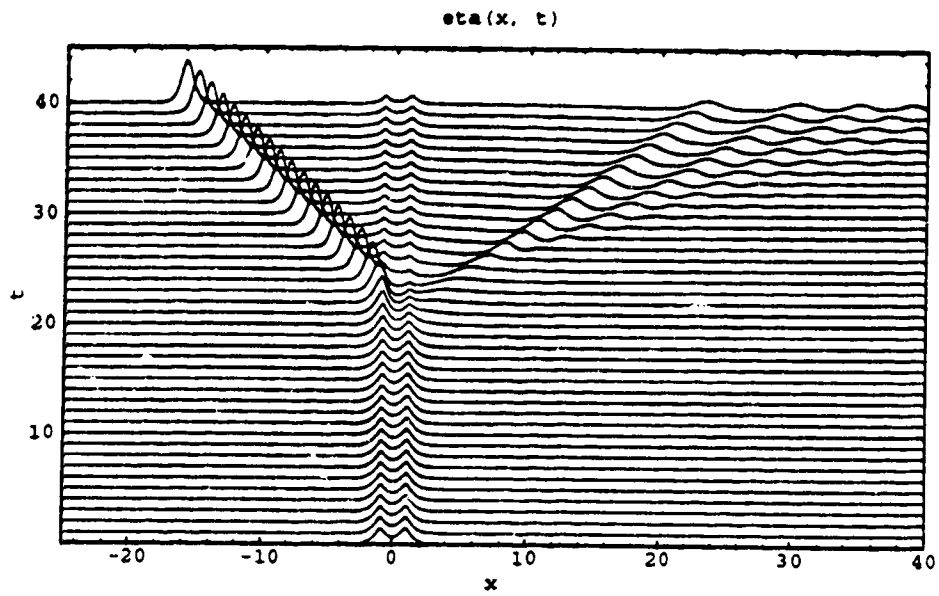
Figure 5.5: Evolution of the symmetric SPSWS $\eta_s^{(2)}(x)$ corresponding to the dashed line in Figure 4.9 (a).

(a)

(b)
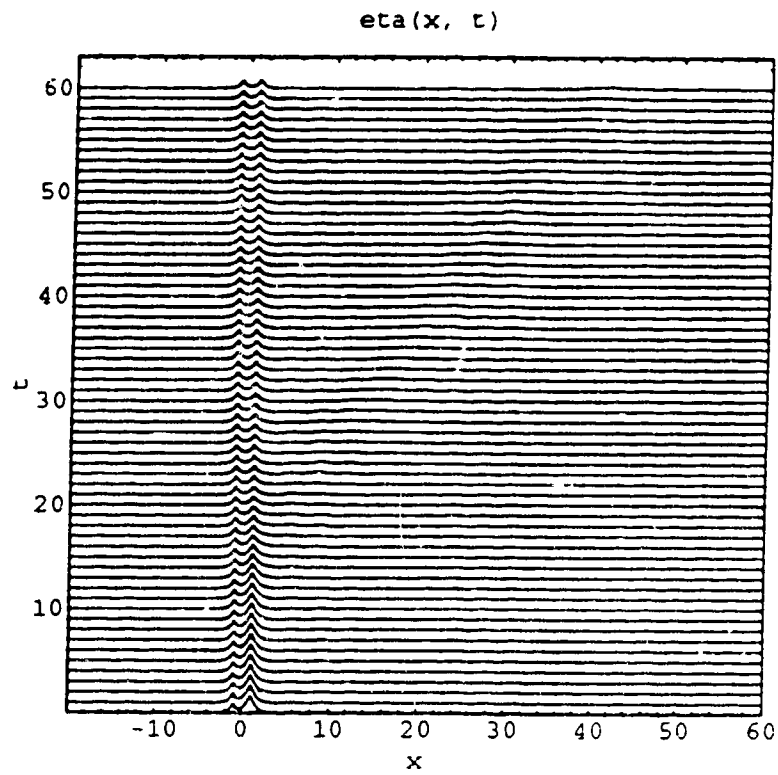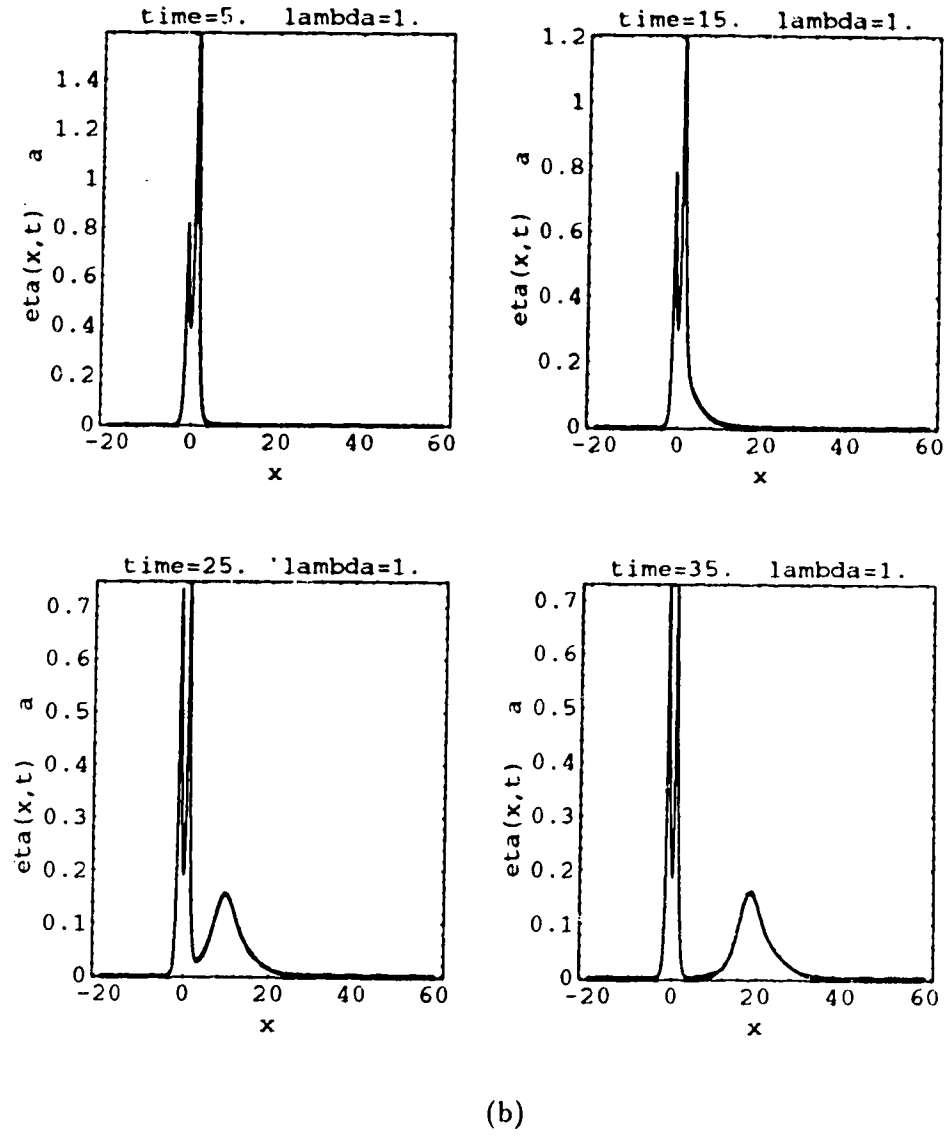
Figure 5.6: (a) Evolution of the symmetric SPSWS $\eta_s^{(3)}(x)$ corresponding to the dashed line in Figure 4.9 (b). (b) Four wave profiles at time $t = 5$, 15, 25, 35.

Figure 5.7 (a) displays the evolution of another nonsymmetric SPSWS up to $t = 60$. Figure 5.7 (b) shows four profiles of wave propagation corresponding to $t = 1$, 10, 20, 30. According to these numerical results, this nonsymmetric SPSWS is unstable as well and it eventually evolves into the stable steady-state with only some weak radiation downstream. In the computation, the infinite domain in space is taken as $(-L, 3L)$ to display the main character of the wave propagation, $L = 20, \Delta x = 80/512$ and $\Delta t = 0.02$.

eta(x, t)

(a)

(b)
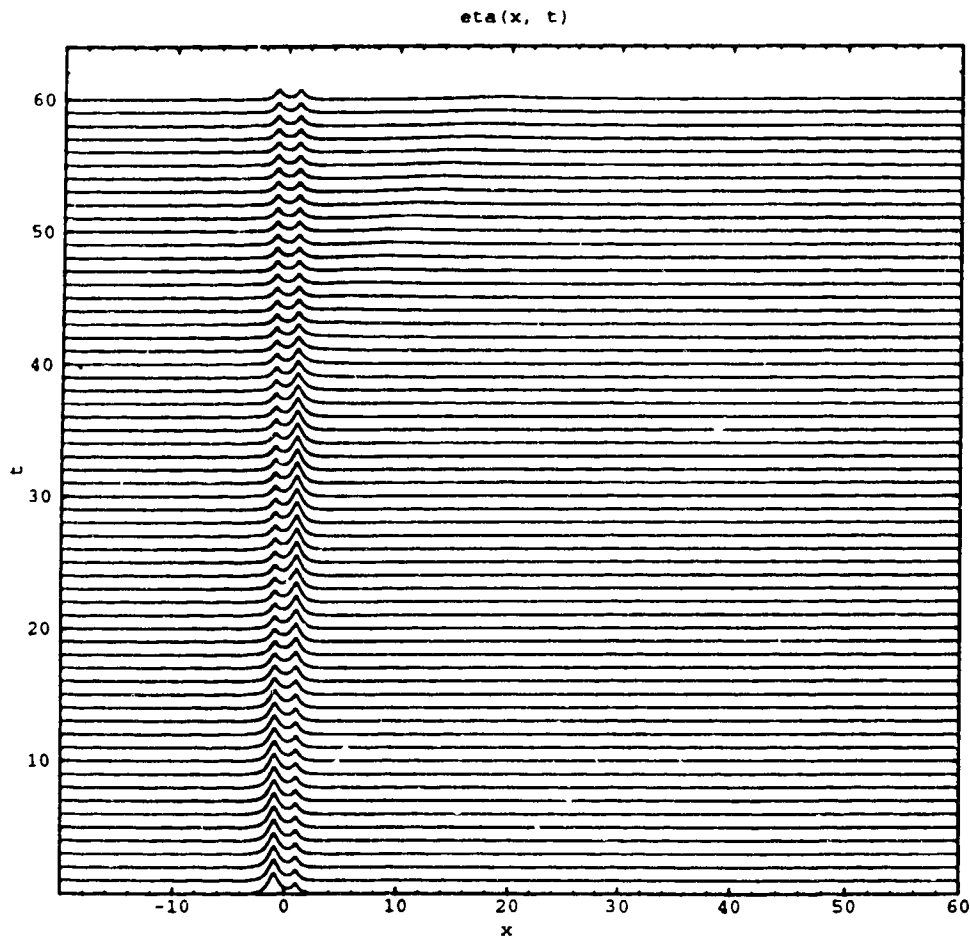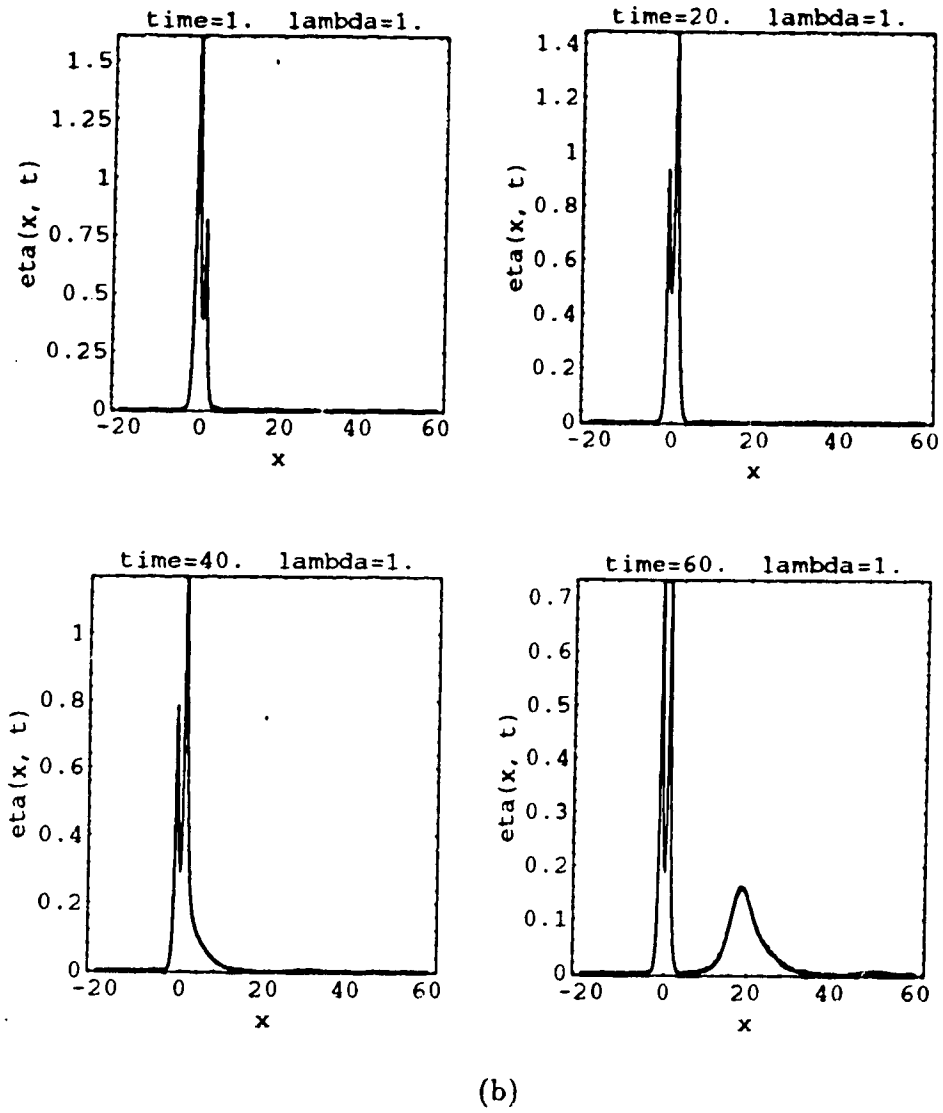
Figure 5.7: (a) Evolution of the symmetric SPSWS $\eta_s^{(4)}(x)$ corresponding to the dot-dashed line in Figure 4.9 (b). (b) Four wave profiles at time $t = 1$, 20, 40, 60.

It is clearly observed that there is a "basin of attraction" in the system. Indeed, the system absorbs energy initially in generating the stable stationary wave in the vicinity of the forcing. The terminology "the basin of attraction" is adopted from Camassa and Wu's paper [7]. Besides the above, there is another interesting feature of the fKdV system. By observing Figure 5.5, we find that a single soliton is generated by the external forcing and advances along the upstream while a train of dispersive waves propagate away along the downstream. It is different from the periodic generation of solitons, discovered by Wu and Wu [47], in transcritical region. This leads us to conjecture that this fKdV system in supercritical region might also generate one soliton running away along the upstream provided that the initial state possesses enough mass. Figure 5.8 demonstrates another evidence of this conjecture, which is to be studied further.
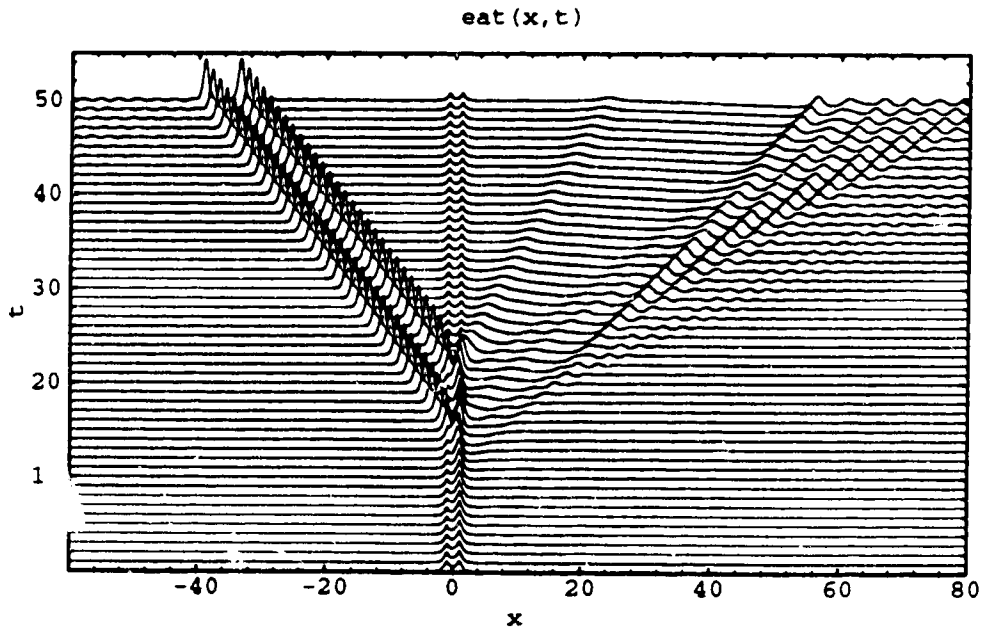
Figure 5.8: Evolution of the initial profile $\eta(x,0) = 0.8\ \eta_s^{(2)}(x)$ in the fKdV system.

Chapter 6

Solitary Waves on a Shelf

The study in this chapter is concentrated on free-surface waves of a steady open channel flow over a shelf as depicted in Figure 6.1. The motivation of the study is to reveal a qualitative description of wave motion in the ocean disturbed by a long body steadily moving close to the seabed. The application of this problem may be found in hydraulic and coastal engineering.

The sfKdV equation (3.1) is used to model this physical problem. Particularly, the shelf forcing can be put in the form $f(x) = (P/2)\mathcal{H}(x)$, where P is a positive constant representing the height of the shelf and $\mathcal{H}(x)$ is a Heaviside unit step function in dimensionless variables, i.e. $\mathcal{H}(x)$ takes the value 1 for $x > 0$ and vanishes for $x < 0$. The parameters α and β are negative constants.

By solving an sfKdV BVP, we have found that there are two branches of stationary waves: the solitary wave branch (§6.2) and the uniform flow branch (§6.3) [38]. For the first branch, an almost complete solitary wave profile is sustained on the downstream shelf and a tail of a solitary wave, whose base is lower than that of the downstream one, remains in the upstream flat bottom. There is a smooth transition

73
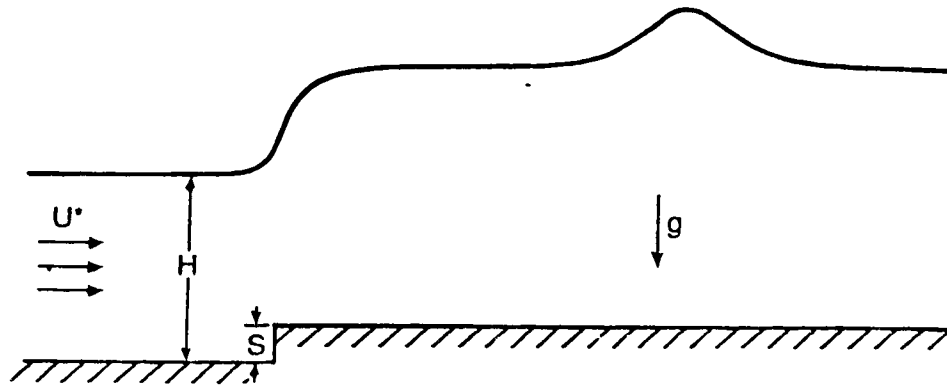
Figure 6.1: The sketch of a stationary solitary wave on the shelf

region which connects the downstream solitary wave with the upstream tail. This stationary solitary wave is different from the case of a solitary wave that surges from an upstream deeper water zone to a downstream shelf and disintegrates into a train of smaller solitary waves, which is a soliton fission problem, as first studied by Madsen and Mei [23]. A second branch of uniform flow solutions can be found analytically, which agree with the results obtained through numerical computation by King and Bloor [18]. According to the criterion described in §5.1.2, this uniform flow branch is stable, but, the numerical simulations await future research since the package "sspsws.m" cannot work for non-periodic boundary conditions.

6.1 Mathematical description

Let us first give a complete mathematical description of the problem. For the shelf forcing, the boundary condition $\eta(+\infty) = b$ is required, where b is a positive constant. Hence, the first order asymptotic approximation of the elevation of the free surface and the boundary conditions satisfy the following sfKdV BVP

$$\lambda \eta_x + 2\alpha \eta \eta_x + \beta \eta_{xxx} = \frac{P}{2} \mathcal{H}_x, \quad -\infty < x < \infty, x \neq 0 \tag{6.1}$$

$$\eta(-\infty) = 0, \ \eta(\infty) = b, \tag{6.2}$$

$$\eta_x(\pm\infty) = \eta_{xx}(\pm\infty) = 0. \tag{6.3}$$

Any solution $\eta(x)$ of the sfKdV BVP (6.1)–(6.3) must have the first order continuous derivative for all $x \in \mathcal{R}$, i.e., $\eta(x) \in \mathcal{C}^1$ and the second order continuous derivative for all $x \in \mathcal{R}$ except at $x = 0$. Under this circumstance, integrating (6.1) and using (6.2)–(6.3) yields

$$\lambda b + \alpha b^2 = \frac{P}{2}. \tag{6.4}$$

Therefore, there are two possible values for b, i.e.,

$$b_\pm = \frac{-\lambda \pm \sqrt{\lambda^2 + 2\alpha P}}{2\alpha}, \tag{6.5}$$

if $\lambda^2 \geq -2\alpha P$. It is easy to show that when $b = b_-$, the sfKdV BVP (6.1)–(6.3) has no bounded solution satisfying $\eta(+\infty) = b_-$.

Theorem 9 *When* $\lambda^2 \geq -2\alpha P$, *the* sfKdV BVP (6.1)–(6.3) *has no bounded solution, which approaches* b_- *as* x *approaches* ∞.

Proof: Suppose that $\eta(x)$ be a bounded solution of the sfKdV BVP (6.1)–(6.3) with $\eta(+\infty) = b_-$. By a standard procedure, integrating twice (6.1) and using

(6.2)–(6.3), we have

$$\eta_x^2 = -\frac{2\alpha}{3\beta}(W_- + \eta)(b_- - \eta)^2, \quad x > 0, \tag{6.6}$$

where

$$W_- = \frac{\lambda - 2\sqrt{\lambda^2 + 2\alpha P}}{2\alpha}. \tag{6.7}$$

From (6.6), we have $W_- + \eta \leq 0$ for all $x > 0$. Particularly, $W_- + b_- \leq 0$. This is a contradiction with the fact $W_- + b_- = -3\sqrt{\lambda^2 + 2\alpha P}/(2\alpha) > 0$.

Hence, we take only b_+ in (6.5) to search for the solutions of the sfKdV BVP (6.1)–(6.3) for $\lambda > \lambda_C = \sqrt{-2\alpha P}$ and a given P. Before presenting two branches of solutions to the sfKdV BVP (6.1)–(6.3) we would like to show that the value of any solution $\eta(x)$ at $x = 0$ can be determined by the continuity of η and η_x.

Theorem 10 *Suppose that $\eta(x)$ is a solution to the* sfKdV BVP (6.1)–(6.3). *Then, for $x < 0$,*

$$\eta(x) = -\frac{3\lambda}{2\alpha}sech^2\left\{\sqrt{\frac{\lambda}{-4\beta}}\left[x - \sqrt{\frac{4\beta}{-\lambda}}arcsech\sqrt{-\frac{2\alpha}{3\lambda}\eta(0)}\right]\right\}, \tag{6.8}$$

where

$$\eta(0) = \frac{b_+(2P - \lambda b_+)}{3P}.$$

Proof: It is well-known that, for $x < 0$,

$$\eta(x) = -\frac{3\lambda}{2\alpha}sech^2\left\{\sqrt{\frac{\lambda}{-4\beta}}\left[x - \sqrt{\frac{4\beta}{-\lambda}}arcsech\sqrt{-\frac{2\alpha}{3\lambda}\eta(0)}\right]\right\}$$

Integrating (6.1)–(6.3) over $(-\infty, 0)$ and $(0, \infty)$ twice, respectively, then using the continuity conditions of η and η_x at $x = 0$, we can get

$$\eta(0) = b_+ - \frac{\lambda}{P}b_+^2 - \frac{2\alpha}{3P}b_+^3.$$

Further, by (6.4), we have

$$\eta_0 \equiv \eta(0) = \frac{b_+(2P - \lambda b_+)}{3P}.$$

Hence, the remainder of this problem is to solve a mixed initial value and boundary value problem of the following first order differential equation

$$\frac{3\beta}{2\alpha}(\eta_x)^2 = (W_+ - \eta)(b_+ - \eta)^2, \quad x > 0, \tag{6.9}$$

$$\eta(0) = \eta_0, \quad \eta(+\infty) = b_+, \tag{6.10}$$

where $\eta_0 = (b_+ P - \lambda b_+^2)/(3P)$ and $W_+ = -2b_+ - (3\lambda)/(2\alpha)$.

6.2 Solitary wave branch

We would like to find solutions with $\eta(x) > b_+$ for sufficiently large $x > 0$. The solution for sufficiently large $x > 0$ might be taken in the form

$$\eta(x) = b_+ + (W_+ - b_+)\text{sech}^2 \left\{ \left[\frac{\alpha(W_+ - b_+)}{6\beta} \right]^{1/2} (x - L_1) \right\}.$$

However, we use the ODE solver in Mathematica called NDSolve (cf. Appendix D) to search for this branch of solutions. Some solutions for given parameters $\alpha = -3/4$ and $\beta = -1/6$ are displayed in Figure 6.2, which shows that the upstream flow is a solitary wave tail and the downstream flow is an almost complete solitary wave whose base is higher than that of the upstream solitary wave tail. There is a smooth transition region where the upstream solitary wave tail is connected with the base of the downstream solitary wave. This branch is referred to as *solitary wave branch*.

The existence of solitary waves on a shelf, although not rigorously proved mathematically, can be intuitively justified. It is well known that there exists a stable

solitary wave in each single-layer free-surface flow at a supercritical speed. A bottom obstruction, such as a shelf, only alters the shape of the solitary wave called the free solitary wave, in the flat channel, but does not completely remove it. The altered solitary wave is considered to be a perturbation of the free solitary wave by the obstruction as explained by Vanden-Broeck [43]. The existence of the free solitary wave was mathematically proved by Amick and Turner [3], and was numerically justified by Turner and Vanden-Broeck [42].

6.3 Uniform flow branch

By a standard procedure, under the assumption $\eta < b_+$, integrating (6.9)–(6.10) once yields the following solution for $x > 0$

$$\eta(x) = b_+ + (b_+ - W_+)\text{csch}^2\left[\sqrt{\frac{\alpha(W_+ - b_+)}{6\beta}}x + \text{arccoth}\sqrt{\frac{W_+ - \eta_0}{W_+ - b_+}}\right]. \qquad (6.11)$$

Therefore, an analytic expression for a second branch of solutions can be written as

$$\eta(x) = -\frac{3\lambda}{2\alpha}\text{sech}^2\left\{\sqrt{\frac{\lambda}{-4\beta}}\left[x - \sqrt{\frac{4\beta}{-\lambda}}\text{arcsech}\sqrt{-\frac{2\alpha}{3\lambda}\eta_0}\right]\right\} \qquad (6.12)$$

when $x < 0$ and

$$\eta(x) = b_+ + (b_+ - W_+)\text{csch}^2\left[\sqrt{\frac{\alpha(W_+ - b_+)}{6\beta}}x + \text{arccoth}\sqrt{\frac{W_+ - \eta_0}{W_+ - b_+}}\right] \qquad (6.13)$$

when $x \geq 0$.
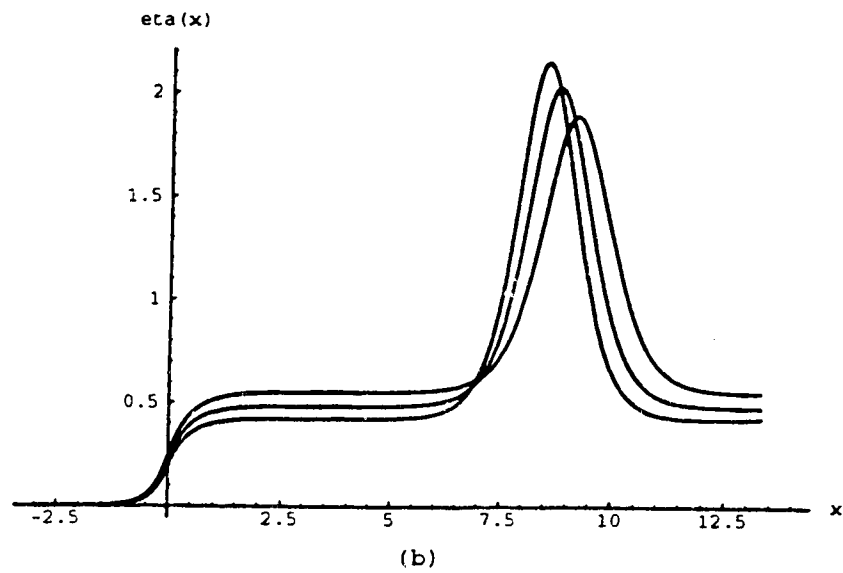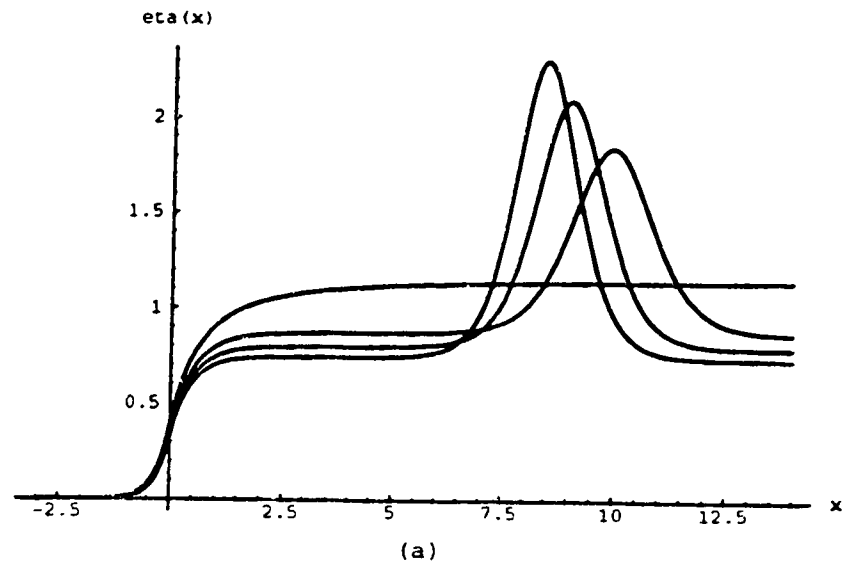
Figure 6.2: (a) Solitary waves on the shelf for fixed $P = 2$ and different $\lambda = \sqrt{3}, 1.8, 1.85, 1.9$. (b) Solitary waves on the shelf for fixed $\lambda = 1.5$ and different $P = 1.0, 1.1, 1.2$

Graphics of solutions on this branch are shown in Figure 6.3 for given parameters $\alpha = -3/4$ and $\beta = -1/6$, which shows that the upstream flow is a solitary wave tail and the downstream flow is an opposite solitary wave tail. Also, there is a smooth transition region that connects the upstream solitary wave tail and the downstream solitary wave tail. This branch is referred to as *uniform flow branch*. According to **Corollary** in §5.1.3, all uniform flows must be stable since $\eta < b_+$.

The bifurcation diagrams in terms of the amplitude of two branch solutions against the upstream velocity for fixed the height of the forcing and the height of the forcing for fixed the upstream velocity are displayed in Figure 6.4 (a) and (b). The dashed line stands for the solitary wave branch and the solid line represents the uniform flow branch. Figure 6.4 (a)-(b) demonstrates that (i) the amplitude of downstream solitary waves on the solitary wave branch is proportional to the upstream velocity and inversely proportional to the height of the shelf is fixed; (ii) the downstream elevation on the uniform flow branch is inversely proportional to the upstream velocity and proportional to the height of the shelf.
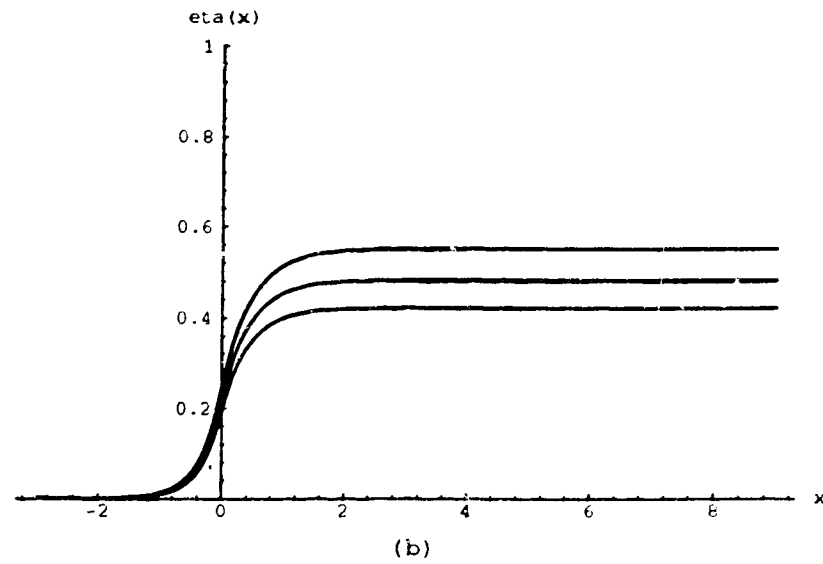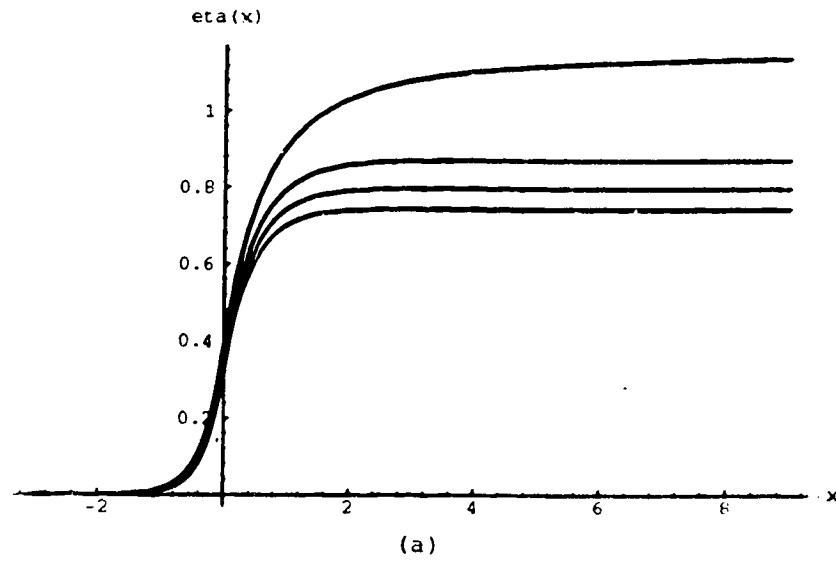
Figure 6.3: (a) Uniform flows on the shelf for fixed $P = 2$ and different $\lambda = \sqrt{3}, 1.8, 1.85, 1.9$. (b) Uniform flows on the shelf for fixed $\lambda = 1.5$ and different $P = 1.0, 1.1, 1.2$
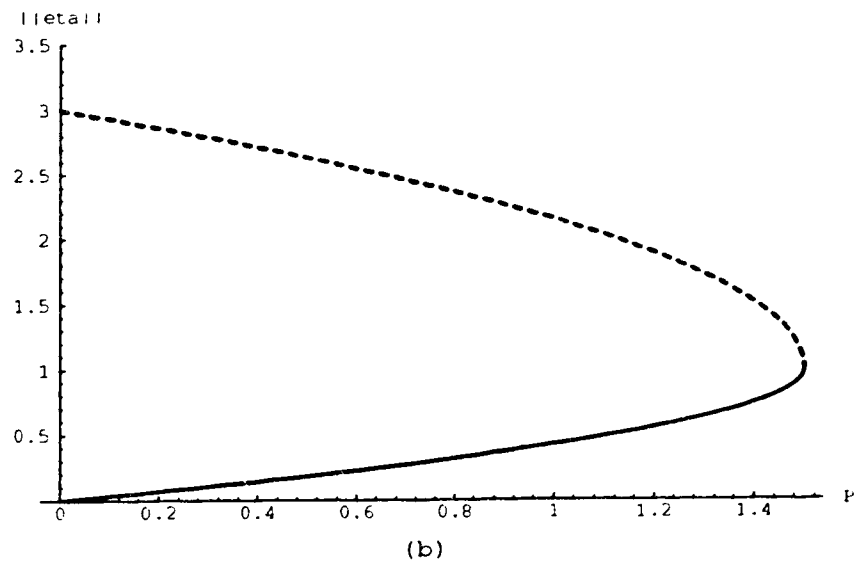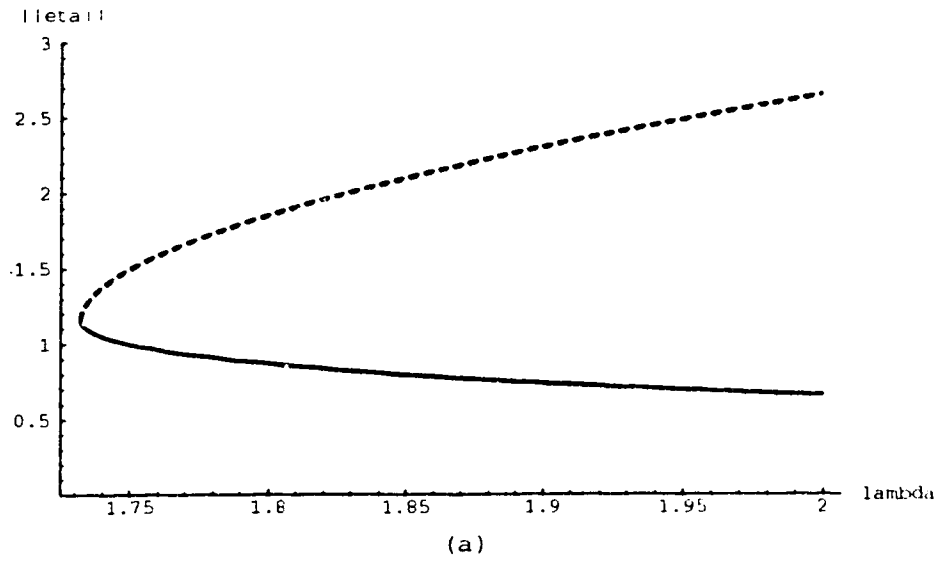
Figure 6.4: (a) Bifurcation diagram of two branch solutions to the sfKdV BVP (6.1)-(6.3) with $P = 2$. (b) Bifurcation diagram of two branch solutions to the sfKdV BVP (6.1)-(6.3) with $\lambda = 1.5$.

Chapter 7

Experimental Validation of the sfKdV model

The fKdV model has been used often since 1984 to describe the motion of two dimensional free-surface waves of an inviscid and incompressible fluid flow over an obstruction in a channel. The validity of this asymptotic model is a noteworthy question and seems impossible to be proved analytically. Much evidence from computational and experimental results has shown that the fKdV model is a good model to within the error of less than 10% when the height of the bump is lower than half of the upstream depth (cf. [21] and [36]). In this chapter, we investigate experimentally stationary open channel flows over a bump to check the validity of the sfKdV model for forced stationary solitary waves and hydraulic falls. The experimental work on forced stationary solitary waves seems not appeared in literature before, although analogue experiments for hydraulic falls were conducted by Forbes (referred to as the critical flow there) [12] and Sivakumaran, et al. [41].

The experimental setup is described in §7.1. All experimental results and their

comparisons with theoretical results obtained from the sfKdV model for forced stationary solitary waves and hydraulic falls will be presented in §7.2 and §7.3, respectively. Meanwhile, the uncertainty of the experiments is analyzed, which seems not to have been reported in the previous literature.

7.1 Experimental apparatus

The experiments are performed in a top-open flume made of a steel frame with glass windows on both vertical side walls and the aluminum bed about 7500 mm long, 650 mm deep and 465 mm wide in T. Blench Hydraulics Laboratory at the University of Alberta (shown in Plate 7.1).

Plate 7.1   Experimental apparatus
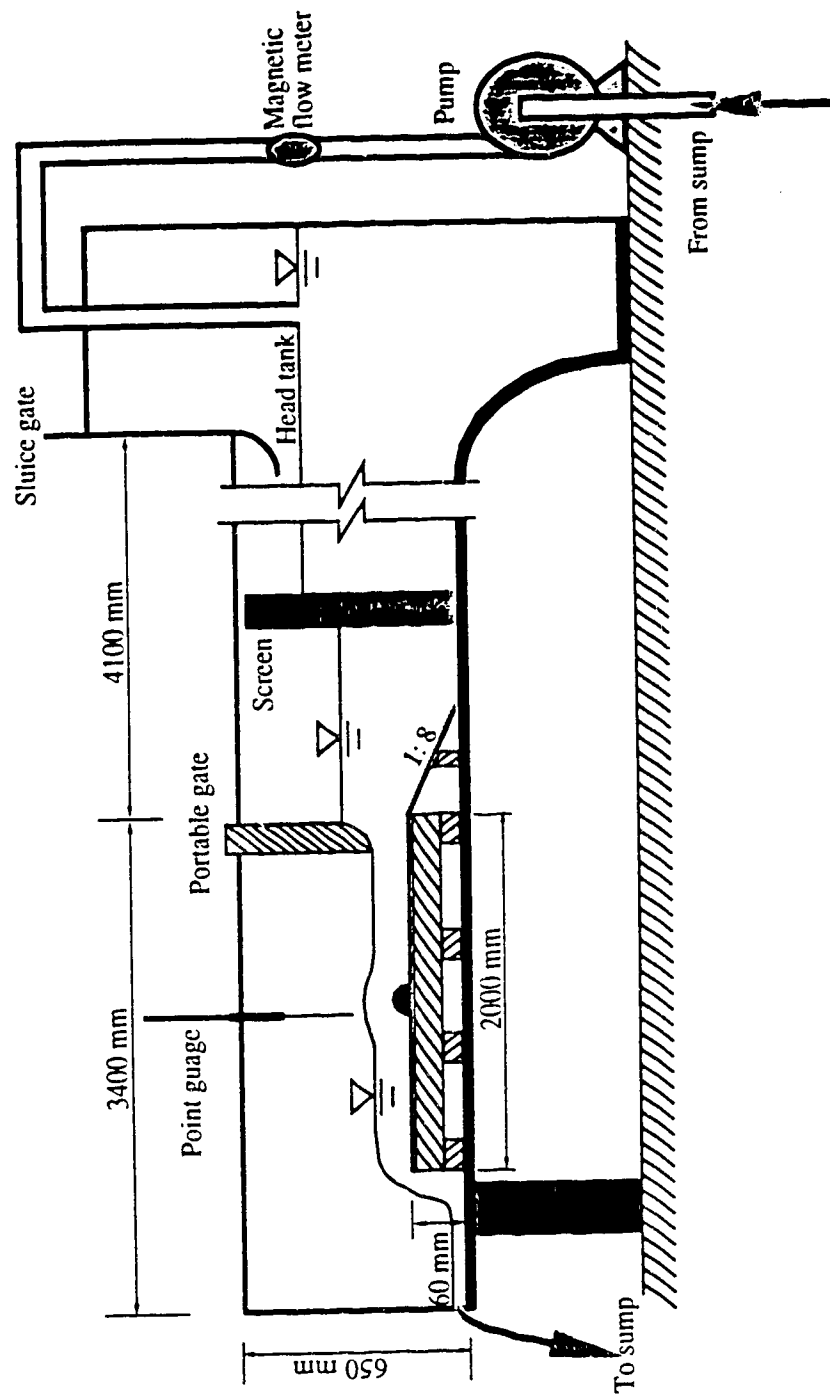
Figure 7.1 Experimental setup

As shown in Figure 7.1, water is pumped into the head tank from the sump. The water discharge Q is controlled by the pump and measured by a magnetic flow meter (1 voltage/sec = 15 litre/sec). The velocity of the flow is then calculated by Q/A, where A is the area of the channel cross section. A portable point gauge is placed on the top frame of the flume to measure the depth of the water at different cross sections along the center line of the flume.

In order to reduce the turbulence of the inflow, a portable gate with a streamline lip is inserted in the flume about 4200 mm distance from the head tank and a screen is placed in the middle of the portable gate and the sluice gate of the head tank. This portable gate is also used to control the depth of the upstream inflow. In addition, we put a piece of 2000 mm long, 465 mm wide and 6 mm thick white plastic board into the flume about 4100 mm distance from the head tank to diminish the roughness of the original bed where there are many holes. To improve the inflow and maintain the downstream supercritical flow, the plastic board is lifted up to about 60 mm high above the original bed so that the length of the valid channel is suitable for testing both forced solitary waves and hydraulic falls.

In our experiments, two different bumps made of clear plastic glass are used, which are referred to as Bump I and Bump II, respectively. Both bumps are a segment of a piece of cylindric pipe with the radius $r = 31.5$ mm. Bump I (flat bump or nonlocal forcing) with the base length $b = 46$ mm and the height $h_c = 10$ mm is used for testing forced stationary solitary waves. Instead, Bump II (high bump or local forcing) with the base length $b = 60$ mm and the height $h_c = 22$ mm is used for testing hydraulic falls. The purpose of using a flatter cylindric segment for testing forced stationary solitary waves is to reduce the effect of the flow separation on the free surface. Instead, when testing hydraulic falls, a higher bump is used to

avoid the occurrence of the downstream hydraulic jump.

7.2 Forced stationary solitary waves

In this section, let us illustrate the experimental results of supercritical forced stationary solitary waves and compare them with those obtained from the sfKdV model. Meanwhile, the uncertainty of the experiment is also analyzed.

7.2.1 Experimental results

A series of experiments have been done for forced supercritical stationary solitary waves. Plate 7.2 displays two pictures of two-dimensional supercritical stationary solitary waves sustained on the bump, which are modelled by the sfKdV equation. In (a) and (b), the flow has the same upstream depth $H = 47$ mm and the different upstream Froude number $F = 1.32$ and 1.46. Here the upstream Froude number is defined as the ratio of the velocity U of the upstream flow to the shallow water wave speed $\sqrt{gH}$, i.e. $F = U/\sqrt{gH}$. The flows at both upstream and downstream are uniform. It is clear that the amplitude of the free surface decreases as the upstream velocity increases for a fixed depth of the upstream flow. Indeed, the amplitude of the free surface is 58 mm in (a) and 55 mm in (b). Also, a real water flow has a nonsymmetric free-surface wave profile, i.e., the downstream free surface is a little higher than the upstream. This nonsymmetric phenomenon might be due to the effects of sidewall friction and the flow stagnation points on the bump, but, the real reason seems still not clear.

Further, Plate 7.3 (a) demonstrates another two-dimensional water surface in the case of the upstream depth $H = 34$ mm and the Froude number $F = 1.48$. Plate

7.3 (b) displays the three-dimensional picture of the free surface corresponding to Plate 7.3 (a). Small ripples on the upstream free surface generated by the sidewalls

FORCED SOLITARY WAVE

(a)
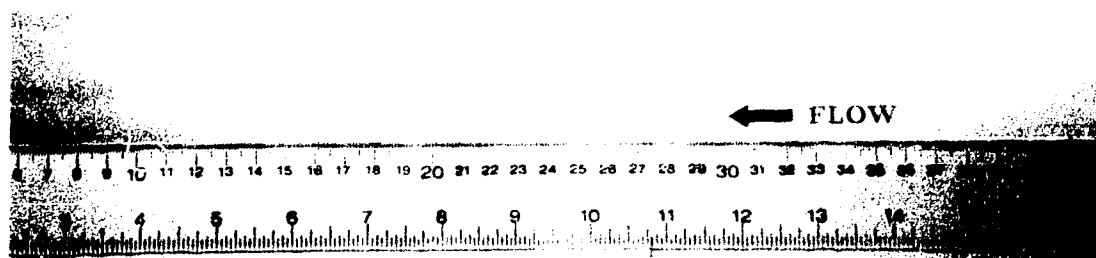
FORCED SOLITARY WAVE
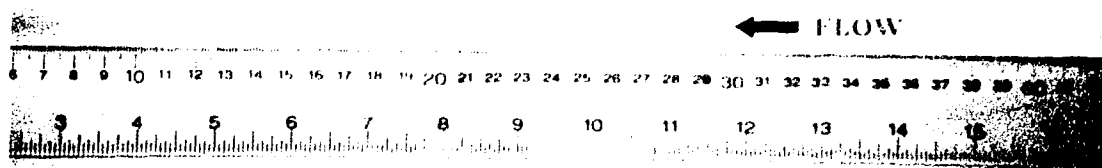
(b)

Plate 7.2   Two-dimensional forced solitary waves: (a) $H = 47$ mm, $F = 1.32$; (b) $H = 47$ mm, $F = 1.46$.

FORCED SOLITARY WAVE

(a)
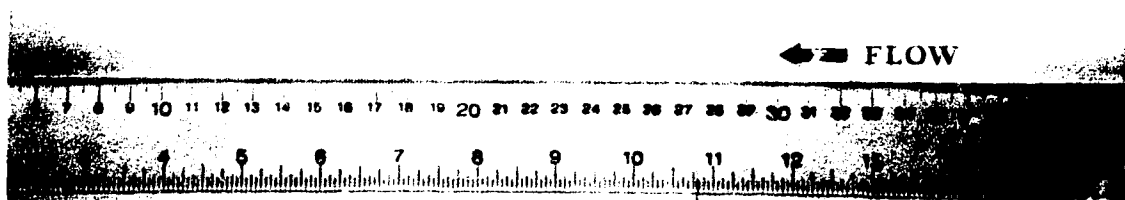
FORCED SOLITARY WAVE
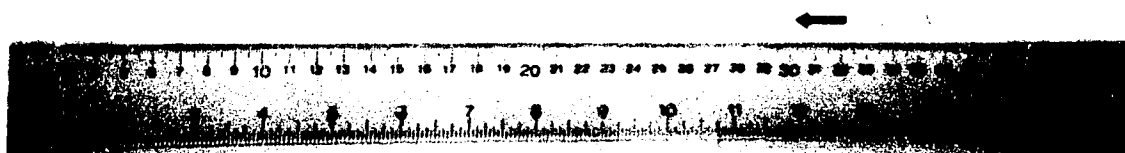
(b)

Plate 7.3   (a) Two-dimensional forced solitary waves: $H = 34$ mm and $F = 1.48$.

(b) The corresponding three-dimensional forced solitary waves.

are amplified when the water flows over the bump. The fluctuation of water surface becomes larger at the downstream. This fluctuation might also increase when the discharge of the flow increases since the flow approaches to a state which is no longer a potential flow. Despite the appearance of these uncertainties, the experimental results we have obtained at least qualitatively demonstrate the basic features of forced stationary solitary waves in supercritical flows.

7.2.2 Comparison of experimental and theoretical results

To compare the results obtained from the sfKdV model and the experimental data in §7.2.1, we may put the sfKdV BVP (3.4)-(3.5) in the laboratory coordinates:

$$(F - 1)\eta^* + \frac{\alpha}{H}\eta^{*2} + \beta H^2 \eta^*_{x^*x^*} = \frac{1}{2}h^*(x^*), \qquad -\infty < x^* < +\infty, \quad (7.1)$$

$$\eta^*(\pm\infty) = \eta^*_{x^*}(\pm\infty) = 0. \tag{7.2}$$

Here, F is the upstream Froude number and H is the depth of the upstream flow. In this section, $\alpha = -3/4$, $\beta = -1/6$, and the forcing function $h^*(x^*)$ can be expressed in the form:

$$h^*(x^*) = \begin{cases} \sqrt{r^2 - x^{*2}} - r + h_c, & |x| \leq b/2, \\ 0, & \text{otherwise,} \end{cases}$$

where b and h_c represent the width and height of the circle segment, respectively. The radius of the circle can be calculated by the formula

$$r = \frac{b^2 + 4h_c^2}{8h_c^2}.$$

This forcing is considered as a nonlocal one since the base of the bump is over 4.5 times of the height. Then, the sfKdV BVP (7.1)-(7.2) must be solved by the numerical method since there are no analytical solutions available. An effective

numerical scheme developed by Shen [34] is used here. To make the numerical method and results self-contained, we briefly describe this scheme. For brevity, the superscript '*' of all variables are dropped off thereafter.

For $x \leq -b/2$, the solution of the sfKdV BVP (7.1)-(7.2) is expressed by

$$\eta(x) = -\frac{3H(F-1)}{2\alpha}\text{sech}^2\sqrt{-\frac{F-1}{4H^2\beta}}(x - L_0),$$

where the phase shift L_0 is to be determined. We need to solve the BVP (7.1)-(7.2) for $x > -b/2$. Different solutions are distinguished by different values of the phase shift L_0. To determine L_0, we solve the following initial value problem

$$(F - 1)\eta + \frac{\alpha}{H}\eta^2 + H^2\beta\eta_{xx} = \frac{1}{2}h(x), \qquad x > -\frac{b}{2}, \tag{7.3}$$

$$\eta\left(-\frac{b}{2}\right) = -\frac{3H(F-1)}{2\alpha}\text{sech}^2\sqrt{-\frac{F-1}{4H^2\beta}}\left(\frac{b}{2} + L_0\right), \tag{7.4}$$

$$\eta_x\left(-\frac{b}{2}\right) = \sqrt{-\frac{F-1}{\beta}}\eta\left(-\frac{b}{2}\right)\tanh\sqrt{-\frac{F-1}{4\beta}}\left(\frac{b}{2} + L_0\right) \tag{7.5}$$

up to $b/2$ for a trial value of L_0, and compute

$$B_F(L_0) \equiv \frac{\beta H^2}{2}\eta_x^2\left(\frac{b}{2}\right) + \left[\frac{F-1}{2} + \frac{\alpha}{3H}\eta\left(\frac{b}{2}\right)\right]\eta^2\left(\frac{b}{2}\right).$$

The solution $\eta(x)$ satisfies $\eta(+\infty) = 0$ if and only if $B_F(L_0) = 0$ and $\eta(b/2) > 0$ for some L_0. If $|B_F(L_0)| < 10^{-5}$, we consider this L_0 as a numerical approximation solution to $B_F(L_0) = 0$. Using a do loop for L_0, a function $B_F(L_0)$ versus L_0 can be plotted in the $(L_0, B_F(L_0))$ rectangular coordinate plane. The number of the intersections of the graph of the function $B_F(L_0)$ with the L_0 axis is equal to the number of SPSWS of the sfKdV BVP (7.1)-(7.2).

Based on this scheme, a Mathematica program (cf. Appendix E) is designed to solve the sfKdV BVP (7.1)-(7.2). We found that there are two branches of solitary wave solutions for the bump we used. Figure 7.2 displays numerical solutions and

experimental data corresponding to those in Plate 7.2 (a)-(b). All solid lines are the solutions of the sfKdV model which are stable. The dashed lines represent the solutions of the sfKdV model which are unstable. The dots are experimental data measured by the point guage.
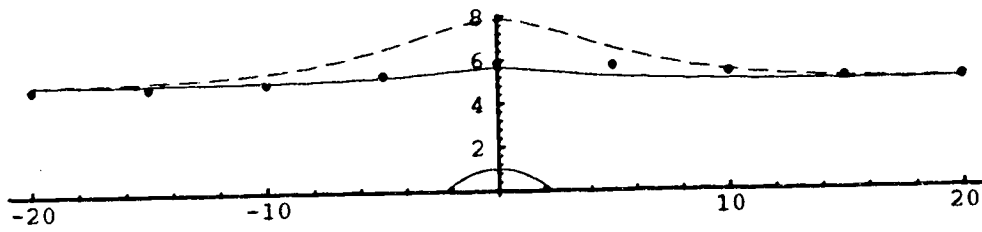
(a)
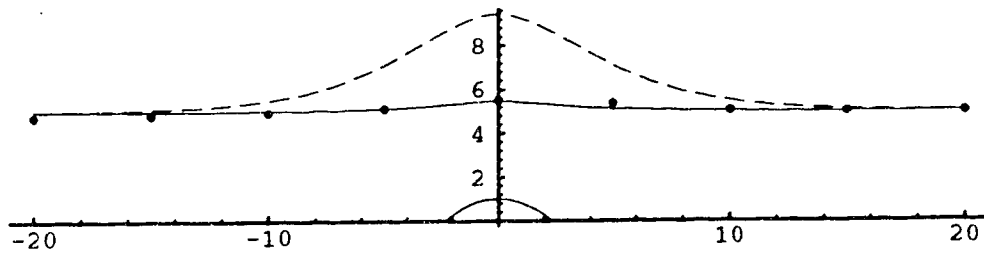
(b)

Figure 7.2: Comparison of experimental and theoretical results: (a) $H = 47$ mm, $F = 1.32$ and (b) $H = 47$ mm, $F = 1.46$.

The results obtained from the r'KdV model agree reasonably well with the experimental results, in term of the amplitude of the free surface. It is noticed that the sfKdV model slightly underestimates the supercritical flows. This is different from the case of transcritical flows and hydraulic falls, where both fKdV models slightly overestimates th⁻ amplitude of transcritical waves [21] and the sfKdV model overestimates the amplitude of hydraulic falls [36], respectively.

7.3 Hydraulic falls

In this section, we first report the experimental results of hydraulic falls, and then compare the experimental results with the theoretical results from the sfKdV model and the extended Rayleigh's formulation due to Shen [36] and Miles [28], respectively.

7.3.1 Experimental results

As mentioned before, Bump II is used for demonstrating hydraulic falls. This bump is considered as a local forcing since the height of the bump is comparable with the width of the bump. A hydraulic fall is a critical flow which is uniform at both upstream and downstream. The subcritical flow at the upstream is changed into the supercritical flow at the downstream when the flow falls over the bump. The basic features of hydraulic falls can be characterized in terms of the upstream Froude number F_L^- and the nondimensional downstream depth H_{ds}/H against the nondimensional area of the bump A/H^2 (or the nondimensional height of the bump h_c/H. When the discharge of the flow increases, the upstream water level rises so that the nondimensional area of the bump A/H^2 decreases. We have observed that the free surface of water is almost smooth everywhere both upstream and

downstream when the discharge is not too large. Plate 7.4 (a) demonstrates a picture
of two-dimensional water surface in the case of the upstream depth $H = 67.2$ mm and
the discharge of the flow $Q = 0.8$ voltage. Plate 7.4 (b) displays the corresponding
three-dimensional picture. All experimental data are shown in Table 1. In this table,
the values H and H_{ds} are measured by the point guage and the discharge Q is read
from the magnetic flow meter. Due to the fluctuation of the income flow, the data
Q showing on the magnetic meter varies within a range about ± 0.099 voltage. We
take an average value of two extrem discharge recordings.

H (mm)	H_{ds} (mm)	Q (voltage)
55.1	19.0	0.5
59.2	22.8	0.6
64.7	25.3	0.7
67.2	27.0	0.8
69.1	29.5	0.9
73.5	32.8	1.0
76.3	35.2	1.1
80.5	39.3	1.2
84.7	41.9	1.3
88.2	44.9	1.4
91.8	47.4	1.5
94.6	50.0	1.6

Table 1:   Experimental data
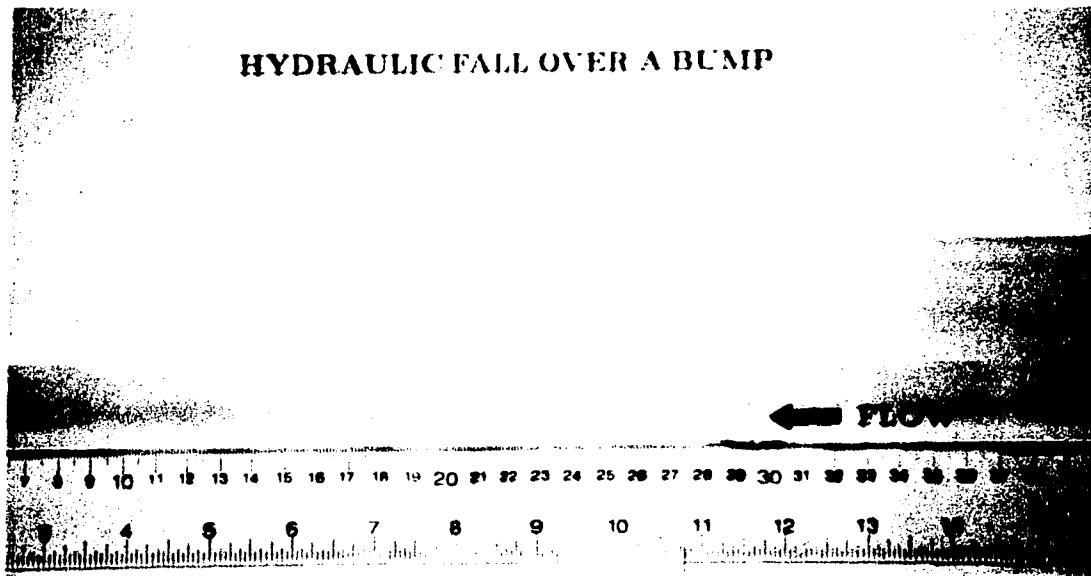
(a)
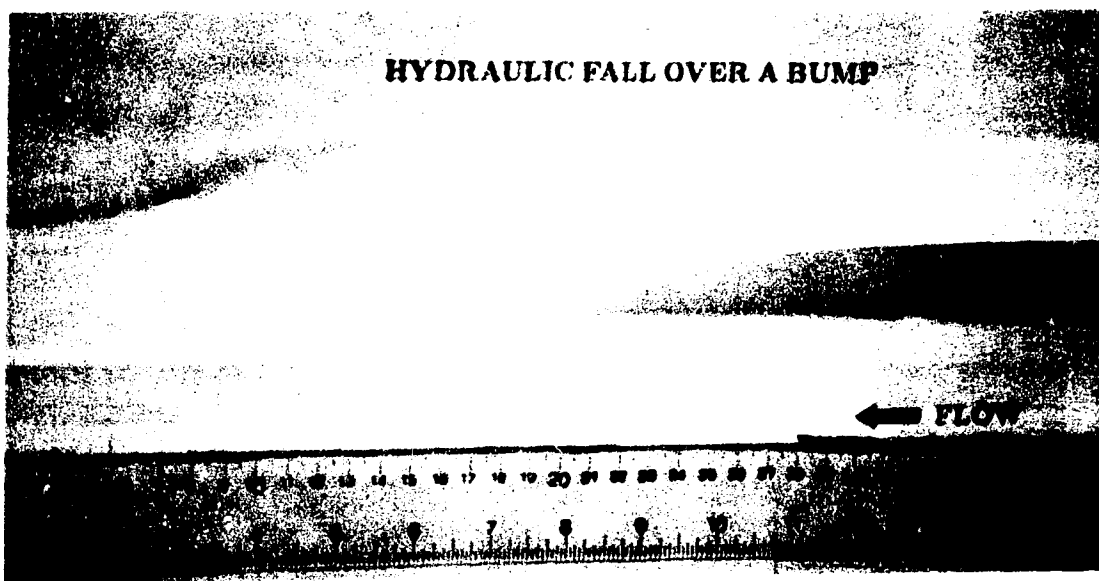
(b)

Plate 7.4   (a) Two-dimensional hydraulic fall: $H = 67.2$ mm, $Q = 0.8$ voltage;

(b) Three-dimensional hydraulic fall: $H = 67.2$ mm, $Q = 0.8$ voltage.

7.3.2 Comparison of experimental and theoretical results

For a compact (or localized) forcing, the forcing function can be approximated by $P\delta(x)$ in nondimensional variables, where P represents the nondimensional area of the bump and $\delta(x)$ is the Dirac delta function. The comparison between the experimental results and theoretical results from two theoretical models: Rayleigh's formulation developed by Miles [28] and the sfKdV model [36] will be illustrated in this subsection. Through this comparison, we can conclude that the sfKdV model is valid when $A/H^2 < 0.25$ and the corresponding physical phenomenon exists. This conclusion confirms Shen's previous results the sfKdV model is valid for $\varepsilon < 0.7$ [36] since we can choose $\varepsilon = (A/H^2)^{1/4}$.

According to the extension of Rayleigh's formulation and the sfKdV model, the dimensionless quantity of the downstream depth can be approximated by

$$\frac{H_{ds}}{H} = 1 - \left(\frac{\sqrt{6}A}{H^2}\right)^{\frac{2}{3}} \tag{7.6}$$

to first order of $(A/H^2)^{2/3}$, where A stands for the area of the obstacle and H is the depth of the far upstream. For the value of F_L, Miles obtained ([28], (4.2))

$$F_L = \sqrt{1 - \left(\frac{9A}{2H^2}\right)^{\frac{2}{3}}} \tag{7.7}$$

while Shen had ([36], (90))

$$F_L = 1 - \frac{1}{2}\left(\frac{9A}{2H^2}\right)^{\frac{2}{3}}. \tag{7.8}$$

Although, from the formal mathematical expressions, (7.8) is a linear approximation of (7.7), it does not mean that (7.8) is a less accurate formula (see Figure 7.3). Equations (7.7) and (7.8) can be rewritten in term of the dimensionless quantity

H_{d_s}/H,

$$F_L = \sqrt{\frac{3H_{d_s}}{2H} - \frac{1}{2}}$$ (7.9)

and

$$F_L = \frac{1}{4}\left(1 + \frac{3H_{d_s}}{H}\right).$$ (7.10)

On the other hand, by Bernoulli's equation, we are able to obtain

$$F_L = \sqrt{\frac{2H_{d_s}^2}{H(H + H_{d_s})}}.$$ (7.11)

According to the experimental data, a detailed comparison is displayed in Figure 7.3-4. The experimental data for F_L in Figure 7.4 are calculated by the formula

$$F_L = \frac{U}{\sqrt{gH}} = \frac{Q}{wH\sqrt{gH}}.$$

The comparison shows that the experimental results agree reasonably well with the predictions by the theoretical models.
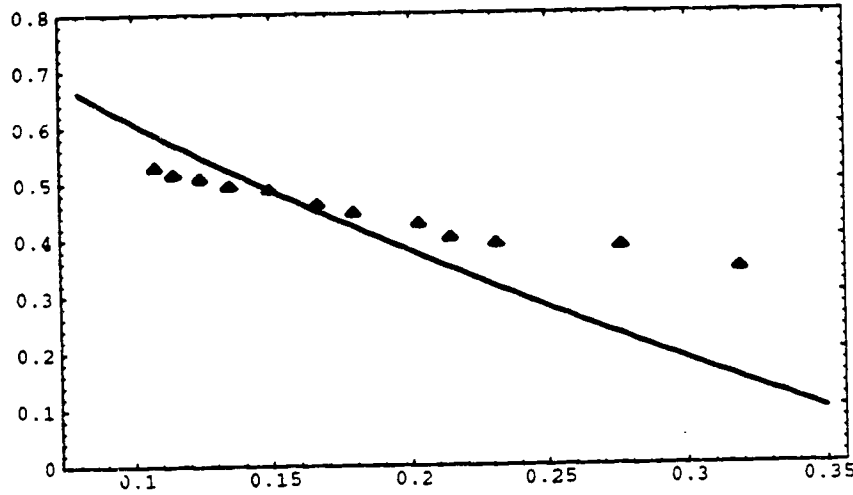
Figure 7.3: the comparison of the experimental and theoretical results for H_{d_s}/H against A/H^2: the experimental data (triangle dots) and the theoretical prediction (solid line).
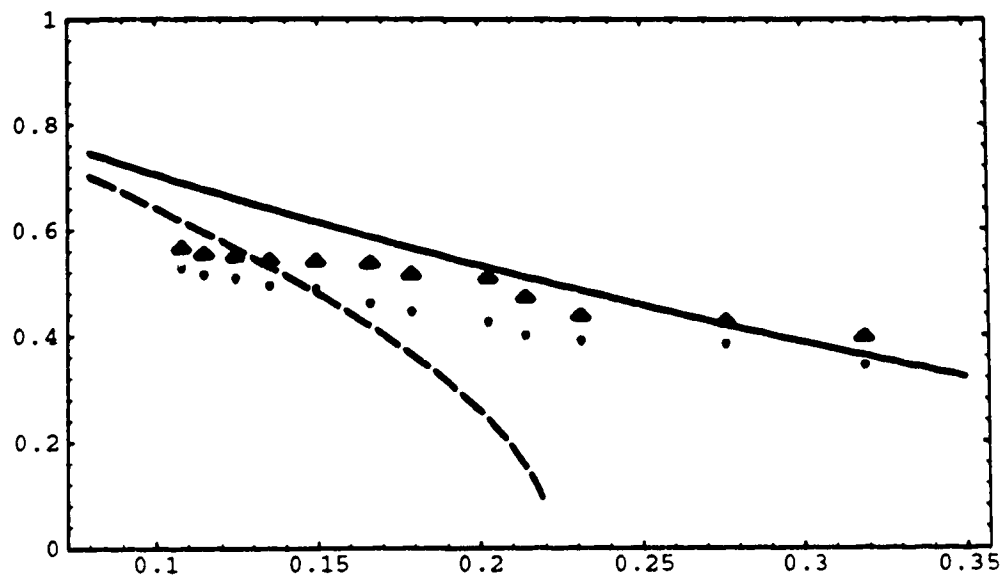
Figure 7.4: The comparison of the experimental and theoretical results for F_L against A/H^2: the experimental data (triangle dots), the Bernoulli's equation (circular dots), Rayleigh's formulation (dashed line), and the theoretical prediction (solid line).

Chapter 8

Summary and Remarks

We started the dissertation with a derivation of the forced Korteweg–de Vries (fKdV) model for nonlinear long internal waves of a two-layer fluid flow in a closed channel subject to external forcings. The fluids are assumed to be inviscid and incompressible. The external forcing is an obstruction mounted on the bottom bed or the top lid in the channel. The response of nonlinear long internal wave modes to the external forcing of order ε^2 is of order ε. The weak nonlinearity is of the second order. There is a balance of the dispersion, the nonlinearity, and the forcing. Then, the study primarily deals with the stationary forced Korteweg–de Vries (sfKdV) equation. The main results can be summarized as follows. Analytic properties of solutions to the sfKdV equation are discussed, which are useful in understanding the difference among multiple forced solitary wave solutions and envisaging the bifurcation behavior of the boundary value problem for the sfKdV equation. When the forcing is a rectangular bump/dent or two local forcings, supercritical solitary wave solutions (SSWS) to the sfKdV equation can be expressed in terms of Weierstrass' elliptic functions in the site of the forcing matched with the solitary wave tails

99

outside of the forcing. The existence of multiple SSWS is illustrated by depicting complicated bifurcation diagrams. There are at most two SSWS for a rectangular bump and more than two SSWS for a rectangular dent and two local bumps. A criterion of the stability of SSWS is provided based on nonlinear stability theory developed by Benjamin. According to numerical simulations, only one SSWS is stable and all the others are unstable. Solitary waves on a shelf are discovered by solving a boundary value problem of the sfKdV equation. The uniform flows on a shelf are analytically found, which agree with the previous results obtained by King and Bloor through numerical computation. A series of experiments are implemented to verify the validity of the sfKdV model for both forced solitary waves and hydraulic falls. Experimental results agree reasonably well with the prediction from the sfKdV model and shows that the sfKdV mode is a good model when nondimensional area of the bump A/H^2 is smaller than 0.25. The application of these results can be found in the areas of meteorology, oceanography, and other related fields.

Next, let us make some remarks for future studies in this area since there remain many interesting and significant open problems. The first remark is about the evolution of nonlinear long waves in the fKdV system. In transcritical region ($\lambda_L < \lambda < \lambda_C$), the periodic soliton generation has been intensively studied since 1982. All the studies have confirmed the remarkable numerical findings by Wu and Wu [47] and the pioneering experimental work by Huang, et al. [16]. Besides this, we have already learned from our stability analysis that a stable steady state always exists in the supercritical region (i.e., $\lambda > \lambda_C$). According to our numerical simulations in the supercritical region, when an initial state possesses sufficiently large mass, it can always evolve into the stable stationary solitary wave sustained on the site of the forcing. The excessive mass is radiated to infinity at both upstream and downstream.

In particular, the mass in the system is redistributed to form the stable steady state in the vicinity of the forcing, a soliton advancing ahead of the forcing, and a train of dispersive waves propagating along the downstream. Usually, an unstable steady state satisfies such an initial condition of sufficiently large mass. Obviously, this wave phenomenon is different from that in transcritical region discovered by Wu and Wu [47] and should be studied further.

The second one is on the bifurcation of multiple SSWS of the sfKdV equation. In the sfKdV model, the forcing is classified into two categories: nonlocal and local forcing. Here, "nonlocal forcing" means that the support of the forcing in the physical problem is of comparable length with the length scale L of the free surface wave. The forced stationary KdV equation has more than two SPSWS for a nonlocal forcing as we have shown in §4.1. Indeed, there may exist $2N$ SPSWS for an arbitrary integer N when a and λ are sufficiently large in the case of the well-shape forcing. At the turning points from two SPSWS to four SPSWS, from four solutions to six solutions, and so on, there may exist pitchfork bifurcations. In addition, nonsymmetric solutions exist in response to the symmetric forcing and must occur in pairs. For two local forcings, the sfKdV equation has also more than two SPSWS for a nonlocal forcing as we have shown in §4.2. As of today, the bifurcation behavior in this case is still unclear.

The third one is associated with the stability problem. Although Camassa and Wu have made a remarkable progress on the study of the stability of forced smooth solitary waves, in general, the stability of the forced stationary solitary waves is very difficult to analyze since the structure of the SPSWS is complicated. For linear theory, what must be overcome is to solve an eigenvalue problem of third order ordinary differential equations. For nonlinear theory, other criteria are necessary to

be developed so that more general cases of forcings can be treated. The approach based on Hamiltonian functional should be paid more attention in this direction.

The final remark is on the existence of solitary waves on a shelf. The verification of the existence of the shelf solitary wave as a solution of the Euler equation is still an open problem. Two approaches may be taken for further studies. One is the computational method developed by King and Bloor [18] and the other one is the theoretical method expounded by Amick and Turner [3].

Bibliography

[1] M. J. Ablowitz and P. A. Clarkson, Solitons, Nonlinear Evolution Equations and Inverse Scattering, Cambridge University Press, Cambridge (1991).

[2] T. R. Akylas, On the excitation of long nonlinear water waves by a moving pressure distribution, J. Fluid Mech., **141** (1984), pp. 455-466.

[3] C. J. Amick and R. E. L. Turner, A global theory of internal solitary waves in two-fluid systems, Trans. Am. Math. Soc., **298** (1986), pp. 431-484.

[4] P. G. Baines, A unified description of two-layer flow over topograghy, J. Fluid Mech., **146** (1984), pp. 127-167.

[5] T. B. Benjamin, The stability of solitary waves, Proc. R. Soc. Lond. A, **328** (1972), pp. 153-183.

[6] J. L. Bona, On the stability of solitary waves, Proc. R. Soc. Lond. A, **344** (1975), pp. 363-374.

[7] R. Camassa and T. Yao-Tsu Wu, Stability of forced solitary waves, Phil. Trans. R. Soc. Lond. A, **337** (1991), pp. 429-466.

[8] R. Camassa and T. Yao-Tsu Wu, Stability of some stationary solutions for the forced KdV equation, Physica D, **51** (1991), pp. 295-307.

103

[9] T. F. Chan and T. Kerkhoven, Fourier methods with extended stability intervals for the Korteweg–de Vries equation, SIAM J. Numer. Anal., **22** (1985), pp. 441–454.

[10] R. C. Ertekin, W. C. Webster, and J. V. Wehausen, Waves caused by a moving disturbance in a shallow channel of finite width, J. Fluid Mech., **169** (1986), pp. 272–295.

[11] A. S. Fokas and M. J. Ablowitz, Forced nonlinear evolution equations and inverse scattering transform, Stud. Appl. Math., **80** (1989), pp. 253–272.

[12] L. K. Forbes, Critical free-surface flow over a semi-circular obstruction, J. Engr. Math., **22** (1988), pp. 3–13.

[13] L. K. Forbes and L. W. Schwartz, Free-surface flow over a semi-circular obstruction, J. Fluid Mech., **114** (1982), pp. 229–314.

[14] L. Gong and S. S. Shen, Multiple supercritical solitary wave solutions of the stationary forced Korteweg-de Vrices Equation and their stability, SIAM J. Appl. Math, 1994 (in press).

[15] R. H. J. Grimshaw and N. F. Smyth, Resonant flow of a stratified fluid over topography, J. Fluid Mech., **169** (1986), pp. 429–464.

[16] D. B. Huang, O. J. Sibul, W. C. Webster, J. V. Wehausen, D. M. Wu and T. Y. Wu, Ships moving in the transcritical range, In Proc. Conf. on Behavior of ships in Restricted Waters, Varna, **2** (1982), pp. 26/1–26/10.

[17] C. Katsis and T. R. Akylas, On the excitation of long nonlinear water waves by a moving pressure distribution, Part 2. Three-dimensional effects, J. Fluid Mech., **177** (1987), pp. 49–65.

[18] A. C. King and M. I. G. Bloor, Free surface flow over a step, J. Fluid Mech., **182** (1987), pp. 193–208.

[19] D. J. Korteweg and G. de Vries, On the change of form of long waves advancing in a rectangular canal, and on a new type of long stationary waves, Philos. Mag., **39** (1895), pp. 422–443.

[20] H. Lamb, Hydrodynamics, Dover, New York (1932).

[21] S. J. Lee, G. T. Yates, and T. Y. Wu, Experiments and analyses of upstream-advancing solitary waves generated by moving disturbances, J. Fluid Mech., **199** (1989), pp. 469–593.

[22] D. Ludwig, Parsimonious asymptotics, SIAM J. Appl. Math., **43** (1983), pp. 664–672.

[23] O. S. Madsen and C. C. Mei, The transformation of a solitary wave over an uneven bottom, J. Fluid Mech., **39** (1969), pp. 781–791.

[24] B. A. Malomed, Interaction of a moving dipole with a soliton in the KdV equation, Physica D, **32** (1988) pp. 393–408.

[25] C. C. Mei, Radiation of solitons by slander bodies advancing in a shallow channel, J. Fluid Mech., **162** (1986), pp. 53–67.

[26] W. K. Melville and K. R. Helfrich, Transcritical two-layer flow over topography, J. Fluid Mech., **178** (1987), pp. 31–52.

[27] J. W. Miles, Solitary waves, Ann. Rev. Fluid Mech., **12** (1980), pp. 11–43.

[28] J. W. Miles, Stationary, transcritical channel flow, J. Fluid Mech., **162** (1986), pp. 489–499.

[29] P. M. Naghdi and L. Vongsarnpigoon, The downstream flow beyond an obstacle, J. Fluid Mech., **162** (1986), pp. 223–236.

[30] A. C. Newell, Solitons in Mathematics and Physics, SIAM, Philadephia (1985).

[31] F. Z. Nouri and D. M. Sloan, A comparison of Fourier pseudospectral methods for the solution of the Korteweg-de Vries equation, J. Comp. Phys., **83** (1989), pp. 324–344.

[32] A. Patoine and T. Warn, The interaction of long, quasi-stationary baroclinic waves with topography, J. Atoms. Sci., **39** (1982), pp. 1018–1025.

[33] A. S. Peters and J. J. Stoker, Solitary waves in liquids having non-constant density, Comm. Pure Appl. Math., **13** (1960), pp. 115–164.

[34] S. S. P. Shen, Disturbed critical surface waves in a channel of arbitrary cross section, J. Appl. Math. Phys. (ZAMP), **40** (1989), pp. 216–229.

[35] S. S. P. Shen, Locally forced critical surface waves in a channel of arbitrary cross section, J. Appl. Math. Phys. (ZAMP), **42** (1991), pp. 122–138.

[36] S. S. P. Shen, Forced solitary waves and hydraulic falls in two-layer flows, J. Fluid Mech., **234** (1992), pp. 583–612.

[37] S. S. P. Shen, A Course on Nonlinear Waves, Kluwer, Boston (1993).

[38] S. S. P. Shen and L. Gong, Solitary waves on a shelf, Phys. Fluids A, **5** (1993), pp. 1071-1073.

[39] S. S. P. Shen and M. C. Shen, A new equilibrium of subcritical flow over an obstruction in a channel of arbitrary cross section, Eur. J. Mech. (B/Fluid), **9** (1990), pp. 59-74.

[40] S. S. Shen, R. P. Manhar and L. Gong, A symbolic program for the Chan-Kerkhoven scheme and the stability of the cusped forced Korteweg-de Vries solitary waves, 1994 (submitted to J. Comp. Phys.).

[41] N. S. Sivakumaran, T. Tingsanchali & R. J. Hosking, Steady shallow flow over curved beds, J. Fluid Mech., **128** (1983), pp. 469-487.

[42] R. E. L. Turner and J. -M. Vanden-Broeck, Broadening of interfacial solitary waves, Phys. Fluids, **31** (1988), pp. 2486-2490.

[43] J. M. Vanden-Broeck, Free surface flow over an obstruction in a channel, Phys. Fluids, **30** (1987), 2315-2317.

[44] Z. X. Wang and D. R. Guo, Special Functions, World Scientific, Singapore (1989).

[45] G. B. Whitham, Linear and Nonlinear Waves, Wiley, New York (1974).

[46] T. Y. Wu, Generation of upstream-advancing solitons by moving disturbances, J. Fluid Mech., **184** (1987), pp. 75-99.

[47] D. M. Wu and T. Y. Wu, Three-dimensional nonlinear long waves due to moving surface pressure, In Proc. 14th Symp. Naval Hydrodyn., Washington: National Academy of Sciences (1982), pp. 103-125.

Appendix A

```
(**********************************************************)
(*                                                        *)
(*-------------- Program I      rectbifsol.m -------------*)
(*                                                        *)
(*  This MATHEMATICA program "rectbifsol.m" is designed   *)
(*  to plot the bifurcation and solutions of the sfKdV BVP *)
(*  with a rectangular bump or well-shape forcing discussed *)
(*  in Section 4.1.2.                                     *)
(*                --written by Lianger Gong, May 7, 1994   *)
(*                                                        *)
(**********************************************************)


(* Input the values of 'gamma' and 'al' first. Here, gamma *)
(* and al represent the height of the bump or the depth of *)
(* the dent and the length of the bump or dent, respectively*)


alpha = -3/4;
beta = -1/6;
b1 = -2*alpha/(3*beta);
b2[x_]:= -x/beta;
b3 = 2*gamma/beta;
c1 = 4/b1;
c2[x_]:= -b2[x]/(3*b1);
u0[x_,t_]:=-(b2[x]/b1)*Sech[Sqrt[0.25*b2[x]]*(0.5*al+t)]^2;
u1[x_,t_]:=Sqrt[b2[x]]*u0[x,t]*Tanh[Sqrt[0.25*b2[x]]*(0.5*al+t)];
g2[x_]:=-(b2[x]*c2[x]+b3)/c1;
g3[x_,t_]:=-(b1*c2[x]^3+b2[x]*c2[x]^2+b3*c2[x]-b3*u0[x,t])/(c1^2);

hw1[x_,t_]:=WeierstrassP[al,g2[x],g3[x,t]];
hw2[x_,t_]:=c1*WeierstrassPPrime[al,g2[x],g3[x,t]]-u1[x,t];
hw3[x_,t_]:=c1*hw1[x,t]-u0[x,t]+c2[x];
hw4[x_, t_]:= 0.25*(hw2[x, t]/hw3[x, t])^2 - hw1[x, t];
bl0[x_, t_]:= c1*hw4[x, t] + 2*c2[x] - 2*u0[x, t];
bif[x1_, x2_, t1_, t2_]:= ContourPlot[bl0[x,t],{x, x1, x2}, {t, t1, t2},
          PlotRange->{0, 0}, PlotPoints ->30, FrameLabel->{"lambda","L0"},
        ContourShading->False, Contours->1, ContourSmoothing->True];

(* bl0[x, t] defines the equation (4.11) in Section 4.1.1    *)
(* where x and t represent the cooresponding lambda and L0.  *)
(* bif[x1, x2, t1, t2] plots the bifurcation diagram, where  *)
(* x1=lambda_min, x2=lambda_max, t1=L0_min and t2_=L0_max.    *)


(* Input lambda here. 'pltb' plots the curve of bl0[lambda,t]*)
(* 'frt' finds a root L0 of bl0[x, t]=0 close to t1 and t2.   *)
pltb[t1_,t2_]:= Plot[bl0[lambda,t],{t,t1,t2},PlotPoints->30];
```

```
frt[t1_,t2_]:= N[FindRoot[bl0[lambda,t]==0,{t, t1, t2}], 10];

(* The following section is designed to plot the solution *)
ul[x_,t_]:=If[x<=-al/2,(-b2[lambda]/b1)
           *Sech[Sqrt[0.25*b2[lambda]]*(x-t)]^2,0];
urn[x_,t_]:=If[x >=al/2,(-b2[lambda]/b1)
           *Sech[Sqrt[0.25*b2[lambda]]*(x-al-t)]^2,0];
ur[x_,t_]:=If[x >=al/2,(-b2[lambda]/b1)
           *Sech[Sqrt[0.25*b2[lambda]]*(x+t)]^2,0];
gwp[x_, t_]:=WeierstrassPPrime[x + 0.5*al,g2[lambda], g3[lambda,t]];

gw1[x_, t_]:=c1*gwp[x, t] - u1[lambda, t];
gw2[x_, t_]:= WeierstrassP[x + 0.5*al, g2[lambda], g3[lambda, t]];
gw3[x_, t_]:=c1* gw2[x, t] - u0[lambda, t] + c2[lambda];
gw4[x_, t_]:= gw2[x, t] + (u0[lambda, t] - c2[lambda])/c1;
gw5[x_, t_]:= 0.25*(gw1[x, t]/gw3[x, t])^2 - gw4[x, t];
u[x_, t_]:= If[Abs[x] < al/2, c1*gw5[x, t] + c2[lambda], 0];

us[x_,t_]:=ul[x,t]+ur[x,t]+u[x,t];       (* symmetric solution *)
usn[x_,t_]:=ul[x,t]+urn[x,t]+u[x,t];     (*  nonsymmetric solution  *)

(* 'plts' and 'pltns' plot the symmetric and nonsymmetric    *)
(*  solution in [x1,  x2]. Input the value L0 here.          *)
plts[x1_,x2_,t1_,t2_]:=Plot[{us[x,t1],us[x,t2]},{x,x1,x2},
                 PlotRange->{0, -3*lambda/(2*alpha)},PlotPoints->35,
                 AxesLabel->{x, "eta(x)"},PlotStyle->{{GrayLevel[0],
               Thickness[0.0005]},{Dashing[{0.01}],Thickness[0.0005]}}];
pltns[x1_, x2_, t1_, t2_]:=Plot[{usn[x, t1],usn[x, t2]},{x,x1,x2},
                 PlotRange->{0,-3*lambda/(2*alpha)},PlotPoints->35,
                 AxesLabel->{x, "eta(x)"},PlotStyle->{Dashing[{0.02,0.01}],
               Thickness[0.0005]},{Dashing[{0.01}],Thickness[0.0005]}}];

(****************End of the program ***************************)
```

Appendix B

```
(*****************************************************)
(*                                                 *)
(*-------------- Program II    del2bifsol.m --------------*)
(*                                                 *)
(*  This MATHEMATICA program "del2nifs.m" is designed    *)
(*  to find the roots L0 and L1 and plot solutions      *)
(*  of the sfKdV BVP with a forcing of two delta functions *)
(*  discussed in Section 4.2.                        *)
(*                     --Written by Lianger Gong, May 8, 1994 *)
(*                                                 *)
(*****************************************************)

(* First, set up an equation for L0 *)
(* Input the values of 'gamma' and 'al' first. Here, gamma  *)
(* and al represent the height of the bump of the depth of  *)
(* the dent and the length of the bump or dent, respectively*)

alpha = -3/4;
beta = -1/6;
b1 = -2*alpha/(3*beta);
b2[x_]:= -x/beta;
u0[x_, t_]:= -(b2[x]/b1)*Sech[Sqrt[0.25*b2[x]]*(al+t)]^2;
u1[x_, t_]:= Sqrt[b2[x]]*u0[x, t]*Tanh[Sqrt[0.25*b2[x]]*(al+t)];
s[x_, t_]= pl*(pl + 2*beta*u1[x, t])/beta^2;
c1 = 4/b1;
c2[x_]:= -b2[x]/(3*b1);
d1[x_, t_]:=u1[x, t] + pl/beta;
d2[x_, t_]:=u0[x, t] - c2[x];
g2[x_]:= -(b2[x]*c2[x])/c1;
g3[x_, t_]:= -(b1*c2[x]^3+b2[x]*c2[x]^2+s[x, t])/(c1^2);
hw1[x_,t_]:= WeierstrassP[2*al,g2[x],g3[x,t]];
hw2[x_,t_]:= c1*WeierstrassPPrime[2*al,g2[x],g3[x,t]]-d1[x,t];
hw3[x_, t_]:= c1*hw1[x,t] - d2[x, t];
hw4[x_,t_]:=0.25*c1*(hw2[x,t]/hw3[x,t])^2-c1*hw1[x,t]-d2[x,t]+c2[x];
hw5[x_, t_]:=(pr^2 - s[x, t]*beta^2)/(2*pr*beta);
bl0[x_, t_]:=hw5[x,t]^2-b1*hw4[x,t]^3-b2[x]*hw4[x,t]^2;

(* Input pl and pr here. 'pltb' plots the curve of     *)
(* bl0[lambda, t] and shows possible locations of L.    *)

pltb[t1_,t2_]:=Plot[bl0[lambda,t],{t,t1,t2},PlotRange->All,PlotPoints->30];

(* 'flt' search for an approximate root L0 close    *)
(* to t1 and t2 for a fixed lambda.                 *)
```

```
flt[t1_,t2_]:= N[FindRoot[b10[lambda,t]==0,{t,t1,t2}],7];

(* Second, search for L1 *)

u2[x_, t_]:= -(b2[x]/b1)*Sech[Sqrt[0.25*b2[x]]*(a1-t)]^2;
u3[x_, t_]:= -Sqrt[b2[x]]*u2[x, t]*Tanh[Sqrt[0.25*b2[x]]*(a1-t)];
sr1[x_, t_]= u2[lambda, t] - hw4[lambda, x];
sr2[x_, t_]= u3[lambda, t]-(pr^2 - s[lambda, x]*beta^2)/(2*pr*beta);

(* Input L0 'pltr' plots the curve of sr1[t, L0]        *)
(* and label the possible location of L1.               *)

pltr[t1_,t2_]:=Plot[sr1[L0,t],{t,t1,t2}, PlotPoints->50];

(* 'frt' finds a approximate L_1 root of sr1[L0, t]=0 close *)
(* to t1 and t2 for a fixed lambda and check sr2[L0, L1]=0  *)

frt[t1_, t2_]:= N[FindRoot[sr1[L0, t]==0, {t, t1, t2}], 8];

(* The final paragraph defines an analytic solution        *)

ul[x_, xl_]:= If[x <= -a1, (-b2[lambda]/b1)
                    *Sech[Sqrt[0.25*b2[lambda]]*(x - xl)]^2, 0];
ur[x_, xr_]:= If[x > a1,(-b2[lambda]/b1)
                    *Sech[Sqrt[0.25*b2[lambda]]*(x - xr)]^2, 0];

gwp[x_, xl_]:=WeierstrassPPrime[x + a1,g2[lambda], g3[lambda,xl]];
gw1[x_, xl_]:=c1*gwp[x, xl] - ul[lambda, xl]- (p1/beta);
gw2[x_,xl_]:=WeierstrassP[x+a1,g2[lambda],g3[lambda,xl]];
gw3[x_, xl_]:=c1* gw2[x, xl] - u0[lambda, xl] + c2[lambda];
gw4[x_, xl_]:=c1*gw2[x, xl] + u0[lambda, xl] - 2*c2[lambda];
gw5[x_,xl_]:= 0.25*c1*(gw1[x,xl]/gw3[x,xl])^2-gw4[x,xl];

u[x_, xl_]:= If[ -a1< x <= a1, gw5[x, xl], 0];
us[x_, xl_, xr_]:=ul[x, xl] + ur[x, xr] + u[x, xl];

(* 'plts' and 'pltns' plot symmetric and nonsymmetric SPSWS.  *)

plts[x1_, x2_]:=Plot[{us[x, xl1, xr1],us[x, xl2, xr2]},{x,x1,x2},
                PlotRange->{0,-3*lambda/(2*alpha)},PlotPoints->35,
              AxesLabel->{x,"eta(x)"},PlotStyle->{{GrayLevel[0],
          Thickness[0.0005]},{Dashing[{0.01}],Thickness[0.0005]}}];
pltns[x1_, x2_]:=Plot[{us[x, xl3, xr3],us[x, xl4, xr4]},{x,x1,x2},
                PlotRange->{0,-3*lambda/(2*alpha)},PlotPoints->35,
              AxesLabel->{x,"eta(x)"},PlotStyle->{{Dashing[{0.05,0.01}],
          Thickness[0.0005]},{Dashing[{0.01}],Thickness[0.0005]}}];

(*****************End of the programm ************************)
```

Appendix C

```
(*****************************************************************)
(*                                                             *)
(************  PACKAGE NAME: sspsws.m      ***************)
(*                                                             *)
(* This MATHMATICA code solves the fKdV IVP of                 *)
(*                                                             *)
(*     D[u,t]+lambda*D[u,x]+2*alpha*u*D[u,x]                   *)
(*         +beta*D[u,{x,3}] = D[f, x], t>0, -L < x < L         *)
(*                                                             *)
(*     u(x, 0)=v(x),                                           *)
(*                                                             *)
(* using the spectral method.                                  *)
(*                                                             *)
(*              Modified by L. Gong                            *)
(*              Written originally by S. S. Shen               *)
(*              Department of Mathematics                      *)
(*              University of Alberta                          *)
(*              R. P. Manohar and L. Quinlan                   *)
(*              University of Saskatchewan                     *)
(*              April 1994                                     *)
(*              E-mail:lgong@parabolic.math.ualberta.ca        *)
(*                                                             *)
(*****************************************************************)
BeginPackage["sspsws'"]
sspsws::usage = "sspsws solves the equation using m*lastres time steps"
conser::usage = "conser[m1] checks the conservation of mass at time t=m1"
plt::usage = "plt[m3]  plots the solution u(x,t=m3) at a fixed time t=m3
     where x is in grid point value and the cdw curve"
pltx::usage = "plt[m4]  plots the solution u(x,t=m4) at a fixed time t=m4
     where x is in real x value"
plt3d::usage = "plt3d[x3] plots the 3-Dim graph of u(x,t) in (x3,L) and
     for t running from t=0 to t=lastresand the norm of
     perturbation in 12 against t"
anifKdV::usage = "anifKdV animates the 2-Dim u(x,t) wave
 from t=1 to t=lastres"
pltcd::usage = "pltcd  plots the C_Dw curve against time t"
pltr::usage = "pltr  plots the error between u(x,t) and v(x)
     in 12 space against time t"

<<sspsws.dat;

Begin["'Private'"]

(**********  Begin Computational Procedures  ************)
fourier[g_List]:=Block[{k,n,a},
n = Length[g];
```

```
a = Table[(-1)^(k-1)g[[k]],{k,1,n}];
InverseFourier[a]
        ]; (*end of fourier Block*)


invfourier[gt_List]:=Block[{k,n,a},
   n = Length[gt];
   a = Fourier[gt];
   Table[(-1)^(k-1)a[[k]],{k,1,n}]
  ]; (*end of invfourier Block*)


(****** Calculating one time step for ut at t+deltat  *******)
step[umt_List,ut_List,wt_List]:=
 Block[{j,q,n,a,t1,t2,t3}, n = Length[ut];
        t3=Table[If[Abs[2*(j-1)/n-1]< 0.5*al/1,
   gamma,0.0],{j,1,n}];
        ft=fourier[t3];
        Do[t1 = q - n/2. - 1;
   t2 = N[1/(1.-beta*deltat*s^3*I*t1^3)];
   a[q] = t2*((1+beta*deltat*I*s^3*t1^3)*umt[[q]]
   -2.*lambda*deltat*s*I*t1*ut[[q]]
   -2.*alpha*deltat*I*t1*wt[[q]]
   + 2*deltat*I*s*t1*ft[[q]]),
   {q,1,n}]; (*end of Do loop*)
        Table[a[j],{j,1,n}]
        ]; (*end of step Block*)


tsteps[nsteps_]:=Block[{j},
        Do[w = s u^2; wt = fourier[w];
        upt = step[umt,ut,wt];
        up = invfourier[upt];
        umt = ut;  ut = upt;  u = up   (*updating lists*)
        time = time + 1; (*updating time variables*)
        tottime = deltat + tottime;
        If[Mod[time-1, timesave]==0,
(*then*) Print[tottime];
 <<"!rm intres"; save,
(*else*) Continue],{j,1,nsteps}];
        (*end of Do loop*)
        ]; (*end of tsteps Block*)


init:=Block[{t1}, time=tottime=0.;
  s=N[Pi/1]; w0=s * u0^2; Clear[q];
  umt=fourier[u0]; wmt=fourier[w0]; Clear[q];
  deltat=deltat/initfac ;
  f0=N[Table[If[Abs[2*(j-1)/n-1]<0.5*al/1,gamma,0],{j,1,n}]];
  f0t=fourier[f0];
  ut=Table[umt[[q]]+deltat*N[I*s*(q-n/2-1)*f0t[[q]]]
  -lambda*I*s*(q-n/2-1)*umt[[q]]]
```

```
        -alpha*I*(q-n/2-1)*wmt[[q]]
        +beta*I*((q-n/2-1)^3)*umt[[q]]*s^3],
        {q,1,n}]; Clear[q];
        u=invfourier[ut]; tottime=tottime + deltat;
        tsteps[initfac - 1];
        deltat= initfac * deltat; umt=fourier[u0]; time=1;
            ]; (*end of init Block*)

msteps:=Block[{i}, Do[tsteps[m]; end = ToString[i];
        If[i > 9,
        (*then*) file = StringJoin["res",end],
        (*else*) file = StringJoin["res0",end]];
         reu = Re[u];
         Save[file,reu,tottime,lambda,deltat,cwd],
         {i,firstres,lastres}]; (*end of Do loop*)
            ]; (*end of msteps Block*)


sspsws:=Block[{},
        If [firstres==0, (*then*) Return[Print["If first run, data file is
            not loaded; if sup run, value for firstres is missing."]]
        ];
        If [firstres==1, (*then*) init,
            (*else*) <<intres;
u = invfourier[ut];
        ];
            msteps;
            ];    (*end of sspsws Block*)


save:=Save["intres",l,lambda,n,m,alpha,beta,p,
        deltat,s, timesave,tottime,time,umt,ut]
(******End of Computational Procedures Section******)


conser[m1_]:=Block[{ },
        sufx=ToString[m1];
        If[ m1 < 10,result=StringJoin["res0",sufx],
            result=StringJoin["res",sufx]
            ];
        Get[result];
        Sum[reu[[i]],{i,n}]
        ];
(*********End of Conservation Law Verification*********)


plt[m3_]:=Module[{temp1,temp2,t1,t2,t3,t4},
        sufx=ToString[m3];
        If[ m3 < 10, result=StringJoin["res0",sufx],
            result=StringJoin["res",sufx]
            ];
        Get[result];
```

```
    temp1 = Min[reu];
    temp2 = Max[reu];
    t1 = N[tottime - deltat,4];
    t2 = ToString[t1];
    t3 = ToString[lambda];
    t4 = StringJoin["time=",t2," lambda=",t3];
    ListPlot[reu,PlotJoined->True, PlotRange->{temp1,temp2},
      PlotLabel->t4, Frame->True,
        FrameLabel->{"x (in grid point)","eta(x,t)"}]
  ];
(* End of 2-Dim Plot at t=m3 Section (in grid point) *)

pltx[m4_]:=Module[{temp1,temp2,t1,t2,t3,t4},
 sufx=ToString[m4];
 If[ m4 < 10,result=StringJoin["res0",sufx],
      result=StringJoin["res",sufx] ];
 Get[result];
 temp1 = Min[reu];    temp2 = Max[reu];
 t1 = N[tottime - deltat,4];
 t2 = ToString[t1];
 t3 = ToString[lambda];
 t4 = StringJoin["time=",t2," lambda=",t3];
 xvalues=Table[N[(i-n)*2*l/(n-1) + l], {i,1,n}];
 plotxlist=Table[{xvalues[[i]], reu[[i]]},{i,1,n}];
   ListPlot[plotxlist,PlotJoined->True,
 PlotRange->{temp1,temp2},PlotLabel->t4,
        Frame->True,Axes->False,
      FrameLabel->{"x","eta(x,t)"}]
  ]
(* End of 2-Dim Plot at t=m4 Section (in x value) *)

plt3d[x3_]:=Module[{i, j, tabplot3d},
    cwd=err=Table[0.0, {i, 1, lastres}];d=Table[1, {i,1,n}];
    xit=Table[N[(i-n)*2*l/(n-1) + l], {i,1,n}];
    uit=Table[{xit[[i]], u0[[i]]},{i,1,n}];
    pg[0]=ListPlot[uit,PlotJoined->True, AspectRatio->1.2,
     Axes->False, PlotStyle->{Thickness[0.001]},
    PlotRange->{Min[u0], lastres + Max[u0]},
   DisplayFunction->Identity];
    Do[ sufx=ToString[i];
If[i<10,result=StringJoin["res0",sufx],
result=StringJoin["res",sufx] ];
Get[result];
err[[i]]=Sqrt[Sum[(reu[[j]]-u0[[j]])^2,{j,1,n}]/n];
cwd[[i]]=reu[[1+n*(1-0.5*al)/(2*l)]]
     -reu[[1+n*(1+0.5*al)/(2*l)]];
xvalues=Table[N[(i-n)*2*l/(n-1) + l], {i,1,n}];
    umarch=Take[reu,{1, n}] + i d;
```

```
    xulist=Table[{xvalues[[j]],umarch[[j]]},{j,1,n}];
    pg[i]=ListPlot[xulist, PlotJoined->True, AspectRatio->1.2,
   Axes->False, PlotStyle->{Thickness[0.001]},
   PlotRange->{Min[uO], lastres + Max[uO]},
   DisplayFunction->Identity],{i,1,lastres}];
    Clear[i]; tabplot3d=Table[pg[i],{i,0,lastres}];
    Show[tabplot3d,Frame->True,
 PlotRange->{{x3,-x3},{Min[uO],lastres+2}},
 FrameLabel->{"x","t", "eta(x, t)", ""},
 DisplayFunction->$DisplayFunction ];
 ]
(***** End of 3-Dim Plot Section ***************)


pltcd:=Module[{i, j, tabplot3d},
   cwd=Table[0.0, {i, 1, lastres}];
   Do[ sufx=ToString[i];
       If[i<10,result=StringJoin["res0",sufx],
       result=StringJoin["res",sufx]];
       Get[result]; cwd[[i]]=reu[[1+n*(1-0.5*al)/(2*1)]]
  -reu[[1+n*(1+0.5*al)/(2*1)]],{i,1,lastres}];
    t5 = StringJoin["t"];
    t6 = StringJoin["C_Dw"];
    cwp=Table[{i, cwd[[i]]}, {i, 1, lastres}];
    ListPlot[cwp,PlotJoined->True,AxesOrigin->{1,-0.4},
    AxesLabel->{t5,t6}, PlotStyle->{Thickness[0.001]},
 PlotRange->{-0.5, 0.8}]
 ]
(***** End of C_Dw Plot Section ***************)


pltr:=Module[{i, j, tabplot3d},
     err=Table[0.0, {i, 1, lastres}];
     Do[ sufx=ToString[i];
 If[i<10,result=StringJoin["res0",sufx],
 result=StringJoin["res",sufx]];
 Get[result]; err[[i]]=Sqrt[Sum[(reu[[j]]-uO[[j]])^2,
     {j, 1, n}]/n],{i,1,lastres}];
     ListPlot[err, PlotJoined->True, AxesOrigin ->{1, -0.1},
     AxesLabel->{"t","||zeta ||"},
     PlotStyle->{Thickness[0.001]},PlotRange->{-0.2,0.3}]
  ]
(***** End of Error Plot Section ***************)


<<Graphics`Animation`
anifKdV[min_,max_]:=
    Module[{i,tabanimation},
    Do[ sufx=ToString[i];
If[i<10,result=StringJoin["res0",sufx],
result=StringJoin["res",sufx]];
```

```
Get[result];
xvalues=Table[N[(j - n)*2*1/(n-1) + 1], {j,1,n}];
anilist = Table[{xvalues[[j]], reu[[j]]}, {j,1,n}];
g[i]=ListPlot[anilist,PlotJoined->True,
     PlotRange->{min, max},
DisplayFunction->Identity],{i,1,lastres}];
Clear[i];
tabanimation=Table[g[i],{i,1,lastres}];
ShowAnimation[tabanimation,
     AnimationFunction:>$AnimationFunction]
  ]
(**** End of Animation Procedures Section ****)


End[ ]
Unprotect[anifKdV]
EndPackage[ ]


(**************************************************************)
(***                                                      ***)
(***                 FILE NAME: sspsws.dat                ***)
(***                                                      ***)
(**************************************************************)
(* This file supplies the parameters and initial data    *)
(* for the running sspsws.dat                             *)
(**************************************************************)


alpha = -3/4;beta = -1/6;
gamma=1.0; (*The forcing amplitude *)
lambda = 1.5;al=1.0;
n = 512;l = 8.0;
deltat = 0.01;
m = 100;
firstres = 1;
lastres = 50;
timesave = 100;
waveheight = 1.0;
initfac = 10; (*The first step is divided into initfac sub-steps*)

(**The following is the definition of the initial profile**)
b1 = -2*alpha/(3*beta);
b2[x_]:= -x/beta;
b3 = 2*gamma/beta;
c1 = 4/b1; c2[x_]:= -b2[x]/(3*b1);
u0[x_,t_]:=-(b2[x]/b1)*Sech[Sqrt[0.25*b2[x]]*(0.5*al+t)]^2;
u1[x_,t_]:=Sqrt[b2[x]]*u0[x,t]*Tanh[Sqrt[0.25*b2[x]]*(0.5*al+t)];
g2[x_]:= -(b2[x]*c2[x]+b3)/c1;
g3[x_,t_]:=-(b1*c2[x]^3+b2[x]*c2[x]^2+b3*c2[x]-b3*u0[x,t])/(c1^2);
```

```
x01=0.601315225;
ul[x_]:= If[x <= -al/2,  (-b2[lambda]/b1)
    *Sech[Sqrt[0.25*b2[lambda]]*(x - x01)]^2,0];
ur[x_]:= If[x >= al/2, (-b2[lambda]/b1)
    *Sech[Sqrt[0.25*b2[lambda]]*(x + x01)]^2,0];

 gwp[x_]:=WeierstrassPPrime[x+0.5*al,g2[lambda],g3[lambda,x01]];
gw1[x_]:=c1*gwp[x] - u1[lambda, x01];
gw2[x_]:= WeierstrassP[x + 0.5*al, g2[lambda],g3[lambda, x01]];
gw3[x_]:=c1*gw2[x]-u0[lambda,x01]+c2[lambda];
gw4[x_]:= gw2[x] + (u0[lambda, x01] - c2[lambda])/c1;
gw5[x_]:= 0.25*(gw1[x]/gw3[x])^2 - gw4[x];
u[x_]:=If[Abs[x]<al/2,c1*gw5[x]+c2[lambda],0];
us[x_]:=ul[x]+ur[x]+u[x];
u0=Table[us[l*(2*(q-1)/n -1.)], {q,1,n}];

(************  End of the data file *********************)
```

Appendix D

```
(*********************************************************)
(*                                                      *)
(*---------------- PROGRAM IV    shbifsol.m ------------*)
(*                                                      *)
(*   The Mathematica program "shbifsol.m" is designed   *)
(*   to plot the solutions and bifurcation diagrams of  *)
(*   the sfKdV BVP (6.1)-(6.3) discussed in Chapter 6   *)
(*                                                      *)
(*             --Written by Lianger Gong, May 18, 1994  *)
(*                                                      *)
(*********************************************************)


(* The following section contains the input of all      *)
(* parameters and functions being used in the computation. *)

alpha = -3/4;  beta = -1/6;

(* s[] defines b+ for given parameters lambda and P *)

u[lm_, p_] := Sqrt[ lm^2 + 2 alpha p];
s[lm_,p_]:=(-lm+Sqrt[lm^2+2*alpha*p])/(2*alpha);  (* q[] defines eta(0) *)

r[lm_,p_]:=s[lm, p] (1 - (p + lm s[lm, p] )/(p 3));
q[lm_,p_]:=ArcSech[Sqrt[-r[lm,p]*(2*alpha/(3*lm))]]/Sqrt[-lm/(4*beta)];

(* plt1[] plots the solution for all x < 0 *)

g1[lm_,p_,x_]:=-(3*lm/(2*alpha))*(Sech[Sqrt[-lm/(4*beta)]*(x-q[lm,p])])^2;
plt1[lm_, p_]:=Plot[g1[lm, p, x], {x, -3., 0},
  PlotRange->All,PlotStyle->{Thickness[0.003]}];

(* plt2[] plots the solution for x > 0 on the second branch *)

c[lm_, p_]:= -2 s[lm, p] - 3 lm/ (2 alpha);
v[lm_, p_]:=Sqrt[(c[lm,p]-r[lm,p])/(c[lm,p]-s[lm,p])];
gru[lm_,p_,x_]:=3*u[lm,p]*((Csch[ArcCoth[v[lm,p]]
 +Sqrt[u[lm,p]/(-4*beta)]*x])^2)/(2*alpha)+s[lm,p];
plt2[lm_,p_]:=Plot[gru[lm,p,x],{x,0,9},PlotRange->All,
  PlotStyle->{Thickness[0.003]}];

(* plt3[] plots the solution for x > 0 on the solitary wave branch *)

sol[lm_,p_]:=NDSolve[{lm y[x]+alpha y[x]*y[x]+beta y''[x]-p/2.==0,
     y[0]==r[lm, p],
     y'[0]==Sqrt[-lm/beta]*Tanh[Sqrt[-lm/(4*beta)]
```

```
        *q[lm,p]]*r[lm,p]}, y, {x,0,14} ];
plt3[lm_, p_]:= Plot[Evaluate[y[x]/.sol[lm, p]],{x,0,14},
        PlotStyle->{Thickness[0.003]},PlotRange->All];


(* The following section includes plotting figure 6.2  *)

figas = Show[plt1[1.9, 2],plt3[1.9, 2], plt1[1.85, 2], plt3[1.85, 2],
        plt1[1.8,2],plt3[1.8,2],plt1[Sqrt[3],2],plt3[Sqrt[3],2],
     AxesLabel->{"x", "eta(x)"}];
figbs = Show[plt1[1.5, 1.0],plt3[1.5, 1.0],plt1[1.5, 1.1],
     plt3[1.5, 1.1], plt1[1.5, 1.2], plt3[1.5, 1.2],
        AxesLabel->{"x","eta(x)"}];


$DefaultFont={"Courier", 8};
label2=Show[Graphics[Text[FontForm["(a)",{"Courier",10}], {2.0,0.0}]]];
label1=Show[Graphics[Text[FontForm["(b)",{"Courier",10}], {2.0,0.0}]]];
fig=Show[Graphics[{Rectangle[{-5,-1},{20,3}, figas],
     Rectangle[{-5.3,-1.5},{20,-1}, label2],
     Rectangle[{-5,-6},{20,-2}, figbs],
     Rectangle[{-5.3,-6.5},{20,-6}, label1]}],AspectRatio->1.1]


(* The following is designed to plot figure 6.3.   *)
figau = Show[plt1[1.9, 2], plt2[1.9, 2], plt1[1.85, 2], plt2[1.85, 2],
        plt1[1.8, 2], plt2[1.8, 2],plt1[Sqrt[3], 2], plt2[Sqrt[3],2],
        AxesLabel->{"x", "eta(x)"}];
figbu = Show[plt1[1.5, 1.0],plt2[1.5, 1.0],plt1[1.5, 1.1],
        plt2[1.5, 1.1], plt1[1.5, 1.2], plt2[1.5, 1.2],
        AxesLabel->{"x", "eta(x)"}, PlotRange->{0, 1}];
$DefaultFont={"Courier", 8};
label2=Show[Graphics[Text[FontForm["(a)", {"Courier",10}], {2.0,0.0}]]];
label1=Show[Graphics[Text[FontForm["(b)", {"Courier",10}], {2.0,0.0}]]];
fig=Show[Graphics[{Rectangle[{-5,-1},{20,3}, figau],
     Rectangle[{-5.3,-1.5},{20,-1}, label2],
     Rectangle[{-5,-6},{20,-2}, figbu],
     Rectangle[{-5.3,-6.5},{20,-6}, label1]}],
        AspectRatio->1.1]


(* The following is designed to plot the bifurcation    *)

b[x_, t_]:=(-x + Sqrt[x^2+2*alpha*t])/(2*alpha);
bu=Plot[b[x, 2], {x, Sqrt[-2*alpha*2], 2.},
     PlotStyle->{Thickness[0.003]}, PlotPoints->1000];
w[x_,t_]:=-2*b[x, t]-3*x/(2alpha);
bs=Plot[w[x, 2], {x, Sqrt[-2*alpha*2], 2.}, PlotPoints->1000,
     PlotStyle->{Dashing[{0.01}],Thickness[0.003]}];


bifa=Show[bu, bs, PlotRange->{0, 3},AxesOrigin->{1.725, 0},
     AxesLabel->{"lambda", "||eta||"}]
```

```
bup=Plot[b[1.5, t], {t, 0,  1.5^2/(-2*alpha)},
PlotStyle->{Thickness[0.003]}, PlotPoints->1000];
bsp=Plot[w[1.5, t], {t, 0,  1.5^2/(-2*alpha)},PlotPoints->1000,
  PlotStyle->{Dashing[{0.01}],Thickness[0.003]}];

bifp=Show[bup,bsp,PlotRange->{0,3.5},AxesLabel->{"P","||eta||"}];

$DefaultFont={"Courier", 8};

label2=Show[Graphics[Text[FontForm["(a)",{"Courier",10}], {2.0,0.0}]]];
label1=Show[Graphics[Text[FontForm["(b)", {"Courier",10}], {2.0,0.0}]]];
fig=Show[Graphics[{Rectangle[{-5,-1},{20,3}, bifa],
   Rectangle[{-5.3,-1.5},{20,-1}, label2],
   Rectangle[{-5,-6},{20,-2}, bifp],
   Rectangle[{-5.3,-6.5},{20,-6}, label1]}],
AspectRatio->1.1];
Display["plot2.ps", %]

(*************************THE END****************************)
```

Appendix E

```
(*****************************************************************)
(*                                                             *)
(* ---------------Program V.  sfkdvlab.m-------------------*)
(*                                                             *)
(* This mathematica code is designed to solve the sfKdV    *)
(* equation in the laboratory coordindates by using       *)
(* Shen's scheme. The shape of the bottom bump             *)
(* at the cross section is a segment of a circle with      *)
(* the height 1.1 cm and the width 4.6 cm.                 *)
(*                                                             *)
(*           --------Made by Lianger Gong, May 21, 1994    *)
(*                                                             *)
(*****************************************************************)


(*    nfr[t, y] defines the Froude number as a function   *)
(*    of the voltage t mesured in the experiments.        *)
(*    The parameter y is the depth of the upstream flow.  *)
nfr[t_, y_]:=15 * t /(465 * y Sqrt[9.81 * y]);


(*    h[x] defines the forcing function on the bottom     *)
(*    The bump shape at the cross section is a segment     *)
(*    of a circle with the height hc and the width bp.    *)
hc=1.;
bp=4.6;
r=((0.5*bp)^2 + hc^2)/(2*hc);
 h[x_]:=If[Abs[x] < bp/2, Sqrt[r^2 -  x^2] - r + hc, 0];


(* Plot[h[x], {x, -30, 30}, AspectRatio -> Automatic]  *)
(* Input of volt and H  *)
volt=1.43;
H=5.0;
alp[y_]:=-3./(4*y);
beta[y_]:=-y^2/6;
a=alp[H];
b=beta[H];
lm=nfr[volt, H/100]-1;
x1=-0.5*bp;
eta0[x_]:=-(3*lm/(2*a))*(Sech[Sqrt[-lm/(4 b)](x1-x)])^2;
eta1[x_]:=-(Sqrt[-lm/b])*eta0[x]*Tanh[Sqrt[-lm/(4 b)](x1-x)];


(* The following section is to plot BLO diagram
   in order to locate the phase shift LO.
   n=60;
   Do[l0=-1.+15.0*(i-1)/n;
       sol[i] = NDSolve[{lm*y[x]+a*y[x]*y[x]+ b*y''[x]-0.5*h[x]==0,
                     y[x1] == eta0[l0],
```

```
                    y'[x1]== eta1[10]},
        y, {x, x1, -4*x1} ];
    y1[i]=y[-x1]/.sol[i];
    y2[i]=y'[-x1]/.sol[i];
    bl[i]=(b/2)*y2[i]*y2[i]+(lm/2+a*y1[i]/3)*y1[i]*y1[i],{i,1,n+1}];

    sp=Table[{-1+15.*(i-1)/n, bl[i][[1]]}, {i,1,n+1}];
    g1=ListPlot[sp, PlotJoined -> True,
            PlotRange->All, AxesLabel->{LO, "B(LO)"}];    *)

(* The following section is to plot the two solutions and the bottom bump *)
10=1.56014;
sol = NDSolve[{lm*y[x]+a*y[x]*y[x]+b*y''[x]-0.5*h[x]==0,
            y[x1] == eta0[10],
            y'[x1]== eta1[10]},
            y, {x, x1, -15*x1} ];
y1=y[-x1]/.sol;
y2=y'[-x1]/.sol;
 bl=(b/2)*y2*y2 + (lm/2 + a*y1/3)*y1*y1;

letal[x_]:=-(3*lm/(2*a))*(Sech[Sqrt[-lm/(4*b)]*(x-10)])^2;
letar[x_]:= Evaluate[y[x]/.sol];
leta[x_]:= If[x < x1, letal[x], letar[x]];
gras1=Plot[H + leta[x], {x, -20, 20}, AspectRatio ->  Automatic,
                            PlotStyle->{{Dashing[{0.02, 0.01}]}}];

10= 9.43651;
sol = NDSolve[{lm*y[x]+a*y[x]*y[x]+b*y''[x]-0.5*h[x]==0,
            y[x1] == eta0[10],
            y'[x1]== eta1[10]},
            y, {x, x1, -12*x1}];
y1=y[-x1]/.sol;
y2=y'[-x1]/.sol;
bl=(b/2)*y2*y2 + (lm/2 + a*y1/3)*y1*y1;

letal[x_]:= -(3*lm/(2*a))*(Sech[Sqrt[-lm/(4*b)]*(x-10)])^2;
letar[x_]:= Evaluate[y[x]/.sol];
leta[x_]:= If[x < x1, letal[x], letar[x]];

gras2=Plot[H + leta[x], {x, -20, 20}, AspectRatio ->  Automatic];
grab=Plot[h[x], {x, -20, 20}, AspectRatio -> Automatic];
expd={{-20, 4.81}, {-15, 4.86}, {-10, 5.0}, {-5, 5.34},{0, 5.85},
        {5, 5.74}, {10, 5.42}, {15, 5.17}, {20, 5.10}};
graex=ListPlot[expd];
Show[gras1, gras2, grab, graex, PlotRegion->{{0.1, 0.9},{0.2, 0.8}}];
```